Quantification of Site City Interaction Effects on Responses of Buildings and Basin Under Realistic Earthquake Loading for Development of Economic Smart City

Lav Joshi
IIT Roorkee: Indian Institute of Technology Roorkee
J.P. Narayan (jaypnfeq@iitr.ac.in)
Indian Institute of Technology Roorkee

Research Article

Keywords: Detrimental and beneficial SCI effects, pseudo dynamic rupture, realistic earthquake loading, dynamic parameters of buildings, development of smart city

Posted Date: March 31st, 2021

DOI: https://doi.org/10.21203/rs.3.rs-355609/v1

QUANTIFICATION OF SITE CITY INTERACTION EFFECTS ON RESPONSES OF BUILDINGS AND BASIN UNDER REALISTIC EARTHQUAKE LOADING FOR DEVELOPMENT OF ECONOMIC SMART CITY

Lav Joshi[a] and J. P. Narayan[b]
[a]Department of Earthquake Engineering, Indian Institute of Technology Roorkee, India, Email: ljoshi@eq.iitr.ac.in
[b]Department of Earthquake Engineering, Indian Institute of Technology Roorkee, India, Email: jp.narayan@eq.iitr.ac.in (Corresponding Author)

ABSTRACT

The paper presents the quantification of site-city-interaction (SCI) effects on the responses of buildings of a city and free field motion under realistic earthquake loading for the economic development of a smart city. The state of the art pseudo-dynamic earthquake rupture is implemented in the existing fourth-order viscoelastic staggered-grid SH-wave finite-difference program, and simulated results validated. SH-wave responses of various homogeneous and heterogeneous cities situated on horizontal sediment layer as well as in 2D heterogeneous basins are simulated and analyzed for different dynamic parameters of the buildings. The simulated SCI effects using realistic earthquake loading reveals a reduction of transfer function (TF) of buildings in a wide frequency bandwidth. This finding is conflicting with the reported splitting of bandwidth of the F_0^{SB} in the past SCI studies, carried out using simple plane incident wave-front with a single zero-phase wavelet. The obtained largest SCI effects on a building was highly dependent on the building type, city and basin heterogeneity in contrast to the general perception that it should be maximum at centre of city. It is also obtained that SCI effects are always beneficial to buildings when fundamental frequency of building on rock $F_0^{SR} < 1.4F_0^B$ (F_0^B is the fundamental frequency of basin/sediment layer). The obtained reduction of F_0^{CB} of building of city as well as free field motion due to the effects of SCI corroborates with the past SCI studies. The increase of coupling between the buildings and basin due to an increase of building density causes an increase of SCI effects on the responses of both the buildings and free field motion. The SCI effects in the case of buildings with low damping are beneficial during an earthquake. It is recommended that the smart city should be homogeneous in nature and F_0^{SR} of buildings should be less than around 1.4 times the F_0^B of the underlying basin/sediment deposit and buildings should preferably be a steel one.

Keywords:
Detrimental and beneficial SCI effects, pseudo dynamic rupture, realistic earthquake loading, dynamic parameters of buildings, development of smart city.

Declarations
Funding: Not applicable
Conflicts of interest / competing interests: The authors declare that there is no conflict of interest.
Availability of data and material: Some or all data that support the findings of this study are available from the first author upon reasonable request.
Code availability: The inquiries about the program availability, compilation or usage details may be requested from the first author.
Authors Contribution: Both the authors contributed to the study conception and design. All simulations were performed by Lav Joshi. The first draft of manuscript was written by Lav Joshi and both the authors contributed towards the final version of the manuscript.

1. INTRODUCTION

The explanation of the behaviour of buildings and free field motion during an earthquake loading is a significant challenge for researchers because of the complex soil-structure-soil interaction (SSSI). The study of soil-structure interaction (SSI) started during the 1950s when Merrit and Housner (1954) studied the SSI effects of buildings on the base shear and fundamental frequency of buildings. They reported a decrease in the fundamental frequency of structure resting on soft soil. Later, Jennings (1970) performed an experiment to estimate the ground motion induced by the **Millikan Library Building** at California Institute of Technology, Pasadena/Los Angeles, excited by two vibrators placed on the top of the building. Wirgin and Bard (1996) studied the complex interaction of buildings with the underlying basin using numerical simulation of SH-wave responses of homogenous building blocks. They found that SSI significantly modifies the amplitude and duration of ground motion up to a distance of 1.0 km. The site-city-interaction (SCI) affects the buildings and basin responses due to the combined effects of kinematic soil-structure interaction and inertial structure-soil interaction on a global scale (Merrit and Housner, 1954; Jennings, 1970; Wong and Trifunac, 1975; Wirgin and Bard, 1996; Gueguen et al., 2002). Chavez-Garcia and Cardenas-Soto (2002) recorded micro-tremors around two structures and concluded that the SCI phenomenon is dominant when two conditions are satisfied. Firstly, buildings are on soft soil deposit, and secondly, the fundamental frequency of buildings matches the fundamental frequency of the soft soil deposit. The free-field motion recorded in the vicinity of

structures is altered by the motion radiated to the ground by the vibration of structures. Kham et al. (2006) and Semblat et al. (2008) simulated the SH-wave responses of structures situated in a shallow basin under double resonance condition and concluded that the SCI is beneficial to some part of the city (within the city) and detrimental within and at boundaries of the city. Now, the first question arises whether SCI effects are always beneficial to buildings or detrimental too for some of the buildings of the city.

In most of the past SCI studies, scientists have used incident plane wave-front of SH/SV-wave with simple wavelet shape (Ricker/Gabor wavelet) to excite the site-city model (Kham et al., 2006; Kumar and Narayan, 2018; 2019). **In some of the SCI studies, vertically incident plane waves along with basin-generated surface waves are used to excite the buildings (Kham et al., 2006; Semblat et al., 2008; Sahar et al., 2015; Lu et al., 2018). Isbiliroglu et al. (2015) is an example in which the seismic response of idealized building block models placed in San Fernando Valley corresponding to the 1994 Northridge earthquake is simulated for frequencies up to 5 Hz, apart from this few other studies have also been carried out considering incident wave-field other than simple vertically propagating plane wave (Clouteau and Aubry, 2001; Clouteau et al., 2002; Guidotti et al., 2011; Taborda and Bielak, 2011a; b). On the other hand analytical methods have also been developed to study the SCI effects based on mean impedance of the soil city interface (Boutin and Roussillon, 2004; Boutin and Roussillon, 2006).** Further, in the past SCI studies, the cities were considered in on a sediment layer or in a 2D-shallow basin (shape-ratio<0.25) under double-resonance condition and results were in the form of reduction of fundamental frequencies of building and basin, corresponding transfer function (TF) and splitting of the bandwidth of fundamental mode of vibrations of buildings and basin (Gueguen and Bard, 2005; Kham et al., 2006; Semblat et al., 2008; Kumar and Narayan, 2018). **Double resonance is the matching of the fundamental frequency of basin (F_0^B) with the fundamental frequency of building on rock (F_0^{SR}).** Some researchers have also carried out experimental work to reinforce further the understanding of SCI effects **(Bard et al., 2005;** Schwan et al., 2016, Aldaikh et al., 2016). Now, the second question arises whether the conclusions drawn based on analysis of buildings and basin responses using simple sources such as Ricker wavelet will be intact in the case of realistic earthquake sources.

In SCI studies, buildings are incorporated in the numerical grid as homogenous visco-elastic building block models (BBM) instead of a real one (Wirgin and Bard, 1996; Bard et al, 2005; Sahar et al, 2015). The dynamic parameters for the BBM like values of moduli, damping and density

may vary with the design, type of building, social status of a city/society and the approach followed to finalize the building parameters (IS 1893:2016; Kham et al., 2006; Sahar et al., 2015). Recently, Michel and Gueguen (2018) reported a range for effective S-wave velocity for the buildings as 100-500 m/s depending on the type of building, dimension, and design. **The fundamental frequency of the BBM on rock for the SH-wave can be obtained using simple relation $\mathbf{F_0^{SR} = V_S/4H}$, where 'H' is the height of building (Wirgin and Bard, 1996; Kumar and Narayan, 2019). Means, the SCI results obtained using SH-wave responses of site-city models may be applicable for the shear beam building models** (Bard et al., 2005; Sneider and Safak, 2006; Sahar et al., 2015; Michel and Gueguen, 2018). Now, the third question arises what will be the role of dynamic parameters like density and damping of building in the SCI effects on the responses of buildings and basin.

To fulfil the above-identified scientific gaps as well as for the economic development of the smart city, first, a state of the art pseudo-dynamic earthquake rupture is implemented in the existing fourth-order viscoelastic staggered-grid SH-wave finite-difference program of Narayan and Kumar (2013) to simulate the realistic earthquake ground motion. The simulated ground motion for a postulated earthquake is validated using NGA-West2 (Boore et al., 2014; Campbell and Bozorgnia, 2014; Chiou and Youngs, 2014; Idriss, 2014).) ground motion prediction equations (GMPEs). After that, seismic responses of various homogeneous and heterogeneous city models situated on horizontal sediment layer, as well as in 2D heterogeneous basins, are simulated and analyzed. Seismic responses of homogeneous site-city models with different damping and density of the BBM are also simulated. To quantify the SCI effects on the transfer function (TF) of buildings, the response of a standalone building was considered as a reference. Similarly, the SCI effects on the response of basin were quantified considering the response of basin in the absence of city as a reference.

2. PSEUDO-DYNAMIC RUPTURE IMPLEMENTATION, SGM SIMULATION AND VALIDATION

The process of development of ground motion time histories can be traced back to the revolutionary work of Hartzell (1978) and Irikura (1983), in which a methodology for the simulation of strong ground motion (SGM) due to damaging earthquakes was proposed using smaller earthquake records as an Empirical Green's function. In the past four decades, SGM simulation procedure has come a long way with many new approaches being developed and constant refinements in the same, for example, stochastic method (Boore,1983), theoretical full-waveform Green's functions (Zeng et al., 1994) and different amalgamations of these procedures (Hartzell,

1989). An exhaustive review of all such methodologies is put together and compared in Hartzell et al. (1999), which mainly follows a kinematic rupture implementation. On the other hand, more recent studies have incorporated an entirely spontaneous (Hartzell et al., 2005) or dynamically constrained rupture characterizations (Pulido and Dalguer, 2009) to generate broadband ground motion. Dynamic approach is generally not adopted in the numerical simulation due to the lack of the required rheological and physical parameters around the source volume besides being tedious and computationally exhaustive (Shi and Day, 2013). However, it is possible to simulate earthquake ground motion using a kinematic approach as per the physics of the rupture propagation, which is easier to implement and is comparatively computationally less expensive.

The process of refinement of broadband SGM using a kinematic approach can be found in pioneer works of Graves and Pitarka (2010; 2015), which is a combination of a deterministic approach for low frequency (<1.0 Hz) and a stochastic method for high frequency (> 1.0 Hz) simulations. The crucial work of eliminating the need for a stochastic method for high-frequency ground motion consists of incorporating a so-called pseudo-dynamic rupture in the numerical grid (Guatteri et al., 2004; Schmedes et al., 2010; Mena et al., 2012; Graves and Pitarka, 2016). In the case of pseudo-dynamic rupture, the characterization and inter correlations of kinematic parameters are guided by the rules developed from the statistical analysis of suites of dynamic rupture simulations. Some of the significant recent developments in the pursuit of the reduction of coherency in radiation pattern are the incorporation of a near-fault damage zone (Cochran et al., 2009; Ben-Zion et al., 2015), stochastic crustal velocity perturbations (Graves and Pitarka, 2016) and the effects of fault roughness (Mai et al., 2017).

2.1 Deliberated earthquake rupture models

In the case of most widely used kinematic rupture models, the rupture propagation is simulated by postulating a slip function on a fault plane, in which a set of point sources are distributed along the rupture plane. The ground motion at the desired location is computed by solving the elastodynamic wave equations in an iterative way. The kinematic models simulate earthquakes as the kinematic spreading of a displacement discontinuity along a fault plane as long as the transverse dimension of the fault zone is negligible with respect to the width and length of the fault. The fault length L, fault width W, rupture velocity V_r, permanent slip D, rise time τ_A, slip function, and temporal propagation of slip on the fault is known before a postulated earthquake. Generally, the source is represented in a deterministic manner following the methodology given by Hartzell and Heaton (1983). The whole rupture plane is divided into small sub-faults, which act

as individual point sources. Utmost care is taken in the positioning and size of these point sources such that they do not behave independently. This is achieved by keeping the distance between the consecutive sub-faults less than that of the minimum resolvable wavelength of interest. The time separation is also managed using the rise-time of source time function (STF) and the rupture arrival time in such a manner that there is no time lag between any two adjacent point sources. In the present study, STF directs the temporal evolution of slip at every point source.

In order to study the SCI effects under realistic earthquake loading, five pseudo-dynamic rupture models, namely PRM1-PRM5, are proposed based on the past studies and implemented into the fourth-order SH-wave staggered-grid visco-elastic finite difference program of Narayan and Kumar (2013). The required input parameters for this FD program are unrelaxed shear modulus, density, and anelastic coefficients. The details of the computation of unrelaxed modulus and anelastic coefficients using S-wave velocity and quality factor at a reference frequency is explained in Narayan and Kumar (2013). A layered earth model is considered, and corresponding rheological parameters are given in Table 1. In order to incorporate a point source on the rupture plane shear stress components σ_{xy} and σ_{zy} are required. **The details of implementation of PRM1-PRM5 pseudo-dynamic ruptures for a postulated earthquake of moment magnitude Mw=6.0 and average slip 18 cm are given in the following sub-sections. The dip angle (δ), rake (γ), strike direction (ϕ_s) for the rupture plane of the postulated earthquake are taken as 90º, 180º, and 180º, respectively**. The grid size is taken as 50 m in both the horizontal and vertical directions to give reliable deterministic results up to 5 Hz. The time step (Δt) in the simulation is taken as 0.004 seconds keeping in mind the stability criteria for 4th order accurate finite difference simulations. The length and width of the rupture zone are finalized for the postulated earthquake as 40 km and 15 km, respectively, based on the available empirical relations (Wells and Coppersmith, 1994; Leonard, 2010). The focal depth is taken as 18 km, and ground **motion is recorded towards right of epicentre at a distance of 65 km.**

The number of considered point sources on the rupture plane are 2.4x10^5 (300x800), the distance between the two consecutive point source in both the horizontal and vertical directions is 50 m. A particular point source is inserted into the numerical grid (velocity-stress scheme) using STF and stress tensor components.

$$(\sigma_{zy})^{n}_{i,j+1/2} = (\sigma_{zy})^{n}_{i,j+1/2} - \frac{STF(t) * \Delta t * M_{zy}}{V} \quad (1a)$$

$$(\sigma_{xy})^{n}_{i+1/2,j} = (\sigma_{xy})^{n}_{i+1/2,j} - \frac{STF(t) * \Delta t * M_{xy}}{V} \quad (1b)$$

Where STF(t) is the value of the STF at time instant *'t'*, M_{xy} and M_{zy} are the moment tensor components and V is the volume of the FD grid.

The STF used is a Kostrov-like pulse proposed by Liu et al. (2006), as given below.

$$\dot{s}(t) = \begin{cases} C_N[0.7 - 0.7\cos(\pi t/\tau_1) + 0.6\sin(0.5\pi t/\tau_1)] & 0 \le \tau < \tau_1 \\ C_N[1.0 - 0.7\cos(\pi t/\tau_1) + 0.3\cos(\pi(t-\tau_1)/\tau_2)] & \tau_1 \le \tau < 2\tau_2 \\ C_N[0.3 + 0.3\cos(\pi(t-\tau_1)/\tau_2)] & 2\tau_1 \le \tau < \tau \end{cases} \quad \textbf{(2)}$$

Where $\dot{s}(t)$ is the slip-velocity, $C_N = \pi/(1.4\pi\tau_1 + 1.2\tau_1 + 0.3\pi\tau_2)$, τ is rise time, τ_1 is peak time and equal to 0.13τ and $\tau_2 = \tau - \tau_1$.

The summation of product of value of STF(t) with Δt throughout slip-duration should be unity. The temporal evolution of the slip was characterized using a STF compatible with dynamic rupture simulations proposed by Liu et al. (2006) for all the considered PRM rupture models. In all the considered PRM models, the stress tensor components can be computed using moment tensor formulation (Aki and Richards, 1980).

$$M_{xy} = m_o(sin\delta\, cos\gamma\, cos\, 2\phi_s + 0.5 sin2\delta\, sin\gamma\, sin2\phi_s) = M_{yx} \quad \text{(3a)}$$

$$M_{zy} = -m_o\,(cos\delta\, cos\gamma\, sin\,\phi_s - cos2\delta\, sin\gamma\, cos\phi_s) = M_{yz} \quad \text{(3b)}$$

where, m_o is the seismic moment for a sub-fault. The seismic moment release due to the postulated earthquake is $1.12*10^{25}$ dyne-cm, based on the following equation.

$$M_w = \frac{log\, M_o}{1.5} - 10.7 \quad (4)$$

2.2 SGM simulation using deliberated earthquake rupture models

In the following subsections, implementation of PRM1-PRM5 rupture models and validation of the simulated SGM is presented. Table 2 gives the variability or non-variability in the slip distribution (moment release), rake, rise-time, rupture arrival time, as well as the incorporation of the damage zone in the PRM1-PRM5 models.

2.2.1 SGM simulation using PRM1 rupture model

In the case of PRM1 rupture model, a constant average slip **18** cm and rake **180º** were taken for each point source throughout the rupture plane. The rise-time of the STF was kept constant for all the point sources and was calculated using modified Somerville et al. (1999) relation by Graves and Pitarka (2016). The obtained rise-time (τ_A) for the postulated earthquake of Mw=6.0 is 0.36 second.

$$\tau_A = \alpha_T c_1 M_0^{1/3} \quad (5)$$

Where $c_1 = 1.6 * 10^{-9}$;

$\alpha_T = [1 + F_D F_R c_\alpha]^{-1}$

$$F_D = \begin{cases} 1 - (\delta - 45^0)/45^0, & 45^0 < \delta \leq 90^0 \\ 1, & \delta \leq 45^0 \end{cases}$$

$$F_R = \begin{cases} 1 - (\gamma - 90^0)/90^0, & 0 < \gamma \leq 180^0 \\ 0, & otherwise \end{cases}$$

Where $c_\alpha = 0.1$.

The rupture arrival time at different point sources was calculated using the procedure given by Vidale (1988) using a constant rupture velocity as 0.8 times Vs. The left, middle and right panels of Figure 1a show the slip distribution, rise-time distribution and rupture arrival times for different point sources on the fault-plane, respectively for PRM1 the rupture model.

So, in the case of PRM1 model, the slip (moment release) and rise-time are kept constant throughout the fault plane, and rupture arrival time is also unperturbed; the only heterogeneity that is present is due to the velocity profile, as given in Table 1. The left panel of Figure 2a shows the simulated SGM at an epicentral distance of 65 km (right of epicentre). The simulated SGM reveals a peak ground acceleration (PGA) of the order of 0.13g. **The obtained relatively large PGA may be due to the taken shearing strength of the fault as that of the surrounding rock mass, coherency in ground motion, and the rupture directivity effects to some extent. The coherency in ground motion in the high-frequency range causes over prediction of SGM (Graves and Pitarka, 2016). The right panel of figure 2a shows the comparison of pseudo-spectral acceleration (PSA) using simulated SGM with 5% damping with that obtained using four NGA-West2 attenuation relationships, namely BSSA14 (Boore et al., 2014), CB14 (Campbell and Bozorgnia, 2014), CY14 (Chiou and Youngs, 2014) and I14 (Idriss, 2014). The computed PSAs are substantially more throughout the period range of interest 0.2 to 5.0 seconds.** The coherency effect can be minimized by adding heterogeneity in the source implementation process.

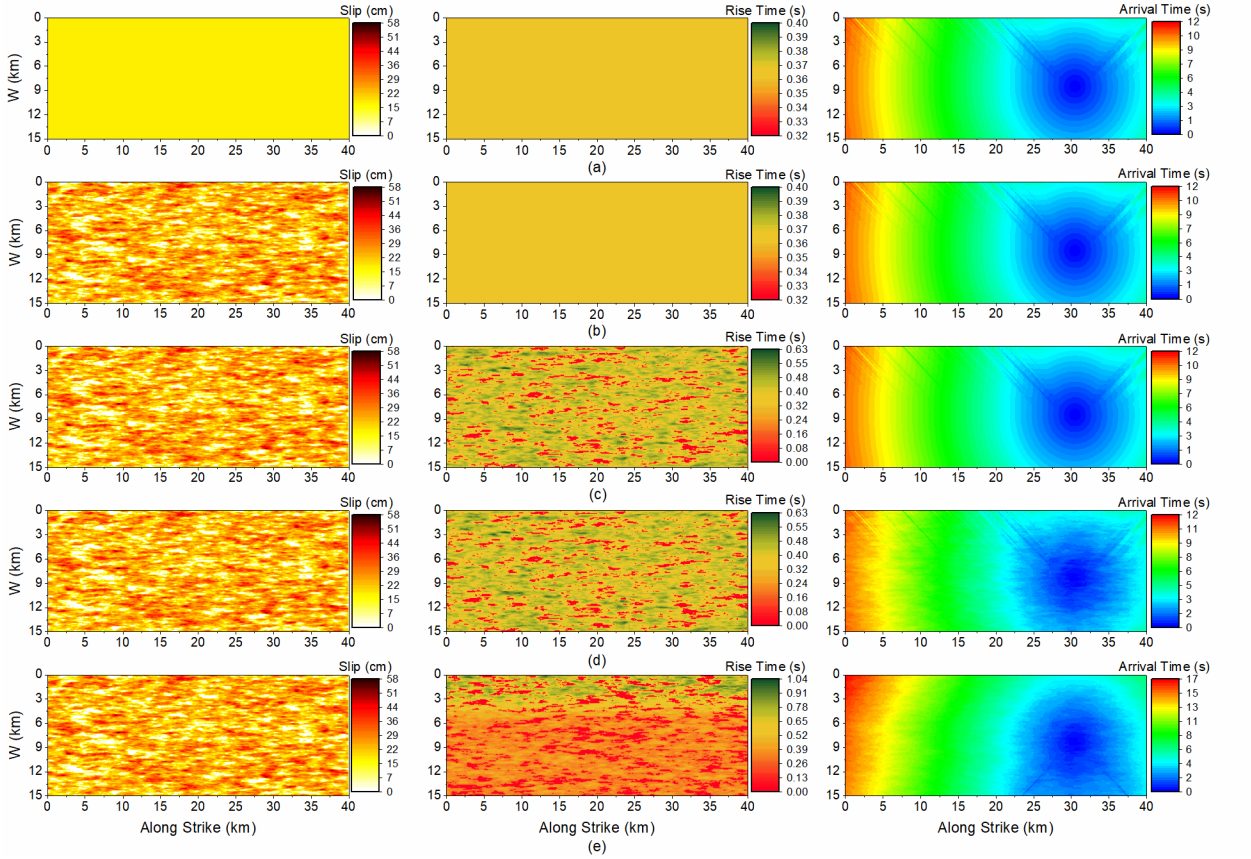

Fig.1a-e Spatial variation of slip (left panel), rise-time (middle panel) and rupture arrival time (right panel) on the rupture plane of the considered PRM1-PRM5 pseudo-dynamic rupture models, respectively.

Table 1 Rheological parameters for the considered layered earth model

Layer Thickness (km)	Density (kg/m^3)	Vs and Qs at reference frequency 1.0 Hz		Unrelaxed shear modulus (GPa)	Anelastic coefficients			
		Velocity (m/s)	Qs		a1	a2	a3	a4
0 – 1	2468	1636	163.6	6.8360	0.0176	0.0107	0.0115	0.0183
1 – 9	2667	3200	320	27.7917	0.0093	0.0055	0.0060	0.0093
9 – 17	2750	3600	360	36.1979	0.0083	0.0049	0.0053	0.0083
17 – 25	3000	3800	380	43.9621	0.0079	0.0047	0.0050	0.0078
≥ 25	3300	4400	440	64.7047	0.0068	0.0041	0.0043	0.0067

2.2.2 SGM simulation using PRM2 rupture model

In the case of PRM2 model, the STF, rise-time, rake and rupture arrival times for different point sources are the same as used in the PRM1 model (Table 2). **Nevertheless, the moment release**

as per-slip was varied from one-point source to another, and the spatial slip distribution was done using the methodology of Mai and Beroza (2002). Mai and Beroza (2002) concluded based on the study of several past earthquakes that the slip distribution in the wavenumber domain follows the Von Karman autocorrelation function as given bellow

$$A\,(k_s, k_d) = \left[\frac{a_s a_d}{(1+K^2)^{H+1}}\right]^{1/2} \quad (6)$$

Where a_s and a_d are the correlation lengths in the strike and dip direction, H is the Hurst exponent which is taken as 0.75, and K is given as

$$K^2 = a_s^2 k_s^2 + a_d^2 k_d^2$$

Table 2 Details of perturbation incorporated in slip, rake, rise time, rupture velocity and damage zone in the PRM1-PRM5 considered pseudo-dynamic rupture models.

PRM models	PRM1	PRM2	PRM3	PRM4	PRM5
Slip	Constant	Variable	Variable	Variable	Variable
Rake	Constant	Constant	Constant	Constant	Variable
Rise-time	Constant	Constant	Variable	Variable	Variable
Variable rupture velocity	Constant	Constant	Constant	Variable	Variable
Damage zone	N.A.	N.A.	N.A.	N.A.	Applied

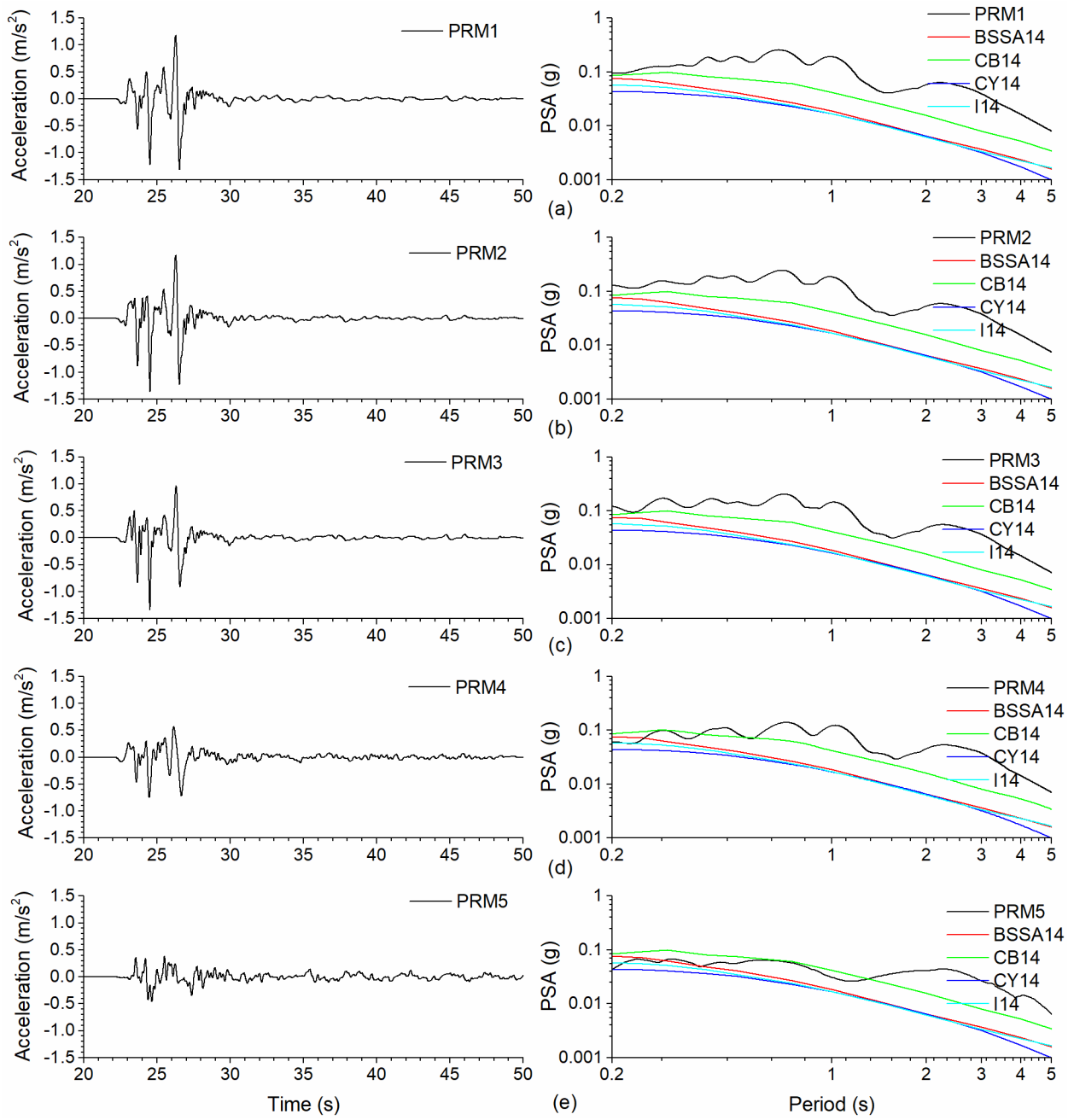

Fig. 2a-e Simulated ground motion acceleration at the free surface (left panels) and a comparison of computed PSA using simulated ground motion with the same calculated using NGA-West2 empirical relations in the case of PRM1-PRM5 pseudo-dynamic rupture models, respectively (right panels).

The correlation lengths in down-dip and strike directions are directly proportional to the magnitude of earthquake and are calculated using the scaling equation 7. For the postulated M_w=6.0 earthquake, the correlation lengths are taken as 3.16 km and 3.14 km in the strike and down-dip

directions, respectively. The obtained 2D random wavenumber distribution is transformed back to the spatial domain to give the slip distribution for the event.

$$log_{10}a_s = 0.5 \times M_w - 2.5 \quad (7a)$$

$$log_{10}a_d = 0.333 \times M_w - 1.5 \quad (7b)$$

The random slip distribution, constant rise-time, and rupture arrival times for different point sources on the fault-plane are shown in the left, middle, and right panels of Figure 1b, respectively (Table 2). **The randomization of moment release at each point source is in proportion of the slip at that point, and the sum of moment released on all the point sources is equal to the total seismic moment of the postulated earthquake.** The simulated SGM at the same epicentral distance is shown in the left panel of Figure 2b. A comparison of computed PSA using simulated SGM with that obtained using NGA-West2 relation is shown in the right panel of Figure 2b. A relative improvement as compared to PRM1 model can be inferred, but still, there is over-prediction of ground motion amplitude and PSA. A minor increase of PGA may be due the randomization of the slip.

2.2.3 SGM simulation using PRM3 rupture model

In the PRM3 model, randomization of rise-time over the fault plane is done, and the randomization of slip as well as rupture arrival times to different point sources are the same as in the PRM2 and PRM1 models, respectively. In the past SGM simulation studies, scientists have used many different methodologies for the randomization of the rise-time (Liu et al., 2006; Graves and Pitarka, 2010; Schmedes et al., 2013; Graves and Pitarka, 2016). **In the case of PRM3 model, we have proposed a method based on ideas borrowed from the past studies. Firstly, we begin with a 2D random wavenumber array, as in the case of random slip distribution, filtered with the same Von Karman autocorrelation function having the same value of correlation lengths and Hurst exponent. This array is correlated to the slip array with a correlation coefficient of 0.61. The particular choice of the correlation coefficient is based on the studies of Schmedes et al. (2010), who have analyzed 315 dynamic strike-slip rupture models to develop a covariance matrix between the fault parameters. Once the rise time matrix has been developed, it is multiplied by a factor 'k' chosen such that the rise time-averaged over the entire fault is equal to the rise time calculated by a modified Somerville et al. (1999) relation (Graves and Pitarka, 2016)**. The source parameters for the PRM3 model are shown in Figure 1c. The simulated ground motion at an epicentral distance of 65 km and a comparison of the corresponding computed PSA with the NGA-West2 relation is

shown in the left and right panels of Figure 2c. Very subtle improvements are noticeable in comparison with Figures 2a and 2b.

2.2.4 SGM simulation using PRM4 rupture model

The randomization in slip, rise-time over the fault plane are the same as used in PRM2 and PRM3 models, respectively in this case (Table 2). The perturbations in the rupture arrival times at different point sources are applied in the PRM4 model using a 2D random wavenumber matrix having a Von Karman power spectral decay. Although, it is not correlated with the slip distribution as no correlation between the rupture velocity and slip was reported in Schmedes et al. (2010). The source parameters for the PRM4 model are shown in Figure 1d. The simulated ground motion at an epicentral distance of 65 km and a comparison of the computed PSA with that obtained using NGA-West2 relations is shown in the left and right panels of Figure 2d, respectively. A comparison with Figures 2a-c reveals a considerable reduction of PGA and PSA in high frequency range after randomization of the rupture arrival time. For example, the obtained PGA is 0.07g using the PRM4 model as compared to PGA obtained as 0.13g, 0.14g, and 0.13g in the case of PRM1, PRM2, and PRM3 models, respectively. So, it can be concluded that randomization in the rupture arrival times to different point sources is playing a significant role in reducing the coherency effects on high frequency seismic radiations.

2.2.5 SGM simulation using PRM5 rupture model

Finally, in the most complex PRM5 rupture model of the present study, the randomization in slip is the same as used in the PRM2 model (Table 2). In this PRM5 model, the perturbations to the rake is applied (Table 2). The rake on the fault plane is varied throughout the fault plane, having a mean value of 180º and a standard deviation of 10º. Apart from the above, a shallow weak zone has also been incorporated in the fault plane up to a depth of 5 km where the rupture velocity is reduced to 56% of V_s to represent the weak zone in near surface rupturing events (Marone and Scholz, 1988; Dalguer et al., 2008; Pitarka et al., 2009). Apart from this the rise time is doubled in the top 5 km of the fault plane (Kagawa et al., 2004), however the average rise time is kept the same as in previous models. Additionally, based on the findings of Cochran et al. (2009), a reduction in seismic velocity of up to 50% has been found in the damage zone near the fault plane. In the PRM5 model, the maximum reduction in velocity is taken as 35% in the fault zone which extends to a depth of 1.5 km beyond the depth of fault where it linearly tapers into the background velocity. Figure 1e shows the source parameters for the PRM5 model. Due to the shallow weak zone, the

rise time in the top 2.5 km of the fault shows longer rise times. The rupture time arrivals are also more heterogeneous as compared to the PRM4 model due to the added perturbations, but they are random and not correlated to slip as proposed by Schmedes et al. (2010). **The simulated ground motion at the same epicentral distance using the PRM5 model is shown in the left panel of Figure 2e, and a comparison of PSA with that obtained using NGA-West2 relation is shown in the right panel of Figure 2e. An analysis of Figure 2e reveals a good match with that obtained using NGA-West2 relation. Further, in the time domain response, there is no strong peak, as was evident in the PRM1-PRM4 models. There is better match of the obtained PGA 0.05g with that computed using NGA-West2 relationship as 0.032g. The obtained somewhat larger PGA may be due to the simulation of SH-wave in only one component (transverse to rupture plane) and the occurrence of rupture directivity effect. On the other hand, NGA West2 relations use the average of both the NS and EW components of the recorded ground acceleration.**

The inferred good match of the spectra with those computed using NGA-West2 relation, validates the accuracy and competency of the proposed PRM5 model for SGM simulation. Further, the PRM5 model is competent enough to avoid coherency problems. It is concluded that the proposed PRM5 rupture model can be used for simulation of SGM even in the case of 3D simulations.

3. SCI EFFECTS ON RESPONSES OF STRUCTURES OF CITY AND FREE FIELD MOTION UNDER REALISTIC EARTHQUAKE LOADING

3.1 Building implementation in the FD grid

In this section, the ground motion computed using kinematic model is applied for investigating the SCI effects on the responses of buildings and basin/sediment layer. The site-city model consisting of 30 buildings along with the earthquake rupture and epicenter, is shown in Figure 3. All the horizontal distances are measured with respect to the epicenter, and all the vertical distances are measured with respect to the free surface. In the past, for SCI studies, buildings of a city were incorporated in the numerical grid as a homogenous linear visco-elastic building block model (BBM) with 5% damping (Wirgin and Bard, 1996; Bard et al., 2005; Sahar et al., 2015).

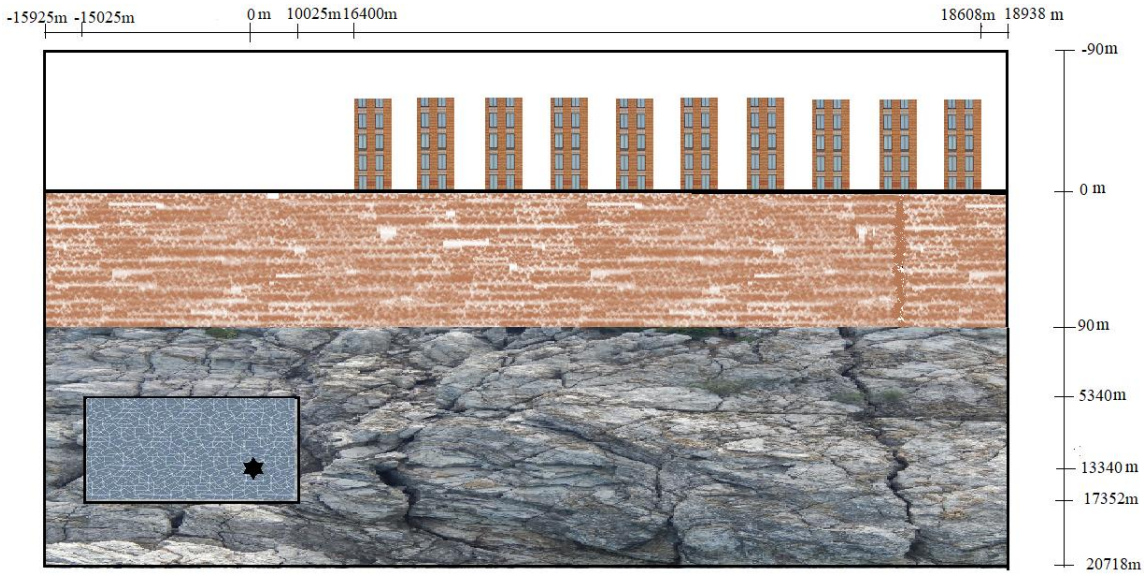

Fig. 3 A vertically staggered site-city model along with the earthquake rupture and epicenter of a postulated earthquake of moment magnitude 5.4 (Note: all the horizontal distances are measured with respect to the epicenter and all the vertical distances are measured with respect to the free surface)

The visco-elastic parameters for the BBM have been assigned in such a way that the different modes of vibrations of the BBM are the same as that of the real building. Although this might be thought of as a simplification of a shear beam or bending beam models, still the block model accounts for both shear and bending effects for out-of-plane and in-plane motion (Wirgin and Bard, 1996; Kham et al., 2006). There have been many studies conducted on the assessment of seismic wave velocity in buildings using the Timoshenko beam theory as well as the shear beam model. In the recent research work of Gueguen et al. (2019), the velocity of S-wave for different types of buildings have been obtained using seismic interferometry and deconvolution from pure bending to pure shear-type buildings, using different cases of Timoshenko beam-like structures (Snieder and Safak, 2006). For example, Sherman Oak, a 12-storey reinforced concrete frame building in Los Angeles (California), can be modelled, assuming it to be a shear beam (Gueguen et al. 2019). Michel and Gueguen (2018) inferred that the equivalent S-wave velocity for the building is highly dependent on the design and the material used and reported that equivalent S-wave velocity in a range of 100 m/s to 500 m/s depending on the building design. The S-wave velocity is taken to be 120 m/s for the BBM, in this study (Sahar et al., 2015). The density of the building was obtained considering the dead load and live load (3 kN/m^2) based on IS-456:2000

and IS-1893:2016. The density of columns, beams, and slabs is taken as **2500 Kg/m^3**, and for walls, it is taken as **2000 Kg/m^3** (Sahar et al., 2015).

The SCI study needs very fine grid (size=3m) to incorporate the building in the numerical model, which in turn requires very large computational memory and time. Further, we are not considering the crustal rock mass in the model for the same purpose as well as to avoid the very large impedance contrast at the base of sediment layer. So, a homogeneous rock layer with shear modulus of the order of 15 GPa is taken. In order to further optimize the required computational memory and time an earthquake with Mw 5.4 is considered. The damage zone is not considered since shearing strength of the considered homogeneous rock is of the same order as that of rupture. Further, the main aim of SGM simulation using pseudo-dynamic rupture is to emanate the seismic energy which is realistic one (spectra of SGM should follow the Brune's model). So, a rupture corresponding to a strike-slip earthquake of magnitude Mw=5.4 (average slip=8.4 cm, average rise time=0.18 s and average rupture velocity=1125 m/s) is implemented into the FD grid using PRM5 model, but, excluding damage zone. **The dip, rake and strike of the fault are taken as 90º, 180º, and 180º respectively.** The length and width of the rupture are taken as 25.5 km and 12.012 km, respectively. The focal depth was taken as 13.340 km. The total horizontal span of the city is 2208 m, and it extends between an epicentral distance of 16.40 km and 18.60 km. Further, the epicentral distance of the first building of the city is 16.40 km. The width of each building is taken as 33 m, and the height of buildings is varied as per the site-city model. The distance between the two consecutive buildings is taken as 42 m. So, the city density is 44.8%. The basin is implemented in the form of a horizontal layer or with a varying sediment thickness. The S-wave velocity (V_S),) and S-wave quality factor (Q_S) at the reference frequency (Fr=1.0 Hz), density (ρ), and unrelaxed moduli for the viscoelastic air, BBM, sediment, and rock are given in Table 3. The grid size was taken as 3 m in the vertical direction from the top of the model to a depth of 930 m and 18 m thereafter. Similarly, the grid size in the horizontal direction in the computational domain (over the span of the site-city model) was taken as 3 m and thereafter 18 m. The time step was chosen to be 0.0012s to avoid stability problems. Buildings are numbered as 1st, 2nd, and so on till 30th from left to right. The recorders are placed at the top of each building at the mid-span of building-width. Similarly, the gaps between the buildings are numbered G1, G2 and so on till G29, and the recorders are placed at the free surface at the mid-span of each gap.

3.2 Response of horizontal sediment layer

The seismic response of a model with a horizontal sediment layer (thickness 84 m) overlying the homogeneous rock is computed. The computed response of the same model in the absence of sediment layer is used as a reference one to quantify the spectral amplification (transfer function) caused by the sediment layer. The rheological parameters of the sediment and rock are given in Table 3. The left panel of Figure 4a shows the recorded ground acceleration and corresponding spectral acceleration on rock at an epicentral distance of 17.45 km. **The obtained PGA is 0.07g. Similarly, the left panel of Figure 4b shows the computed ground acceleration in the horizontal sediment layer and at the same epicentral distance. An increase of PGA (0.21g) can be inferred on the sediment layer due to amplitude amplification caused by combined effects of resonance, damping, and the impedance contrast.**

Table 3 Rheological parameters for the visco-elastic air, building, sediment, and rock

Materials	Velocity at F_R (m/s)	Quality factor at F_R	Density (Kg/m^3)	Unrelaxed moduli (GPa)
Air	0	∞	20	0.0
Building	120	10	350	0.00683
Soil	336	33	1800	0.22194
Rock	1500	150	2400	5.50653

A comparison of spectra of ground acceleration on the free surface in the presence and absence of sediment layer shown in right panel of figure 4a reveals that both the spectra are as per Brune's model. The transfer function (TF) due to the sediment layer is computed using the spectral ratio of response on the horizontal sediment layer with that of the rock motion (Fig. 4b). The numerically obtained fundamental frequency of sediment layer (F_0^B) is 1.0 Hz which matches with the same computed using the well-known empirical relation $F_0^B = V_S/4H$ (Table 3).

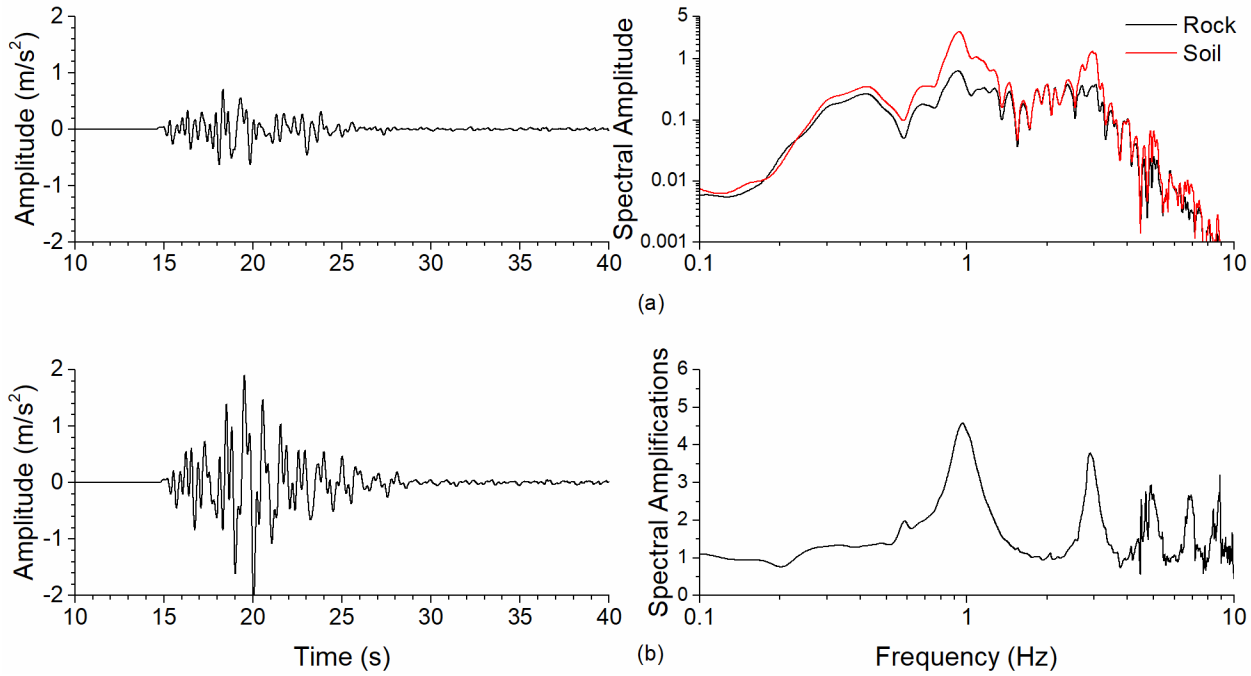

Fig. 4 Free surface ground acceleration recorded on the out-cropping rock and sediment at an epicentral distance of 17.50 km (left panels of Fig. 4a&b); a comparison of spectra of responses of out-cropping rock and sediment (right panel of Fig. 4a) and spectral amplifications (transfer function) caaused by the sediment layer (right panel of Fig. 4b).

3.3 Response of standalone building on rock

Figure 5a shows the motion recorded at the top of the standalone building (height= 30 m and width= 33 m) on rock and at the position of 15th building of the city using the same earthquake loading. The maximum amplitude of motion recorded is 2.55 m/s^2. The spectra of the response of the standalone building was normalized with the spectra of free field motion on the rock at the same location to obtain the TF of the building (Fig. 5d). The obtained F_0^{SR} of standalone building on rock is around 1.0 Hz, and the corresponding spectral amplification is 13.56.

3.4 Response of standalone building on horizontal sediment layer

The seismic response of standalone building situated at the location corresponding to a particular building of the city is computed and used as a reference response for the quantification of SCI effects on the response of that particular building. The computed seismic response of the same standalone building (H5) kept on the horizontal sediment layer ($F_0^B = 1.0\ Hz$) is shown in Figure 5b. Figure 5b reveals that when standalone building and sediment layer are in resonance, then there is a tremendous increase in the response of the building. The recorded ground motion at

481 the top of the building is about 3 times (7.22 m/s^2) to that on a standalone building on rock. This
482 may be due to the occurrence of double resonance phenomenon. The obtained fundamental
483 frequency of standalone building on sediment layer (F_0^{SB}) and corresponding spectral
484 amplification are 0.96 Hz and 36.76, respectively (Fig. 5d). Minor reduction of value of F_0^{SB} as
485 compared to F_0^{SR} can be inferred.
486
487

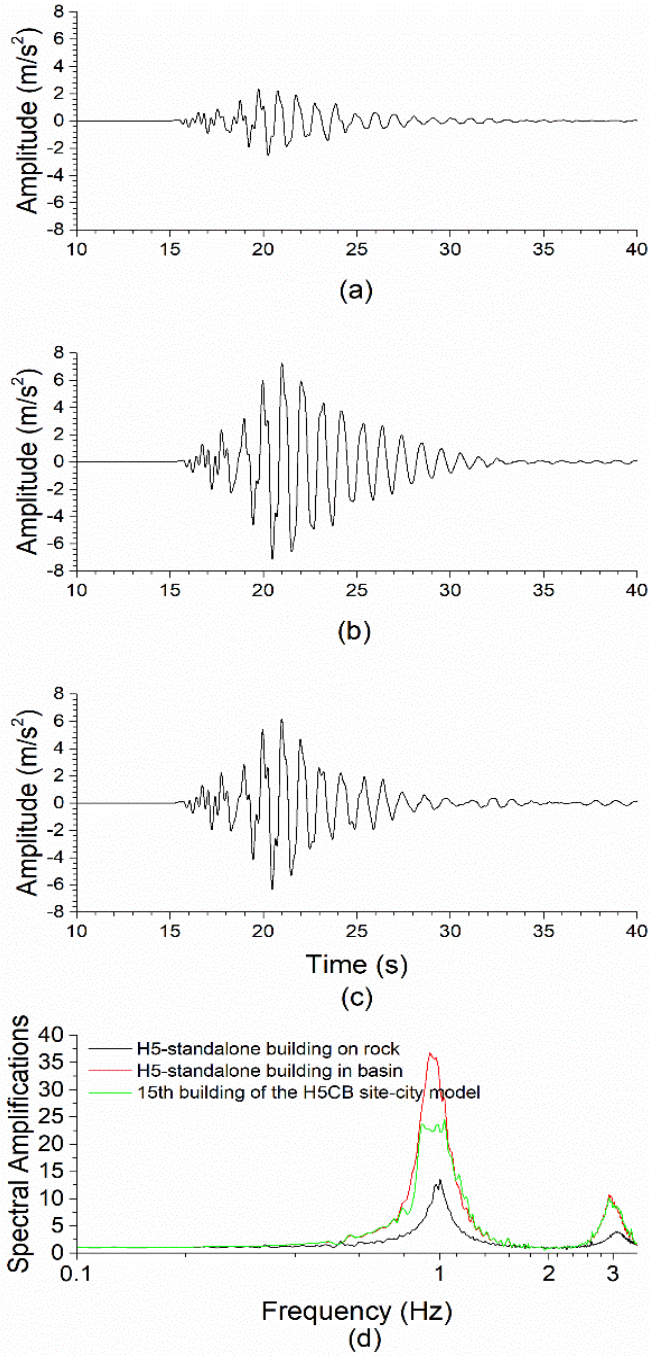

Fig. 5a-c The responses H5-standalone building on rock, H5-standalone building on horizontal sediment layer (H5SB model) and 15th building of the H5CB site-city model, respectively (thickness of sediment is 84 m in both the H5SB and H5CB models); (5d) Comparison of TFs of H5-standalone building on rock, H5-standalone building on horizontal sediment layer (H5SB model) and 15th building of the H5CB site-city model.

3.5 SCI effects on the response of 15th building under double resonance condition

The seismic response of the 15th building (17.45 km epicentral distance) of city made-up of 30 buildings lying on a horizontal sediment layer of $F_0^B = 1.0\ Hz$ was computed. The height and width of all the buildings were taken as 30 m and 33 m, respectively (means $F_0^{SR} = 1.0\ Hz$). Now, both the buildings of the city and sediment layer are under double resonance condition. The computed motion at the top of 15th building and corresponding TF are shown in Figures 5c and 5d. The obtained maximum amplitude as 6.32 m/s^2 is about 12.5% lesser than that in the case of a standalone building (Figure 5b). Even more percentage reduction of amplitude can be inferred in the case of later arrivals of the seismic phases as well as reduction of the duration of shaking.

Table 4 Homogeneous site-city models, fundamental frequency of solo-building (F_0^{SB}) on horizontal sediment layer and bandwidth of plateau (BP) like transfer function of city-buildings located at different positions.

Model	Height (m)	7th Building position		15th Building position		21th Building position		28th Building position	
		F_0^{SB} (Hz)	BP (Hz)	F_0^{SB} (Hz)	BP (Hz)	F_0^{SB} (Hz)	BP (Hz)	F_0^{SB} (Hz)	BP (Hz)
H1CB	18	1.64	1.58-1.86	1.66	1.60-1.74	1.66	1.59-1.92	1.67	1.55-1.91
H2CB	60	0.50	0.46-0.55	0.50	0.46-0.53	0.48	0.47-0.55	0.50	0.48-0.56
H3CB	24	1.05	0.88-1.23	1.03	0.80-1.26	1.11	0.95-1.27	1.08	0.91-1.26
H4CB	36	0.85	0.76-0.95	0.80	0.72-0.90	0.79	0.70-0.84	0.81	0.70-0.97
H5CB	30	0.95	0.84-1.04	0.96	0.76-1.09	0.97	0.89-1.08	0.96	0.87-1.07

It is interesting to infer that the SCI effects on the response of building under realistic earthquake loading has caused a plateau like TF in a wide frequency bandwidth. In contrast to this, in most of the past SCI studies using incident plane wave-front and simple source excitation function (Ricker wave or Gabor wavelet), the reduction of TF was maximum at the F_0^{SR} of building, which in turn caused the splitting of the spectral bandwidth of fundamental mode of vibration of the building (Kham et al., 2006; Semblat et al., 2008; Sahar et al., 2015; Kumar and Narayan, 2019). In most of the past SCI studies under double resonance condition, a further reduction of fundamental frequency of city-buildings (F_0^{CB}) and corresponding TF is reported **due to the SCI effects (Bard et al., 2005; Kham et al., 2006; Semblat et al., 20**08; **Sahar et al., 2015;** Kumar and Narayan, 2019). But, from the present study as the reduction of TF is in a wide frequency band causing a plateau like shape around the F_0^{SB} of building. Hence, we propose a range "bandwidth of plateau (BP)" in place of F_0^{CB} of building and the % reduction of TF at F_0^{CB} is computed in terms of average transfer function (ATF) in the plateau. **Similarly, in the case of**

standalone buildings the average transfer function is computed in the same BP as that of the corresponding city building and is named as average transfer function of single building (ATF-SB). For example, t**he obtained ATF in a frequency band 0.76-1.09 Hz is around 17.27 for 15th building which is around 23.38% lesser than that ~~i~~n the case of standalone building.** Table 4 depicts the fundamental frequency of solo-building (F_0^{SB}) on sediment layer and BP for 7th, 15th, 21st and 28th city-buildings of the homogeneous H1CB-H5CB site-city models. The analysis of table 4 reveals further reduction of F_0^{CB} of city-buildings, particularly under double resonance condition.

4. ROLE OF RESONANCE IN SCI EFFECTS ON RESPONSES OF BUILDINGS AND SEDIMENT LAYER

In the past, most of the SCI studies were conducted under double resonance conditions (Kham et al., 2006; Sahar et al., 2015; Kumar and Narayan, 2018). However, in nature, all the buildings of a city may not be in double resonance condition. The sediment deposit is generally highly variable from one place to another, and there is chance of occurrence of no double resonance, partial double resonance, or a complete double resonance. To study the SCI effects on the responses of buildings of a city and sediment layer under realistic earthquake loading as well as to infer the dependency of the level of this effects on the occurrence of double resonance, partial resonance, and no resonance, five homogeneous site-city models H1CB, H2CB, H3CB, H4CB, and H5CB are considered, wherein only height of buildings is variable and width of all the 30-buildings is 33 m. The height of buildings of the H1CB-H5CB homogeneous city models is H1-H5, respectively as given in Table 4. Similarly, five H1SB-H5SB models with a standalone building at desired location on the same sediment layer with heights as H1-H5, respectively are considered. Table 4 also depicts the F_0^{SB} of standalone buildings of H1SB-H5SB models. There is no resonance between the buildings of the H1CB and H2CB city models with the sediment layer. The buildings of H3CB and H4CB city models are in partial resonance condition and buildings of H5CB city model are in complete resonance condition with the sediment layer. The seismic responses of 7th, 15th, 21st, and 28th buildings of the H1CB-H5CB homogeneous city models are computed using the same realistic earthquake loading. Similarly, the seismic responses of standalone buildings of H1SB-H5SB models located at the position of 7th, 15th, 21st, and 28th buildings of city models are also computed using the same earthquake loading. **The choices of building positions have been made in such a way so as to cover the different regions of the city, ideally we would have wanted to compare the standalone building with city buildings at every location but this requires to run 30 different models (one for each**

building location) which is practically not possible for all the parameters that have to be investigated in the present study.

4.1 Buildings-sediment layer out of resonance

Figure 6a&b shows the comparison of TF of the 7th, 15th, 21st, and 28th buildings of H1CB and H2CB city models with that of a standalone building of the H1SB and H2SB models at the corresponding locations. There is an increase of TF of buildings of H1CB city-model in the frequency bandwidth of fundamental mode of vibration of building, and the reverse is the case for the buildings of H2CB city-model. Based on the past SCI studies, it is a well-established fact that when the buildings are under inertial motion, they radiate motion back to the ground at their different modes of vibrations (Bard et al., 2005; Kham et al., 2006; Sahar et al., 2015). The radiated motion to the ground is out of phase from the incident earthquake motion due to the path difference corresponding to the twice of the height of the building. Further, the frequency content in the radiated motion to the ground is dominant at F_0^{SR} of the building. In a city, when all the buildings of the city are under inertial motion, their collective radiated motion to the ground may cause a reduction or increase of response of buildings of the city, depending on the path difference. Further, the peak reduction of TF may/ may-not occur at F_0^{SB} of building, which in turn may cause a decrease or increase of TF in obtained BP of the building. For example, table 4 depicts the range for BP in the case of 7th building of H2CB city from 0.46 Hz to 0.55 Hz. It is quite surprising to note that in the case of H1CB model, there are detrimental SCI effects on the responses of all the considered buildings (Fig. 6a). The obtained percentage increase of ATF in the BP of buildings of H1CB city model as compared to that the respective standalone building are given in Table 5. **The range of percentage increase of ATF in the BP of buildings of the H1CB city is 9.19% to 18.45%. On the other hand, in the case of H2CB city, there is a decrease of ATF in the BP of all the considered buildings and the range of percentage reduction is 11.95% to 19.94% (Table 5).**

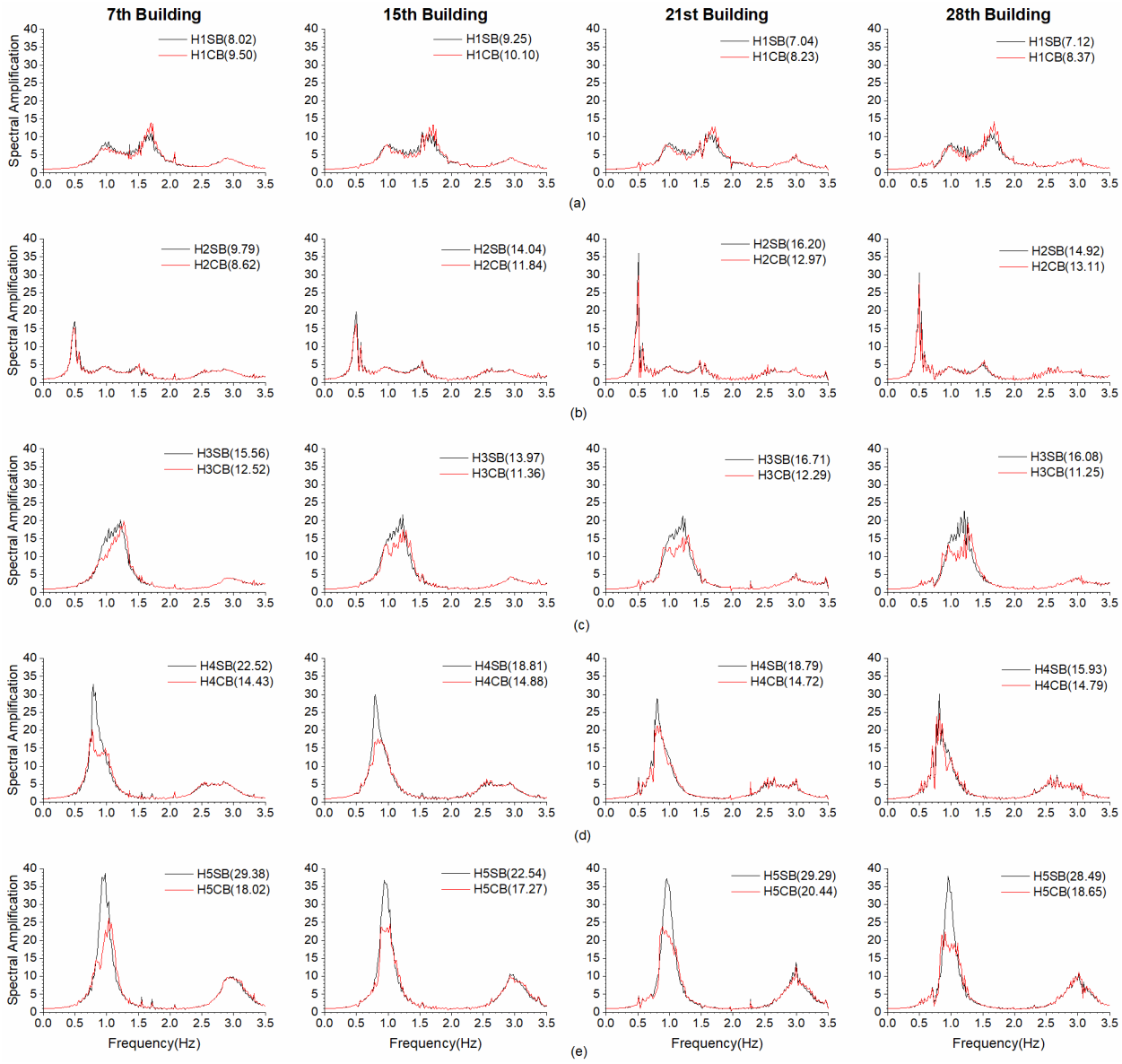

Fig. 6a-e A comparison of transfer functions of standalone buildings of H1SB-H5SB models with that of the corresponding building of cities H1CB-H5CB at different locations (Note: ATF in the BP of buildings of city and standalone buildings are given in brackets).

In order to infer the cause/phenomenon responsible for the observed detrimental effects on the TF of buildings of H1CB city model, seismic responses of buildings of another two homogeneous city models with the height of buildings as 21 m ($F_0^{SB} = 1.4Hz$) and 15 m ($F_0^{SB} = 2Hz$) were simulated. A comparison of the computed TF of the buildings of height 15 m, 18 m and 21 m of

homogeneous cities with the standalone building at the respective location is shown in Figure 7a-c, respectively. In all the three city models, an increase of ATF in the BP of the buildings is obtained. **The range of percentage increase (-ve sign) of ATF in the BP is -7.01% to -11.86%, -9.19% to -18.45% and -3.32% to -11.37%, in the cities with height of buildings as 15 m, 18 m and 21 m, respectively. So, it may be inferred that the SCI effects on the response of buildings may be detrimental when the F_0^{SB} of buildings of the city is larger than around 1.4 times of the F_0^B of underlying basin, although it needs further details study.**

Table 5 Homogeneous site-city models, ATF in the BP of buildings of H1CB-H5CB cities (ATF-BP) as well as standalone buildings (ATF-SB) and percentage increase (- sign) and decrease (no sign) due to SCI effects.

Site-city Models	Height (m)	7th Building position			15th Building position			21th Building position			28th Building position		
		ATF-BP	ATF-SB	% Inc/Dec.	ATF-BP	ATF-SB	% Inc/Dec.	ATF-BP	ATF-SB	% Inc/Dec.	ATF-BP	ATF-SB	% Inc/Dec.
H1CB	18	9.50	8.02	-18.45	10.10	9.25	-9.19	8.23	7.04	-16.90	8.37	7.12	-17.56
H2CB	60	8.62	9.79	11.95	11.84	14.04	15.67	12.97	16.20	19.94	13.11	14.92	12.13
H3CB	24	12.52	15.56	19.54	11.36	13.97	18.68	12.29	16.71	26.45	11.25	16.08	30.04
H4CB	36	14.43	22.52	35.92	14.88	18.81	20.89	14.72	18.79	21.66	14.79	15.93	7.16
H5CB	30	18.02	29.38	38.66	17.27	22.54	23.38	20.44	29.29	30.22	18.65	28.49	34.54

4.2 Building-sediment layer in partial resonance

A comparison of TF of the 7th, 15th, 21st and 28th buildings of H3CB and H4CB city models with that of standalone building of the H3SB and H4SB models at the corresponding locations is given in Figure 6c&d, respectively. There is a decrease of TF of all the buildings of H3CB and H4CB city-models, but this decrease of TF is relatively more in the case of H4CB city model. We can infer the reduction of F_0^{CB} of the buildings of the H3CB and H4CB city-models. Table 5 depicts the percentage reduction of ATF in the BP as compared to that at F_0^{SB} of the standalone building due to the SCI effects and is highly variable from one building to another building. The obtained range of percentage reduction of ATF in BP is 18.68% to 30.04% and 7.16 to 35.92% for the buildings of the H3CB and H4CB site-city models, respectively.

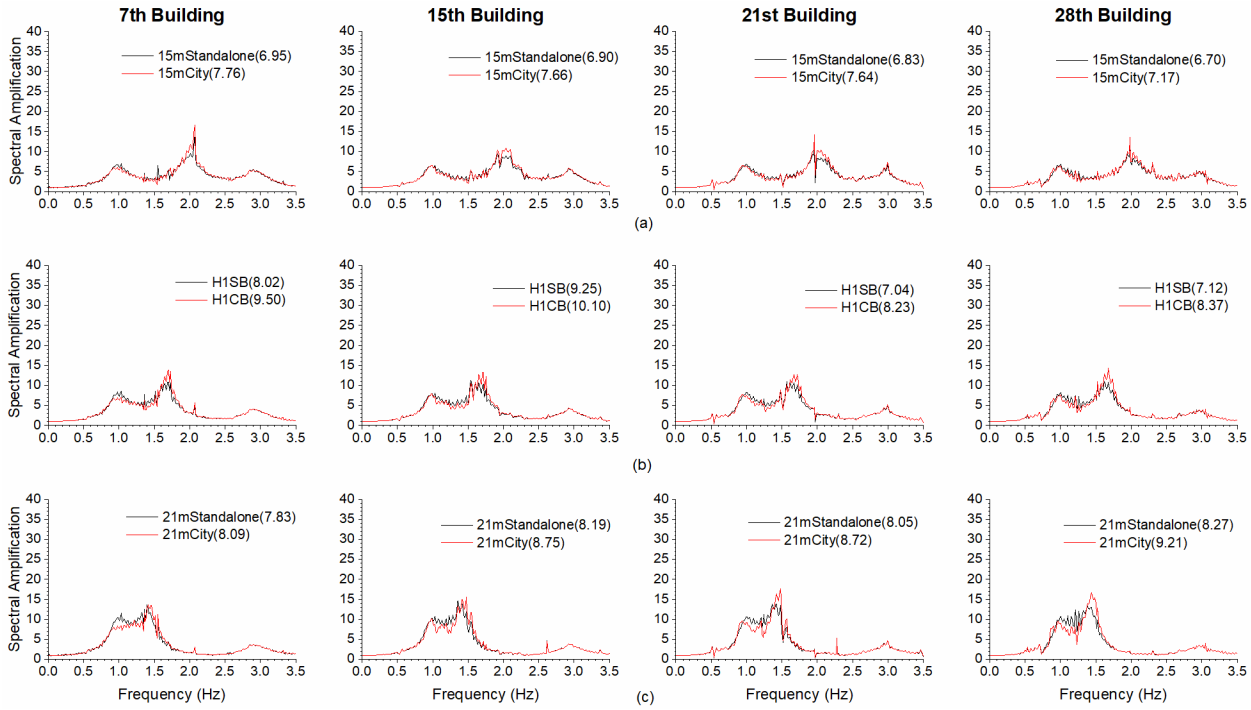

Fig. 7a-c A comparison of transfer functions of buildings of 15m,18m and 21m homogeneous city models, respectively with the standalone building at the corresponding location (Note: ATF in the BP of buildings of city and standalone buildings are given in brackets).

4.3 Building-sediment layer in resonance

Similarly, a comparison of TF of the 7th, 15th, 21st and 28th buildings of H5CB city model with that of standalone building of the H5SB model is shown in figure 6e. The percentage decrease of ATF in the BP of buildings of H5CB city is the largest since both the buildings and basin are in double resonance condition (Table 5). For example, its range in the case of H5CB city is 23.38% to 38.66%. Analysis of Figure 6 and Table 5 clearly reveals that the SCI effects are maximum in the case of H5CB city-model, and these effects are reducing as we move away from the condition of double resonance. The reason for this can be understood by enquiring about the underlying cause of SCI effects. In the case of double resonance, the motion of the building is relatively high as compared to the motion of a building which is not in complete resonance with the sediment layer. This is visible in Figure 6, where TF values are highest in the case of H5CB city model. Hence, the motion radiated back to the ground by the building in double resonance condition will be much higher than other cases, which in turn will cause more reduction in the TF of the buildings.

Arias intensity was also computed for further infer the role of site-city resonance in the SCI effects on the building response (Kramer, 1996). A comparison of the computed Arias

intensity computed for the 15th building of the H1CB-H5CB city models with the corresponding standalone building is shown in Figure 8. The cumulative value of Arias intensity for vibrational time of 25 second is least in the H2CB and largest in the H5CB city model. The higher value of Arias intensity in the case of buildings of H5CB model indicates higher level of shaking which is also evident from the TF shown in figure 6e. The Arias intensity of 15th building of H1CB-H5CB cities is 0.06m/s, 0.03m/s, 0.15m/s, 0.21m/s and 0.42m/s which is 3%, 3.4%, 19%, 14% and 45% lesser than the corresponding standalone building, respectively. Further, there is minor reduction of Areas intensity when buildings of the city are out of resonance with the underlying sediment.

Apart from various generalized conclusions drawn from the past SCI studies using simple plane wave-front with a single wavelet does not hold good while using realistic earthquake loading. For example, Kham et al. (2006), Semblat et al. (2008) and Sahar et al. (2015) reported the splitting of the bandwidth of the fundamental mode frequency of the building due to substantial reduction of TF at F_0^{SR}. In the case of realistic earthquake excitation, a BP is obtained where in the TF is more or less same (Table 4). However, the reported reduction of F_0^{CB} of buildings of city is also observed in the case of realistic earthquake loading (Table 4). The obtained SCI effects on the % reduction of TF of building under realistic earthquake loading reveals that maximum SCI effects can happen on any building irrespective of its location in the city, in contrast to the general perception that it is maximum at the centre of city (Table 5). Although the SCI effects on the TF of buildings are maximum in case of double resonance of the buildings, its impact in other cases is still significant (Table 5), which can be very beneficial in the economic design of buildings and urban planning.

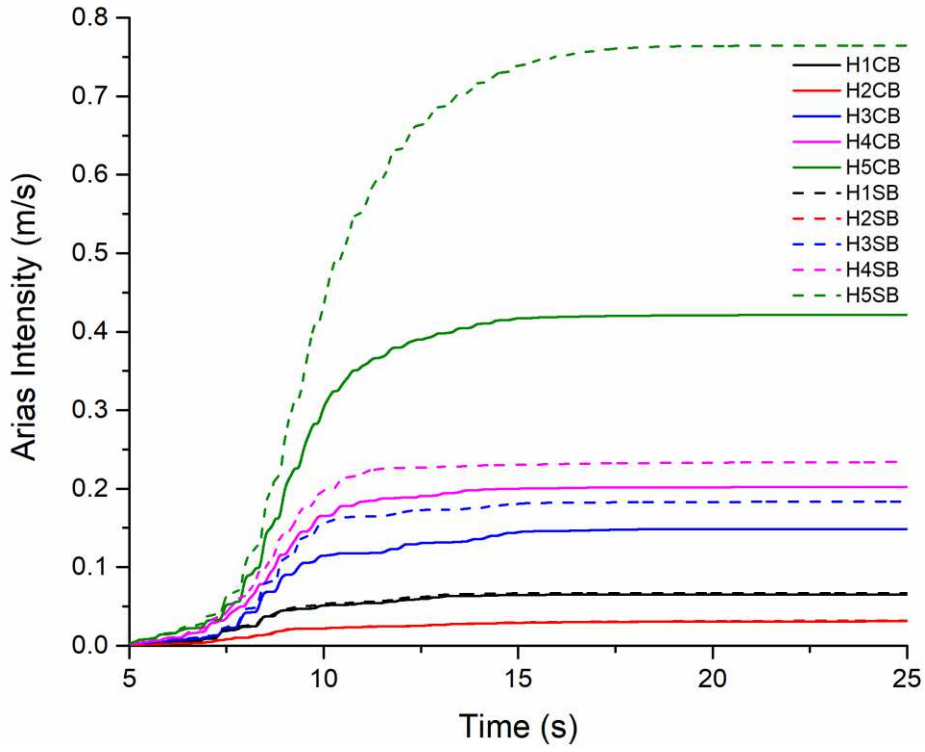

Fig 8 A comparison of Arias intensity of 15th building of the H1CB-H5CB city models with the respective standalone building.

4.4 Role of resonance in SCI effects on the response of sediment layer

In order to study the role of resonance between buildings of a city and sediment layer on the free field motion, the responses are computed at epicentral distances of 16.90 km, 17.50 km, 17.95 km and 18.47 km in the presence and absence of H1CB-H5CB homogeneous city models. Figure 9a-e depicts the comparison of TF of the sediment layer at the above-selected locations in the absence and presence of H1CB-H5CB cities, respectively. **There is only minor change in TF of sediment layer with location (epicentral distance) under realistic earthquake loading. This may be due to not a huge change in the angle of incidence at the free surface with epicentral distance due to the presence of sediment layer, even though there is considerable change of angle of incidence at the base of the sediment layer.** The apparent variation of F_0^B of the sediment layer and corresponding TF at different locations (in between the two consecutive buildings) are given in Figure 10a-e for the H1CB-H5CB site-city models, respectively.

Analysis of Figures 9 reveals that F_0^B of the sediment is affected by the SCI effects when buildings and sediment are partial and complete resonance condition and it is more in case of complete

resonance condition. Further, there is only minor change in the TF of sediment layer at frequency F_0^B when sediment and buildings are out-of-resonance.

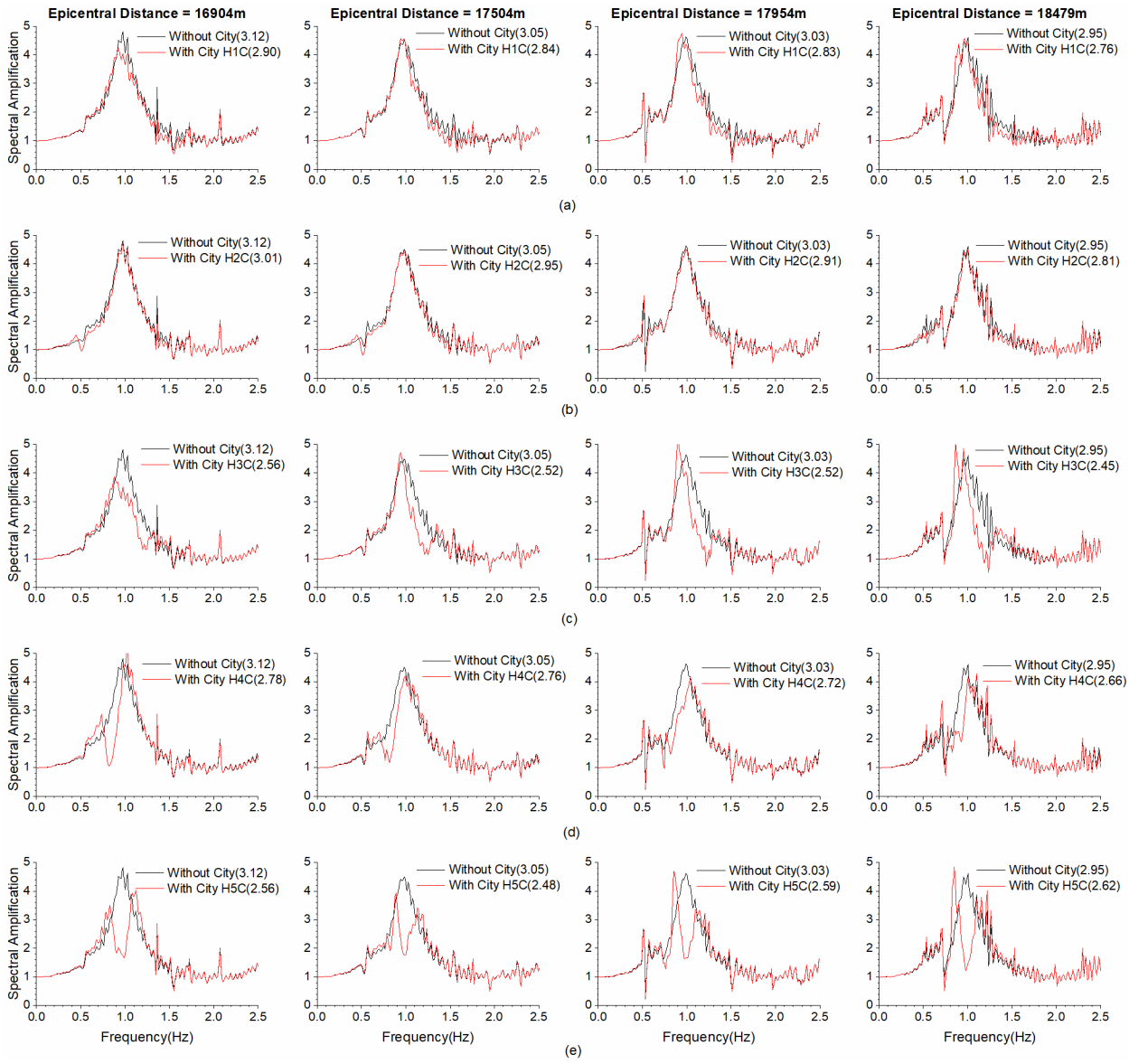

Fig. 9 A comparison of transfer functions of sediment layer at various locations in the absence and presence of homogeneous H1CB-H5CB city models (Note: ATF of sediment layer in absence of city and ATF of the same in a frequency bandwidth (0.75-1.25Hz) in the presence of city are given in brackets).

But, a considerable change in the TF of sediment layer at frequency F_0^B can be inferred when sediment layer and buildings are in partial-resonance condition, and substantial change is

obtained when both are in resonance. For example, the range of TF at apparent F_0^B of the sediment layer is 3.7 - 5.5, 4.1 - 5.2, and 3.3 - 4.9 in the cases of H3CB, H4CB, and H5CB site-city models, respectively. Further, the obtained TF at some of the locations at apparent F_0^B of sediment layer in the cases of H4CB and H5CB site-city models is even higher than that in the absence of the respective cities (detrimental SCI effects on the free field motion). This finding corroborates with the findings of Kham et al. (2006) and Semblat et al. (2008). In contrast to this, the free field ATF in a frequency bandwidth 0.75-1.25Hz in the presence of city is always lesser than that in absence of city (Fig. 9). So, it may be concluded that SCI effects are always beneficial for the free field motion.

Arias intensity was also computed to infer the role of site-city resonance in the SCI effects on the sediment response. Figure 10 a-e depicts a comparison of the free field Arias intensity computed at an epicentral distance 17.5 km in the presence and absence of the H1CB-H5CB city. The obtained free field Arias intensity at epicentral distance of 17.5 km in the presence of H1CB-H5CB city as 0.022m/s, 0.021 m/s, 0.020 m/s, 0.019 m/s and 0.014 m/s which is 2.04%, 5.09%, 8.55%, 16.43% and 38.93% lesser than the corresponding value in the absence of the city, respectively reflects that SCI effect on free field resonance is largest in the case of H5CB city model.

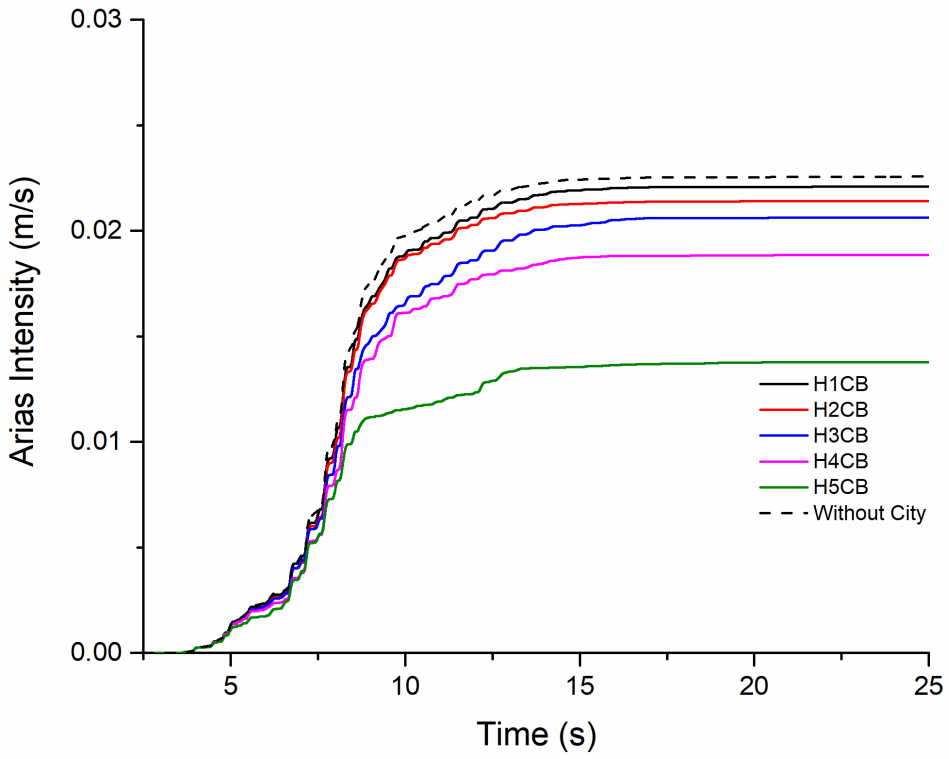

Fig 10 A comparison of free field Arias intensity at an epicentral distance of 17504m in the presence and absence of H1CB-H5CB city.

5. ROLE OF BASIN HETEROGENEITY IN SCI EFFECTS

Nowadays, the city or a particular sector is being developed using a specific design and height of buildings. In nature, the sediment thickness in basin may not be the same everywhere below that city/sector. So, some of the structures may be in double resonance, partial double resonance, and out of double resonance. In order to infer the SCI effects on the responses of a city made up of a particular type of structure but with a varying sediment thickness below it, four B1-B4 basin models are considered. Each basin model is subdivided into five sectors, and the sediment thickness in a particular segment is constant. The thicknesses of sediment in different segments of the basin are given in Table 6. **Although the considered step like basin may seem to be unrealistic but the reason why this type of geometry has been selected is to get an exact match of frequencies with the building frequencies considered in the previous section.**

Table 6 Considered basin models and sediment thicknesses in different segments (Note: width of the segment is the same for all the basin models)

Basin models	Sediment thickness below segments of different basin models				
	Segment1	Segment2	Segment3	Segment4	Segment5
B1	84m	102m	168m	66m	51m
B2	51m	66m	168m	102m	84m
B3	84m	66m	51m	102m	168m
B4	66m	102m	51m	84m	168m

The S-wave velocity in sediment is constant throughout, as given in Table 3. The sediment thickness before and after the city is extending infinitely with the sediment thickness of the first and last segments of different basin models. Figure 11a-d depicts the sketches for the B1-B4 basin models, respectively.

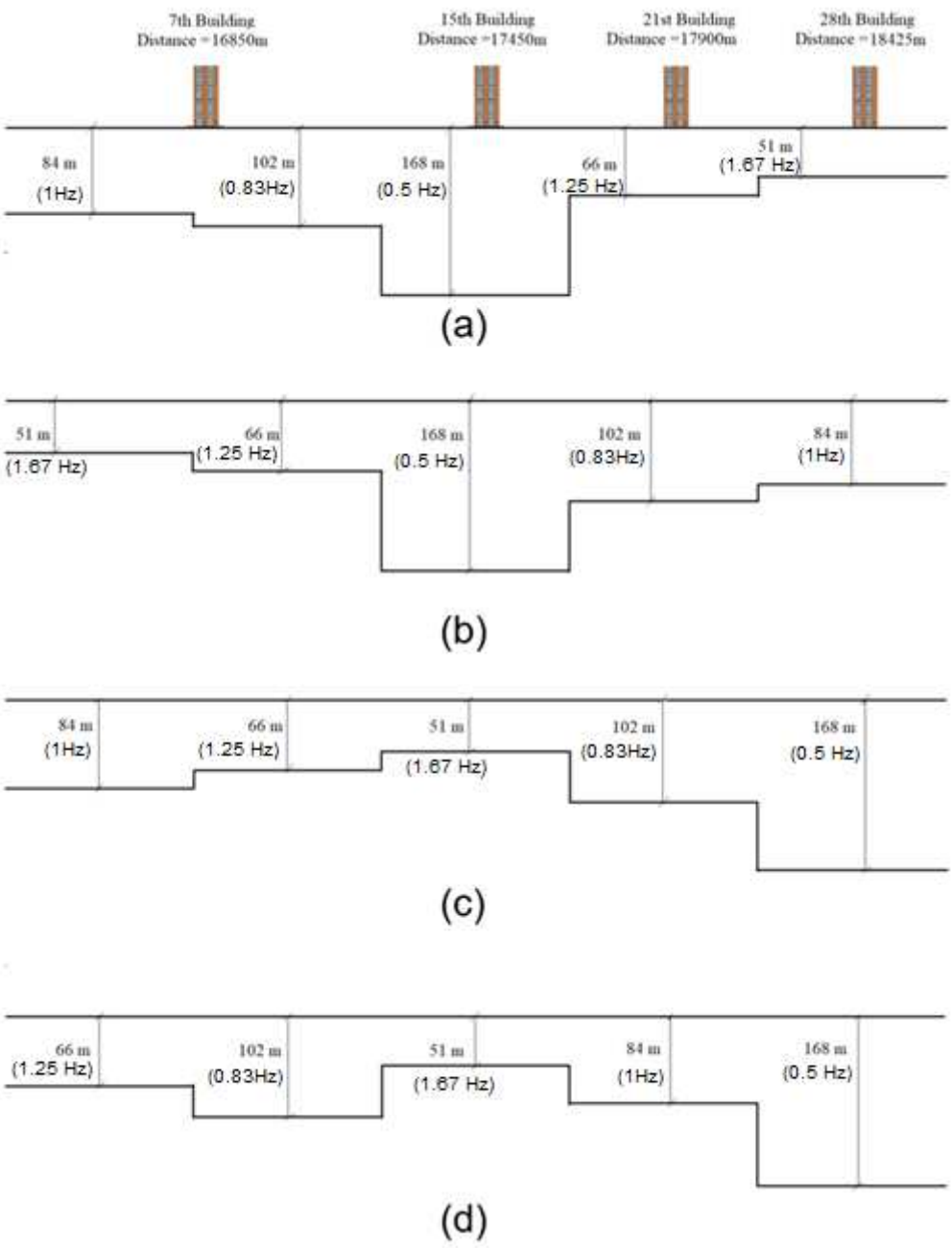

Fig. 11a-d Sketches for B1-B4 basin models, respectively and the sediment thicknesses along with the fundamental frequency in the different segments.

H5CB homogeneous city is considered for the study of the role of basin heterogeneity in the SCI effects. The name of homogeneous site-city models corresponding to B1-B4 basins is B1-H5CB to B4-H5CB, respectively. The buildings of the city are in resonance with the sediment thickness 84 m, and the rest of the buildings are either in partial resonance or out-of-resonance with the underlying sediment depending on its thickness. Seismic responses of the 7th, 15th, 21^{st,} and 28th

buildings of the B1-H5CB to B4-H5CB site-city models were computed using the same realistic earthquake loading. The response of the standalone building located at their respective places in each basin was also computed. A comparison of the TF of the 7th, 15th, 21st, and 28th buildings of the B1-H5CB to B4-H5CB with the standalone buildings are shown in Figures 12a-d, respectively.

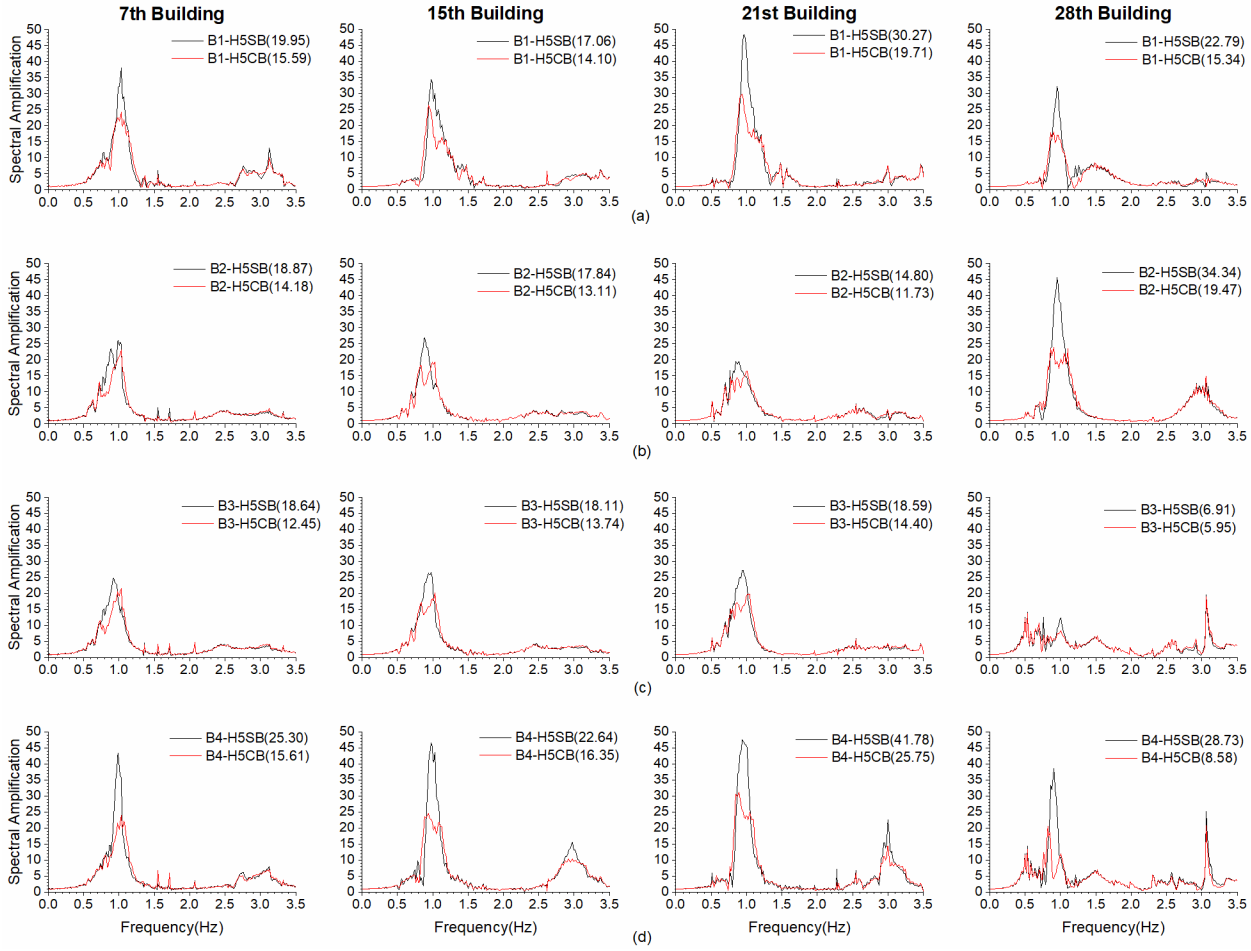

Fig. 12a-d A comparison of transfer functions of standalone buildings of B1-H5SB to B4-H5SB models with that of corresponding building of cities B1-H5CB to B4-H5CB at different locations (Note: ATF in the BP of buildings of city and standalone buildings are given in brackets).

The responses of both the buildings of the city and the standalone buildings are highly variable from one site-city model to another depending on the thickness of sediment in the segment of basin. The response of the standalone building, as well as that of the city is affected by the sediment thickness of the segment below it as well as the sediment thickness in the segment ahead to it.

The effect of site frequency in the response of 15th building is not visible in all the basin models, which may be due to basin effects in the central part. The obtained range of percentage reduction of ATF in the BP of buildings is 13.89%-41.64% due to a city with only 30 buildings with a city-density 44.8% (Table 7). Even, % reduction of ATF of 28th building of B4-H5CB is of the order of 70.34%. It is interesting to note that the minimum percentage reduction of ATF is of the order to 13.89% even for buildings which are out of resonance with the underlying basin. The 28th and 21st buildings of the B2-H5CB and B4-H5CB cities are in resonance with the underlying basin and the corresponding percentage reduction of ATF is of the order of 41.64% and 38.37% which is comparable or more than that of the buildings of the H5CB city (Table 5).

Table 7 ATF in the BP of buildings of B1-H5CB to B4-H5CB city models (ATF-BP) as well as standalone buildings (ATF-SB) and percentage increase (- sign) and decrease (no sign) due to SCI effects.

Site-city Models	7th Building			15th Building			21th Building			28th Building		
	ATF-BP	ATF-SB	% Inc/Dec	ATF-BP	ATF-SB	% Inc/Dec	ATF-BP	ATF-SB	% Inc/Dec	ATF-BP	ATF-SB	% Inc/Dec
B1-H5CB	15.59	19.95	21.85	14.10	17.06	17.35	19.71	30.27	34.87	15.34	22.79	32.69
B2-H5CB	14.18	18.87	24.85	13.11	17.84	26.51	11.73	14.80	20.74	20.04	34.34	41.64
B3-H5CB	12.45	18.64	33.21	13.74	18.11	24.13	14.40	18.59	22.54	5.95	6.91	13.89
B4-H5CB	15.61	25.30	38.54	16.35	22.64	27.78	25.75	41.78	38.37	8.58	28.73	70.34

6. ROLE OF CITY-HETEROGENEITY IN SCI EFFECTS

In this sub-section, the role of city heterogeneity in the SCI effects on the responses of buildings and sediment layer are simulated and analysed. **There have been a few studies in the past where the role of heterogeneity in cities have been studied** (**Clouteau et al., 2002; Varone et al., 2020; Taborda and Bielak, 2011a; b).** In the present study two types of heterogeneous city namely HT1CB and HT2CB, containing 30-buildings of width 33 m and varying height, are considered. There are five types of buildings of height H1, H2, H3, H4, and H5 (Table 4). Further, there are six buildings corresponding to each height of building. The sketches for the HT1CB and HT2CB heterogeneous city models are shown in Figure 13a&b, respectively. The rheological parameters for the buildings, sediment, and rock are given in Table 3. The sediment thickness is taken as 84 m. As in the previous cases, the seismic responses of the 7th, 15th, 21st, and 28th buildings of the cities were computed. The seismic response of the standalone building of HT1SB

and HT2SB model located at the respective locations were also computed. The buildings of the city with height 30 m are in resonance with the underlying sediment, and the rest of the buildings are either in partial resonance or out-of-resonance with the underlying sediment. A comparison of ATF of the 7th, 15th, 21st, and 28th buildings of the HT1CB and HT2CB city model with that of a standalone building at the respective locations are given in Figure 14a&b, respectively. There is a reduction of ATF at BP of all the buildings of both the heterogeneous cities except the 15th building of height 18 m ($F_0^{SB} = 1.7\ Hz$) of the HT2CB city model, where there is an increase of ATF in the BP by –17.06%. On the other hand, the range of percentage increase of ATF for the H1 building (18 m height) is -9.19% to -18.45% (Table 5). For rest of the buildings of both the HT1CB and HT2CB city models, the range of percentage reduction of ATF in the BP of buildings is 8.98% to 37.68% (Table 8).

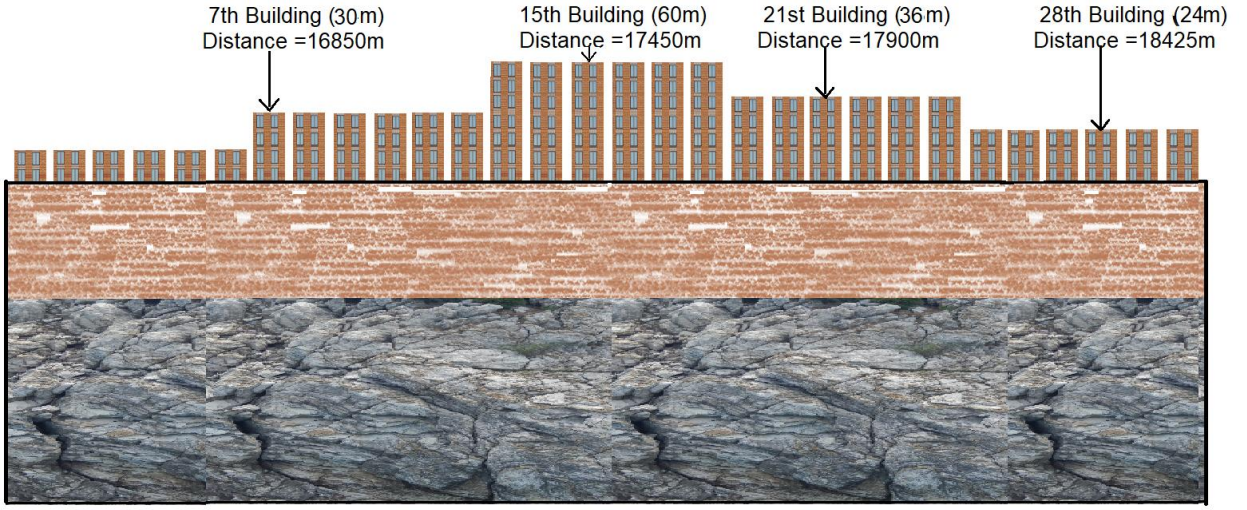

(a)

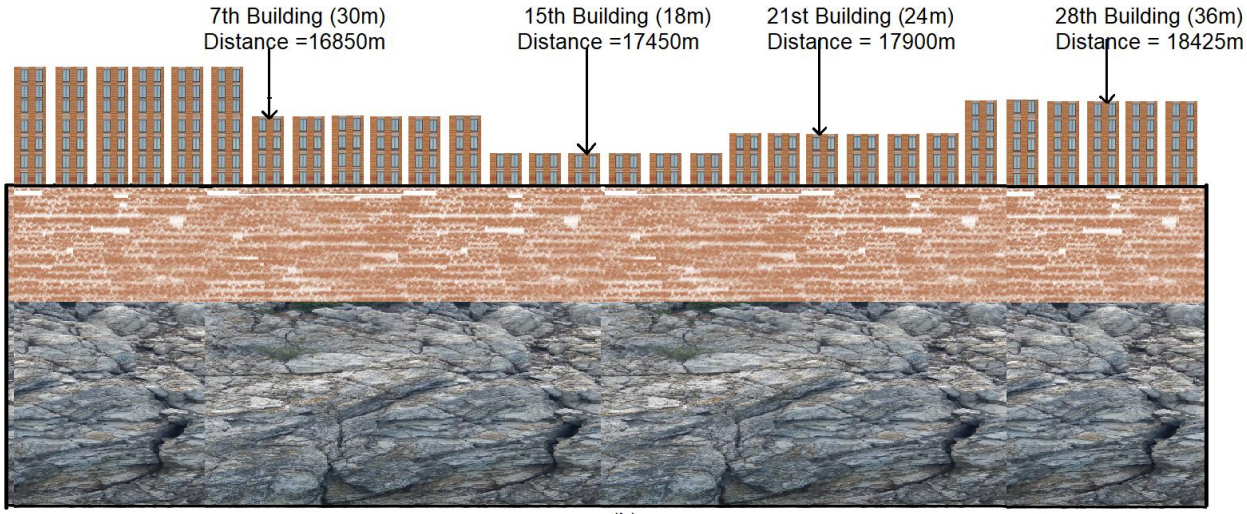

(b)

Fig. 13a&b Sketches for the HT1CB and HT2CB heterogeneous site-city models, respectively

Another interesting result is the obtained percentage reduction of ATF in the case of 7th building, with F_0^{SR} as 1.0 Hz and common to both the HT1CB and HT2CB city models, as 12.77% and 13.46%, respectively which is much lesser than that obtained in the case of buildings of the H5CB city as 23.38% to 38.66% (Table 5). This may be because there are different buildings (18m and 60m) before the 7th building, which may modify the ground motion at the location of 7th building distinctively by radiating motion back to the ground. In contrast to this, the obtained percentage reduction of ATF in the BP of 21st and 28th buildings of HT1CB and HT2CB city as 37.68% and 35.63 % (Table 8) is larger than the same obtained in the case of buildings of H4CB city as 21.66% to 7.16%. So, finally it may be concluded that in the case of heterogeneous city models, there can be both percentage reduction or increase of ATF in the BP of the buildings with a lower magnitude than the same in case of homogeneous city in heterogeneous basin (Tables 7 & 8).

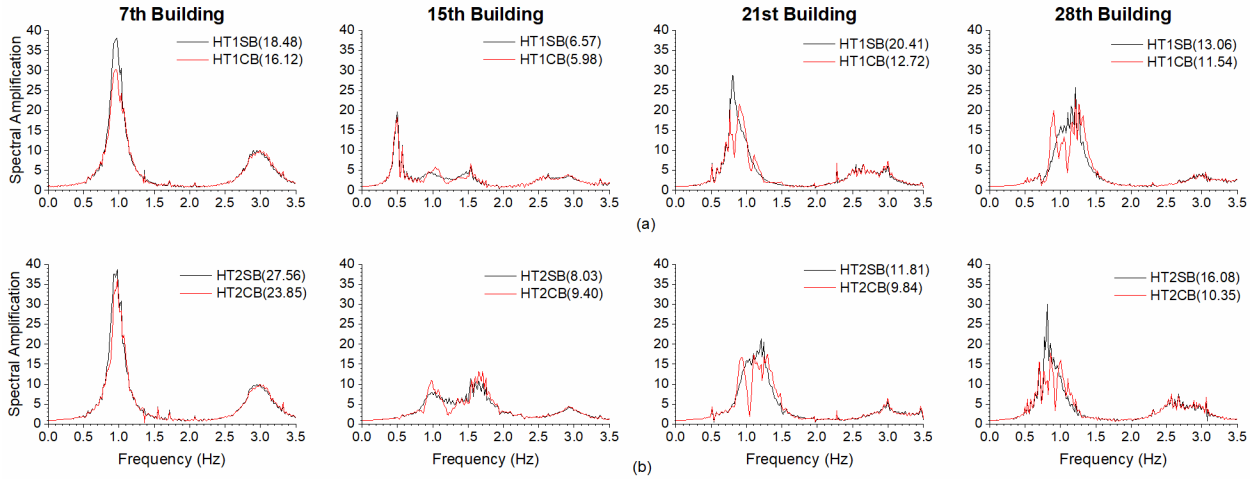

Fig. 14a&b A comparison of transfer functions of standalone building at different location with that of corresponding building of heterogeneous cities HT1CB and HT2CB (Note: ATF in the BP of buildings of city and standalone buildings are given in brackets).

Table 8 ATF in the BP of buildings HT1CB and HT2CB city models (ATF-BP) as well as standalone buildings (ATF-SB) and percentage increase (- sign) and decrease (no sign) due to SCI effects.

	7th Building			15th Building			21th Building			28th Building		
	ATF-BP	ATF-SB	% Inc/Dec	ATF-BP	ATF-SB	% Inc/Dec	ATF-BP	ATF-SB	% Inc/Dec	ATF-BP	ATF-SB	% Inc/Dec
HT1CB	16.12	18.48	12.77	5.98	6.57	8.98	12.72	20.41	37.68	11.54	13.06	11.64
HT2CB	23.85	27.56	13.46	9.40	8.03	-17.06	9.84	11.81	16.68	10.35	16.08	35.63

7. ROLE OF WEIGHT OF BUILDINGS OF CITY IN SCI EFFECTS

The overall density of a building depends on the majority of building material (steel, RCC, or masonry), dimension, and design. The density of a building can be obtained using the weights of all the walls, beams, columns, slabs of building, and the live load (Sahar et al., 2015). The live load can vary depending on the different types of occupancies like residential buildings, educational buildings, and industrial or storage buildings. So, the computed effective density for the BBM may have a range depending on type, design, residential, and occupancy. In order to study the role of density or impedance contrast (IC) in the SCI effects on the responses of building and sediment layer, the responses of H2CB, H4CB and H5CB city models were computed using BBM density as 250 kg/m^3, 350 kg/m^3 and 450 kg/m^3 and analysed. The density of the building was increased, keeping in mind that the S-wave velocity for the BBM is unchanged. The responses of the standalone buildings at the selected locations corresponding to the H2SB, H4SB, and H5SB models were also computed using BBM density as 250 kg/m^3, 350 kg/m^3 and 450 kg/m^3. Further, the free field motion in between the buildings was simulated for with and without the city in the model for BBM density as 250 kg/m^3, 350 kg/m^3, and 450 kg/m^3. The time-domain responses of the buildings revealed that the role of density in SCI effects is tremendous in the form of reduction of response at the top of building with an increase of density of the BBM, particularly after the first arrival (result not shown here).

7.1 Transfer function of buildings

The left, middle and right panels of Figure 15a shows a comparison of TF of 15th building of the H2CB city model with the H2SB model using BBM density as 250 kg/m^3, 350 kg/m^3, and 450 kg/m^3, respectively.

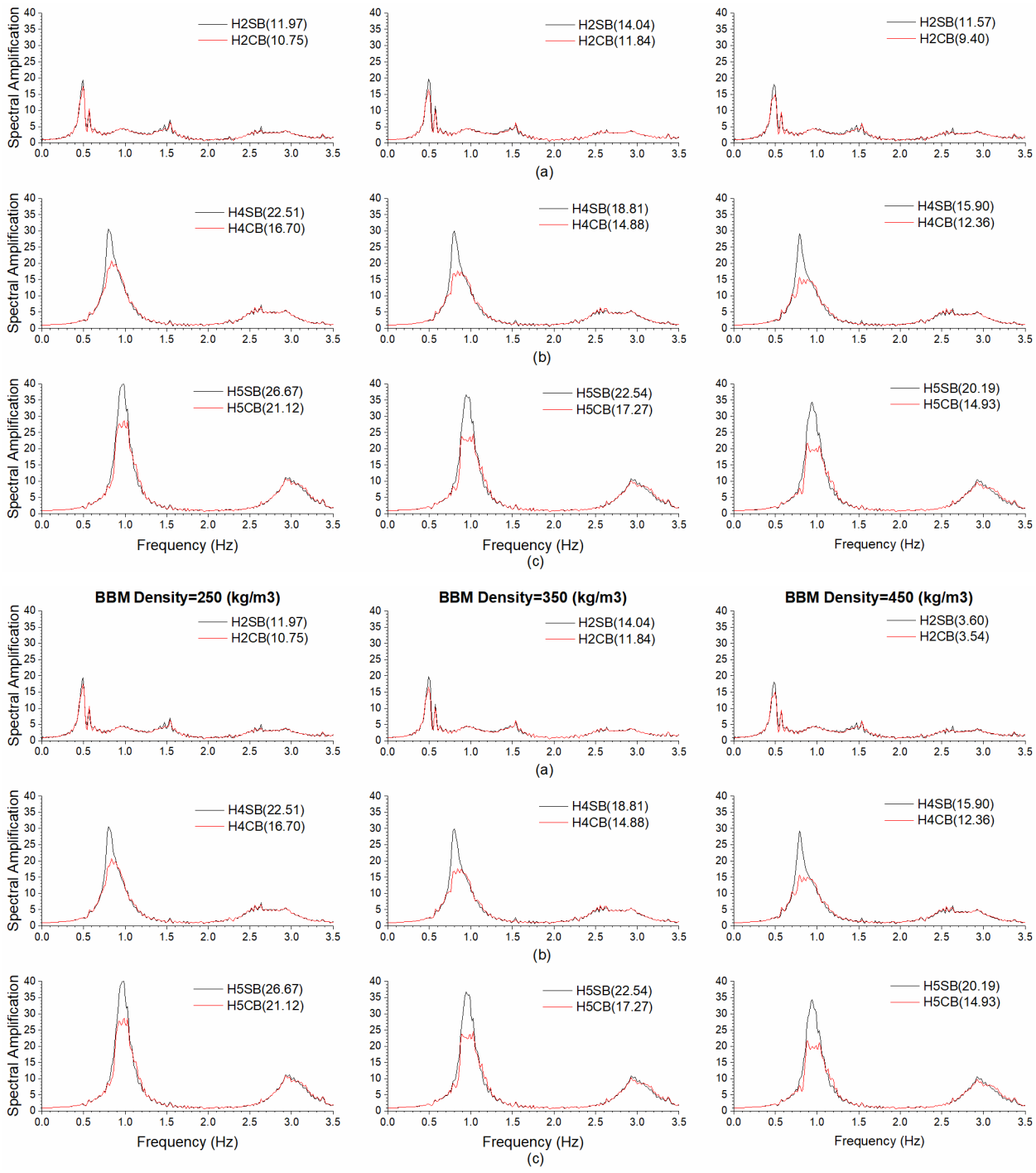

874

875

876 **Fig. 15a-c** A comparison of transfer functions of standalone buildings of H2SB, H4SB and H5SB
877 models with that of corresponding 15th building of cities H2CB, H4CB and H5CB, respectively for
878 different density of the BBM (Note: ATF in the BP of buildings of city and standalone buildings are
879 given in brackets).

880

881 A decrease of TF of both the 15th building of H2CB and standalone building of H2SB with an

increase of density can be inferred due to an increase of impedance of the BBM. However, the percentage reduction of ATF in the BP of 15th building is 10.19%, 15.67% and 18.75% in the case of BBM density as 250 kg/m^3, 350 kg/m^3 and 450 kg/m^3, respectively in the case of H2CB city model (Table 9). The obtained increase of percentage reduction of ATF in the BP of 15th building with an increase in density of the BBM may be due to an increase of coupling between the building and the underlying sediment. An increase of coupling will cause more energy transfer to the building and back to the ground with a phase change of 180^0. Similarly, the left, middle and right panels of Figures 15b&c depict a comparison of TF of 15th building of H4CB and H5CB city models with the standalone buildings of the H4SB and H5SB models for BBM density as 250 kg/m^3, 350 kg/m^3 and 450 kg/m^3, respectively. An increase in the decrease of TF of buildings of H4CB, H4SB, H5CB and H5SB models with an increase of density can also be inferred. An increase of BP with an increase of density of the BBM can also be inferred. An increase of percentage reduction of ATF in the BP of 15th building of the city models with an increase of density of BBM is obtained, irrespective of whether buildings are in resonance or not with the sediment layer (Table 9).

To further enquire the effects of BBM density of buildings, Arias intensity was computed for all the 30 buildings of the H5CB model for the mentioned three density values. The average value of Arias intensity in the case of BBM density as 250 kg/m^3, 350 kg/m^3 and 450 kg/m^3 was found out to be 0.48 m/s, 0.39 m/s and 0.32 m/s with a standard deviation of 0.13, 0.11 and 0.09, respectively. The higher value of Arias intensity at 250 kg/m^3 indicates higher level of shaking of buildings which is also evident from the TF shown in figure 15c. The interesting point to notice is that when we compare the Arias intensity of a particular building of a city (say 15th building) with its standalone counterpart the reduction in the Arias intensity for the city building was found to be 44.83%, 50.23% and 54.28% for the BBM density as 250 kg/m^3, 350 kg/m^3 and 450 kg/m^3, respectively and CD as 44.8%. The obtained larger percentage reduction of ATF in the BP of buildings, Arias intensity and increase of width of BP in the case of higher density reveals that the SCI effects will be more beneficial when the overall density of the buildings is more.

Table 9 Homogeneous city models, ATF in the BP of 15th building of city (ATF-BP) as well as standalone buildings (ATF-SB) and percentage increase (- sign) and decrease (no sign) due to SCI effects for different density of the BBM.

Site-city Models	BBM Density=250 (kg/m^3)			BBM Density=350 (kg/m^3)			BBM Density=450 (kg/m^3)		
	ATF-SB	ATF-BP	% Inc/Dec	ATF-SB	ATF-BP	% Inc/Dec	ATF-SB	ATF-BP	% Inc/Dec
H2CB	11.97	10.75	10.19	14.04	11.84	15.67	11.57	9.40	18.75
H4CB	22.51	16.70	25.81	18.81	14.88	20.89	15.90	12.36	22.26
H5CB	26.67	21.12	20.81	22.54	17.27	23.38	20.19	14.93	26.05

915

916

917 **7.2 Transfer function of sediment layer**

918 The left, middle and right panels of Figure 16a depict a comparison of TF of sediment at an
919 epicentral distance of 17.50 km in the case of presence and absence of H2CB city for BBM density
920 as 250 kg/m^3, 350 kg/m^3 and 450 kg/m^3, respectively. The TF of sediment layer reveals a
921 considerable reduction in the bandwidth of fundamental mode of vibration of the H2-building and
922 there is almost no change in TF at fundamental frequency of sediment layer due to the SCI effects.
923 Further, the fundamental frequency of basin is almost not affected by the SCI effects caused by
924 the H2CB city as well as due to an increase of density of the buildings.

925

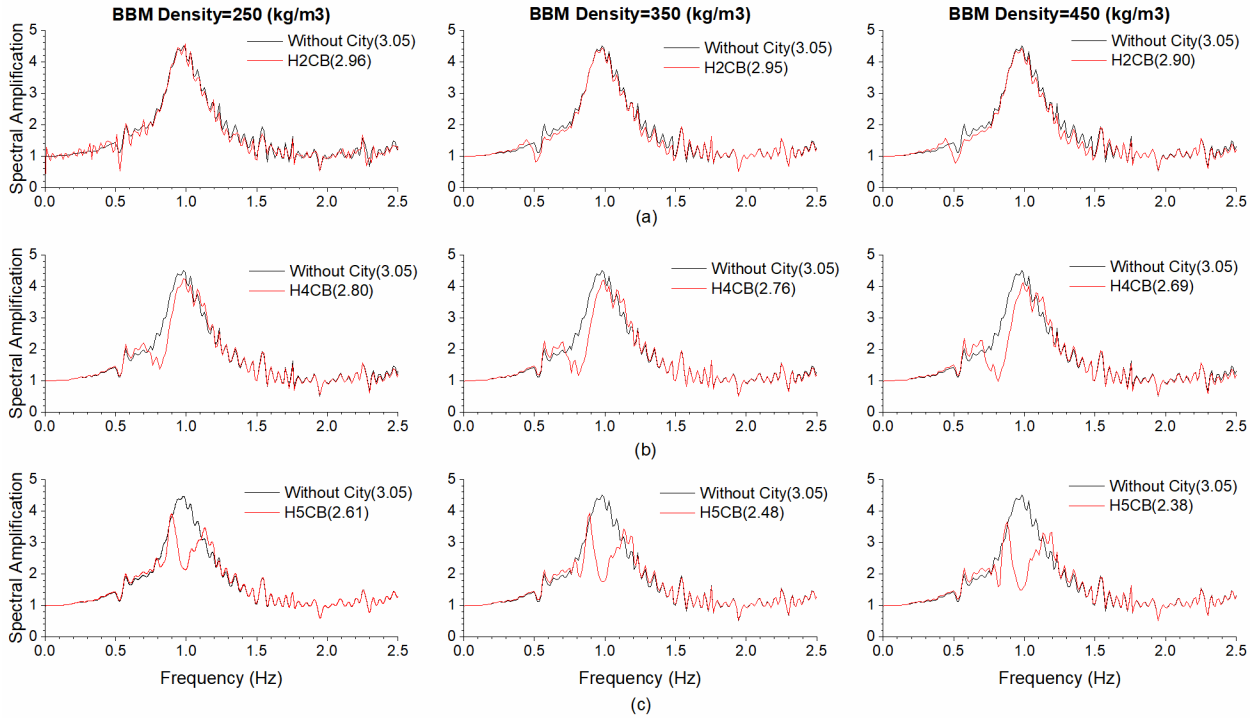

926

927 **Fig. 16a-c** A comparison of transfer function of sediment layer in the presence and absence of
928 H2CB, H4CB and H5CB cities, respectively at an epicentral distance of 17.50 km for different

density of BBM (Note: ATF of sediment layer in absence of city and ATF of the same in a frequency bandwidth (0.75-1.25Hz) in the presence of city are given in brackets).

However, an increase of observed reduction of TF in the bandwidth of fundamental mode of vibration of buildings of H4CB model as well as minor apparent increase of F_0^B of sediment layer can be inferred with an increase of density of the buildings (Figure 16b). Similarly, Figure 16c shows a substantial decrease of TF function of sediment layer in the bandwidth of fundamental mode of buildings of H5CB city model as well as considerable apparent decrease of F_0^B of the sediment layer due to SCI effects. Further, an increase in these effects can be inferred with an increase in the density of the buildings of the H5CB city model. **The obtained percentage reduction of ATF of sediment layer in frequency band 0.75-1.25 Hz in the case of H5CB city model were of the order of 14.43%, 18.69%, and 21.97% for BBM density as 250 kg/m^3, 350 kg/m^3, and 450 kg/m^3, respectively (Table 10).** The obtained decrease of ATF in the bandwidth of F_0^B of the sediment layer when the sediment deposit is under partial or complete resonance condition with the buildings of the city with an increase of density of the BBM reflects the need for consideration of SCI effects in smart city development.

Table 10 Homogeneous city models, ATF of sediment layer in absence of city and ATF in a frequency bandwidth (0.75-1.25Hz) in the presence of city at a distance of 17.45 km as well as percentage increase (- sign) and decrease (no sign) for different density of the BBM.

Site-city Models	BBM Density=250 (kg/m^3)			BBM Density=350 (kg/m^3)			BBM Density=450 (kg/m^3)		
	ATF-B	ATF (0.75-1.25)	% Inc/Dec	ATF-B	ATF (0.75-1.25)	% Inc/Dec	ATF-B	ATF (0.75-1.25)	% Inc/Dec
H2CB	3.05	2.96	2.95	3.05	2.95	3.28	3.05	2.90	4.92
H4CB	3.05	2.80	8.20	3.05	2.76	9.51	3.05	2.69	11.80
H5CB	3.05	2.61	14.43	3.05	2.48	18.69	3.05	2.38	21.97

8. ROLE OF DAMPING OF BUILDINGS IN THE SCI EFFECTS

The damping of a building depends to a great extent on the type of building (steel, RCC, or masonry) as well as dimension and design. Generally, the damping for steel, RCC, and masonry is taken of the order of 2.5%, 5%, and 10%, respectively (IS:456:2000; Clough and Penzien, 2003). To quantify the role of damping of the building in the SCI effects on the responses of buildings and sediment layer, the responses of the H2CB, H4CB and H5CB city models were

computed using BBM damping as 2.5%, 5%, and 10%. The sediment thickness was taken as 84 m. The unrelaxed moduli of the BBM were computed as per the damping taken (Narayan and Kumar, 2013). The response of standalone building at the selected locations corresponding to the H2SB, H4SB, and H5SB models was computed using BBM damping as 2.5%, 5%, and 10%. The free-field motion in between the buildings was also simulated for with and without city in the model for the same BBM damping to quantify the role of BBM damping in the SCI effects on the free field motion. The time-domain responses of the buildings revealed a drastic decrease of amplitude and duration of shaking with an increase of damping of the BBM (result not shown).

8.1 Building response

The left, middle and right panels of Figure 17a-c depicts a comparison of TF of the 15th building of the H2CB, H4CB, and H5CB city models with that of the corresponding standalone building, respectively, using BBM damping as 2.5%, 5%, and 10%. A decrease of TF of the 15th building of H2CB, H4CB, and H5CB city models and corresponding standalone building with an increase of damping can be inferred (Table 11). For example, the percentage reduction of ATF in the BP of building of H2CB model is 22.0%, 15.6% and 10.4% in the case of BBM damping as 2.5%, 5% and 10%, respectively (Table **11). To further enquire the effects of damping on buildings, Arias intensity was computed for all the 30 buildings of the H5CB model for the mentioned three damping values. The average value of Arias intensity for damping 2.5%, 5% and 10% was found to be 0.61 m/s, 0.39 m/s and 0.21 m/s with a standard deviation of 0.18, 0.11 and 0.06, respectively. The higher value of Arias intensity at 2.5% damping indicates higher level of shaking in steel buildings which is also evident from the TF shown in figure 17c. The interesting point to be noticed is that when we compare the Arias intensity of a particular building of the city (15th building) with its standalone counterpart, the reduction in the Arias intensity for the city building was found to be 55.5%, 50.2% and 40.1% for 2.5%, 5% and 10% damping, respectively. So, the inferred larger percentage reduction of ATF in the BP and Arias intensity in the case of low damping reveals that the SCI effects will be more beneficial when a city is developed with steel buildings.**

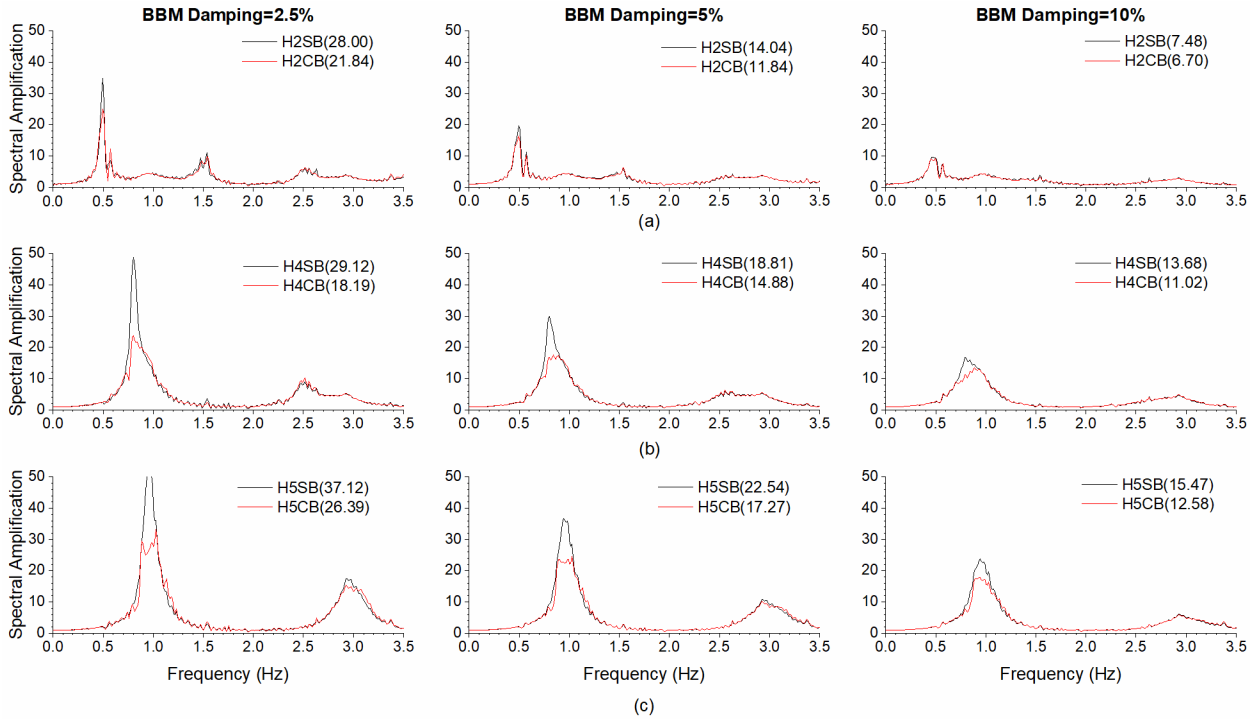

Fig. 17a-c A comparison of transfer functions of standalone buildings of H2SB, H4SB and H5SB models with that of corresponding 15th building of cities H2CB, H4CB and H5CB, respectively for different damping of BBM (Note: ATF in the BP of buildings of city and standalone buildings are given in brackets).

Table 11 ATF in the BP of 15th building of city (ATF-BP) as well as standalone buildings (ATF-SB) and percentage increase (- sign) and decrease (no sign) due to SCI effects for different damping of the BBM.

Site-city Models	BBM Damping=2.5%			BBM Damping=5%			BBM Damping=10%		
	ATF-SB	ATF-BP	% Inc/Dec	ATF-SB	ATF-BP	% Inc/Dec	ATF-SB	ATF-BP	% Inc/Dec
H2CB	28.00	21.84	22.00	14.04	11.84	15.67	7.48	6.70	10.43
H4CB	29.12	18.19	37.53	18.81	14.88	20.89	13.68	11.02	19.44
H5CB	37.12	26.39	28.91	22.54	17.27	23.38	15.47	12.58	18.68

8.2 Response of sediment layer

The left, middle and right panels of Figure 18a depict a comparison of TF of the sediment layer at an epicentral distance of 17.50 km in the presence and absence of H2CB, H4CB, and H5CB city models, respectively for BBM damping as 2.5%, 5%, and 10%. Although there is a considerable percentage reduction of TF in the bandwidth of the fundamental mode of vibration of the buildings,

but, there is almost no change in the fundamental frequency of sediment layer and corresponding TF due to the SCI effects in the case of H2CB city. A decrease of reduction of TF as well as a minor apparent increase of F_0^B of the sediment layer can be inferred in the case of H4CB city model with an increase of damping of the buildings (Figure 18b). Similarly, Figure 18c shows a substantial decrease of TF function and considerable apparent decrease of F_0^B of the sediment layer due to SCI effects in the case of H5CB city model with increase of damping. Further, a decrease of SCI effects can be inferred with an increase in the damping of the buildings. **The obtained percentage reduction of TF of the sediment layer in the frequency bandwidth of 0.75 – 1.25 Hz in H5CB city model were of the order of 19.34%, 18.69%, and 9.51% in the case of BBM damping as 2.5%, 5%, and 10%, respectively (Table 12).** This can be because buildings with higher damping value radiate lesser motion back to ground which causes the reduction in TF of the sediment layer.

Table 12 Homogeneous city models, ATF-B of sediment layer in absence of city and ATF in a frequency bandwidth (0.75-1.25Hz) in the presence of city at a distance of 17.45 km as well as percentage increase (- sign) and decrease (no sign) for different density of the BBM.

Site-city Models	BBM Damping=2.5%			BBM Damping=5%			BBM Damping=10%		
	ATF-B	ATF (0.75-1.25)	% Inc/Dec	ATF-B	ATF(0.75-1.25)	% Inc/Dec	ATF-B	ATF(0.75-1.25)	% Inc/Dec
H2CB	3.05	2.92	4.26	3.05	2.95	3.28	3.05	2.98	2.29
H4CB	3.05	2.68	12.13	3.05	2.76	9.51	3.05	2.80	8.19
H5CB	3.05	2.46	19.34	3.05	2.48	18.69	3.05	2.76	9.51

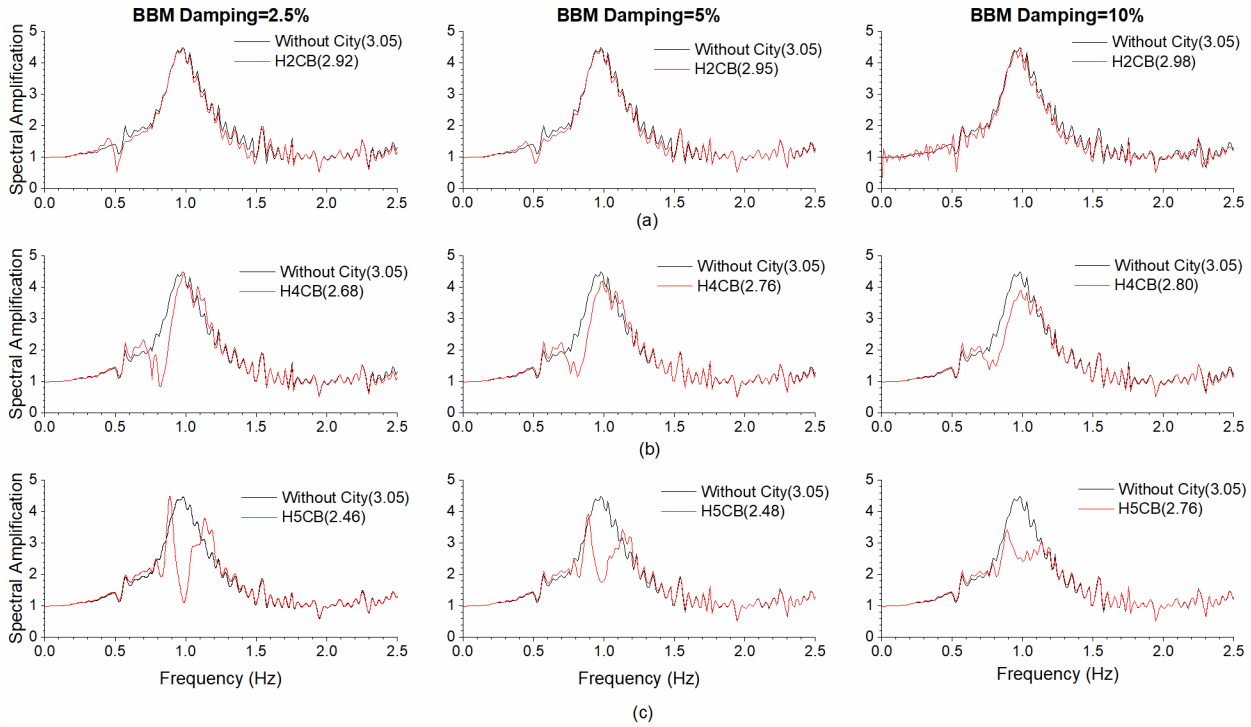

Fig. 18a-c A comparison of transfer function of sediment layer in the presence and absence of H2CB, H4CB and H5CB cities, respectively at an epicentral distance of 17.50 km for different damping of BBM (Note: ATF of sediment layer in absence of city and ATF of the same in a frequency bandwidth (0.75-1.25Hz) in the presence of city are given in brackets).

9. DISCUSSION AND CONCLUSIONS

An analysis of the computed pseudo-spectral acceleration (PSA) using simulated SGM and NGA-West2 empirical relations reveals that the pseudodynamic rupture models (PRM1 & PRM2) over-predict SGM due to use of constant slip, rupture velocity, and rise-time (Graves and Pitarka, 2016). A considerable reduction of coherency effect was not observed even after applying randomization in slip and rise-time of the STF in the case of PRM3 model. However, a considerable reduction of coherency effect was obtained by using the randomization of slip, rise-time, and rupture arrival time in the case of PRM4 model. **The desired reduction of coherency effects on high frequency and a good match of the computed PSA with NGA-West2 was obtained when randomization in the slip, rise-time, rupture arrival time, and rake was done along with the incorporation of a damage zone around the rupture plane in the case of PRM5 model (Liu et al., 2010; Schmedes et al. 2010; 2013; Graves and Pitarka, 2010; 2016). It is concluded that ground motion with a frequency bandwidth of earthquake engineering**

interest can be predicted using PRM5 pseudodynamic rupture model wherein the spectra of radiated seismic energy from different point sources match with the Brune's model (Graves and Pitarka, 2010; 2016).

Some of the various generalized conclusions drawn from the past SCI studies using simple plane wave-front with a single wavelet does not hold good while using realistic earthquake loading. For example, Kham et al. (2006), Semblat et al. (2008), Sahar et al. (2015) and Kumar and Narayan, (2018) reported the splitting of the bandwidth of the fundamental mode frequency of the building due to substantial reduction of TF at F_0^{SR}. The results of the present SCI study using realistic earthquake loading reveals a reduction and flattening of TF for a band of frequency (BP) within the bandwidth of the fundamental mode of vibration of building (Table 5). The maximum SCI effects on a building was highly dependent on the building type, city and basin heterogeneity and not on its location at centre of city, in contrast to the general perception that it is maximum at the centre of city (Kham et al., 2006; Semblat et al., 2008; Sahar et al., 2015).

An interesting inference is made based on the analysis of simulated results of H1CB-H5CB and HT2CB city models as well as two more homogeneous city models with the height of buildings as 15 m and 21 m. When the F_0^{SB} of buildings of the cities (BBM with height 15m, 18m and 21m) are greater than 1.4 times the F_0^B of the sediment layer, there is detrimental SCI effect on the buildings. For example, the range of percentage increase (-ve sign) of ATF in the BP of building is -7.01% to -11.86%, -9.19% to -18.45% and -3.32% to -11.37%, in the cities with height of buildings as 15 m, 18 m and 21 m, respectively. **Although, we feel it needs further detailed study.** The computed percentage reduction of ATF in a frequency band (like BP) instead at a single frequency reveals that the SCI is always beneficial to both the buildings and free field motion, except the case when F_0^{SR} of building is around 1.4 times larger than F_0^B, wherein building response is detrimental. This finding also do not hold good (Kham et al., 2006; Semblat et al., 2008).

The analysis of responses of buildings of homogeneous city situated in a heterogeneous basin and heterogeneous cities situated on the sediment layer with same city density (44.8%) revealed that the percentage reduction of ATF in the BP of buildings is highly dependent on its location, city heterogeneity, and the heterogeneity of the basin. In the case of B1-H5CB to B4-H5CB heterogeneous basin models (some of the buildings are out of resonance with underlying basin),

the obtained range of percentage reduction of ATF in the BP of buildings is 17.35%-41.64% (Table 7). On the other hand, in case of heterogeneous city (HT1CB & HT2CB), the range of percentage reduction of ATF in the BP of buildings is 8.98% to 35.63% (Table 8) and an increase of ATF of the order of –17.04%. Another interesting result is the obtained percentage reduction of ATF in the case of 7th building (in double resonance condition) of the HT1CB and HT2CB city models, as 12.77% and 13.46%, respectively is lesser than that in the case of buildings of the H5CB city (23.38% - 38.66%) (Table 5). So, the obtained lesser beneficial SCI effect as compared to homogeneous city along with detrimental SCI effect in the case of heterogeneous city models, reveals that the development of a smart homogeneous city either in homogeneous or heterogeneous basin is the better option as compared to the heterogeneous city. **The limitation of this study is the computation of 2D linear visco-elastic out of plane response which may not be applicable for the bending beam model. There is need of computation of 3D non-linear viscoelastic response of a site-city model with realistic earthquake loading, wherein in-plane, out-of-plane and vertical motions will act simultaneously, for better quantification of SCI effects.**

The increase of density of building for a fixed value of S-wave velocity is causing the increase of impedance of building, which in turn reduces the impedance contrast and finally an increase of coupling between the building and basin. The increase of coupling has caused an increase of energy transfer of incident earthquake waves to the BBM, and an increase of the amplitude of seismic waves radiated back to the sediment, which in turn increases the SCI effects on the responses of buildings and sediment. For example, the obtained percentage reduction of ATF in the BP of buildings and Arias intensity are largest in the case of highest BBM density. Apart from this, an overall increase in density of a building for a fixed dimension also implies an increase in the weight of the building. Building with more weight will consequently have more counteracting force and moment against the horizontal earthquake load. The obtained largest percentage reduction of ATF in the BP and Arias intensity in the case of low damping of buildings reveals that the SCI effects will be beneficial for urban planning when a city is developed with steel buildings. Also from an earthquake engineering point of view, the steel buildings are more ductile as compared to RCC and masonry buildings which makes them good at resisting forces which are dynamic in nature such as earthquake or wind loads. In order to develop an economical and smart city, it is recommended that the city should be homogeneous in nature and F_0^{SR} of buildings should be less than around 1.4 times the F_0^B of the underlying sediment deposit and buildings should preferably be a steel one.

ACKNOWLEDGEMENTS

The authors are thankful to both the learned reviewers which led the tremendous improvement in the quality of the manuscript. Authors are also thankful to Indian Institute of Technology Roorkee, India for providing computational facility.

References

1. Aki, K., and P. G. Richards (1980). Quantitative Seismology: Theory and Methods, W. H. Freeman and Company, San Francisco, California.
2. Aldaikh, H., Alexander, N.A., Ibraim, E. and Knappett, J., 2016. Shake table testing of the dynamic interaction between two and three adjacent buildings (SSSI). Soil Dynamics and Earthquake Engineering, 89, pp.219-232.
3. Bard PY, Chazelas JL, Guéguen P, Kham M, Semblat JF.,2005. Site-city Interaction. Chapter 5 of the book "Assessing and Managing Earthquake Risk (Geo-Scientific and Engineering Knowledge for Earthquake Risk Mitigation: Developments, Tools and Techniques)", Oliveira CS, Roca A, Goula X Editors, SPRINGER (new book series on Geotechnical, Geological and Earthquake Engineering). Hardcover ISBN 1-4020-3524-1:91-114.
4. Ben-Zion, Y., Vernon, F.L., Ozakin, Y., Zigone, D., Ross, Z.E., Meng, H., White, M., Reyes, J., Hollis, D. and Barklage, M., 2015. Basic data features and results from a spatially dense seismic array on the San Jacinto fault zone. Geophysical Journal International, 202(1), pp.370-380.
5. Boore, D.M., 1983. Stochastic simulation of high-frequency ground motions based on seismological models of the radiated spectra. Bulletin of the Seismological Society of America, 73(6A), pp.1865-1894.
6. Boore, D.M., Stewart, J.P., Seyhan, E. and Atkinson, G.M., 2014. NGA-West2 equations for predicting PGA, PGV, and 5% damped PSA for shallow crustal earthquakes. Earthquake Spectra, 30(3), pp.1057-1085.
7. Boore, D.M., Stewart, J.P., Seyhan, E. and Atkinson, G.M., 2014. NGA-West2 equations for predicting PGA, PGV, and 5% damped PSA for shallow crustal earthquakes. Earthquake Spectra, 30(3), pp.1057-1085.
8. Boutin C., Roussillon, P., 2004. Assessment of the urbanization effect on seismic response. Bulletin of Seismological Society of America, 94 (1), pp. 251-268.
9. Boutin C., Roussillon P., 2006. Wave propagation in presence of oscillators on the free surface. International Journal of Engineering Science, 4, pp.180-204.
10. Campbell, K.W. and Bozorgnia, Y., 2014. NGA-West2 ground motion model for the average horizontal components of PGA, PGV, and 5% damped linear acceleration response spectra. Earthquake Spectra, 30(3), pp.1087-1115.

11. Chávez-García, F.J. and Cárdenas, M., 2002. The contribution of the built environment to the 'free-field'ground motion in Mexico City. Soil Dynamics and Earthquake Engineering, 22(9-12), pp.773-780.
12. Chiou, B.S.J. and Youngs, R.R., 2014. Update of the Chiou and Youngs NGA model for the average horizontal component of peak ground motion and response spectra. Earthquake Spectra, 30(3), pp.1117-1153.
13. Clough, R.W. and Penzien, J., (2003), Dynamics of structures. Berkeley. CA: 1105 Computers and Structures, Inc.
14. Clouteau, D., and D. Aubry (2001). Modification of ground motion in dense urban areas, J. Comput. Acoust. 6, 1659–1675.
15. Clouteau, D., O. Ishizawa, and N. Mezher (2002). Seismic wave propagation in a random city, in 7th National Conf. on Earthquake Eng., Boston.
16. Cochran, E. S., Y.-G. Li, P. M. Shearer, S. Barbot, Y. Fialko, and J. E. Vidale (2009). Seismic and geodetic evidence for extensive, long-lived fault damage zones, Geology 37, no. 4, 315–318, doi: 10.1130/G25306A.1.
17. Gallipoli, M.R., Mucciarelli, M., Castro, R.R., Monachesi, G. and Contri, P., 2004. Structure, soil–structure response and effects of damage based on observations of horizontal-to-vertical spectral ratios of microtremors. Soil Dynamics and Earthquake Engineering, 24(6), pp.487-495.
18. Graves, R. and Pitarka, A., 2015. Refinements to the Graves and Pitarka (2010) broadband ground-motion simulation method. Seismological Research Letters, 86(1), pp.75-80.
19. Graves, R. and Pitarka, A., 2016. Kinematic ground-motion simulations on rough faults including effects of 3D stochastic velocity perturbations. Bulletin of the Seismological Society of America, 106(5), pp.2136-2153.
20. Graves, R.W. and Pitarka, A., 2010. Broadband ground-motion simulation using a hybrid approach. Bulletin of the Seismological Society of America, 100(5A), pp.2095-2123.
21. Guatteri, M., Mai, P.M. and Beroza, G.C., 2004. A pseudo-dynamic approximation to dynamic rupture models for strong ground motion prediction. Bulletin of the Seismological Society of America, 94(6), pp.2051-2063.
22. Gueguen, P. and Bard, P.Y., 2005. Soil-structure and soil-structure-soil interaction: experimental evidence at the Volvi test site. Journal of Earthquake Engineering, 9(05), pp.657-693.

23. Guéguen, P., Bard, P.Y. and Chávez-García, F.J., 2002. Site-city seismic interaction in mexico city–like environments: an analytical study. Bulletin of the Seismological Society of America, 92(2), pp.794-811.
24. Guéguen, P., Diego Mercerat, E. and Alarcon, F., (2019), Parametric Study on the Interpretation of Wave Velocity Obtained by Seismic Interferometry in Beam-Like Buildings. Bulletin of the Seismological Society of America, 109(5), pp.1829-1842.
25. Guidotti, R., I. Mazzieri, M. Stupazzini and P. Dagna (2012). 3D numerical simulation of the Site-City Interaction during the 22 February 2011 MW 6.2 Christchurch earthquake. Proceedings of the 15th World Conference of Earthquake Engineering, Lisboa, 2012 (Paper # 2290, 10 pages)
26. Hartzell, S., 1989. Comparison of seismic waveform inversion results for the rupture history of a finite fault: Application to the 1986 North Palm Springs, California, earthquake. Journal of Geophysical Research: Solid Earth, 94(B6), pp.7515-7534.
27. Hartzell, S., Guatteri, M., Mai, P.M., Liu, P.C. and Fisk, M., 2005. Calculation of broadband time histories of ground motion, Part II: Kinematic and dynamic modeling using theoretical Green's functions and comparison with the 1994 Northridge earthquake. Bulletin of the Seismological Society of America, 95(2), pp.614-645.
28. Hartzell, S., Harmsen, S., Frankel, A. and Larsen, S., 1999. Calculation of broadband time histories of ground motion: Comparison of methods and validation using strong-ground motion from the 1994 Northridge earthquake. Bulletin of the Seismological Society of America, 89(6), pp.1484-1504.
29. Hartzell, S.H. and Heaton, T.H., 1983. Inversion of strong ground motion and teleseismic waveform data for the fault rupture history of the 1979 Imperial Valley, California, earthquake. Bulletin of the Seismological Society of America, 73(6A), pp.1553-1583.
30. Hartzell, S.H., 1978. Earthquake aftershocks as Green's functions. Geophysical Research Letters, 5(1), pp.1-4.
31. Idriss, I.M., 2014. An NGA-West2 empirical model for estimating the horizontal spectral values generated by shallow crustal earthquakes. Earthquake Spectra, 30(3), pp.1155-1177.
32. Irikura, K. (1978). Semi-empirical estimation of strong ground motions during large earthquakes, Bull. Disast. Prev. Res. Inst., Kyoto Univ. 33, 63–104.
33. IS: 1893 (Part 1), (2016), Criteria for Earthquake Resistant Design of Structures. Part 1: General Provision and Buildings, Bureau of Indian Standards, New Delhi.

34. IS: 456, (2000), Plain and Reinforced Concrete-Code of Practice, Bureau of Indian Standards, New Delhi.

35. Isbiliroglu, Y., Taborda, R. and Bielak, J., 2015. Coupled soil-structure interaction effects of building clusters during earthquakes. Earthquake Spectra, 31(1), pp.463-500.

36. Jennings, P.C., 1970. Distant motions from a building vibration test. Bulletin of the Seismological Society of America, 60(6), pp.2037-2043.

37. Kham, M., Semblat, J.F., Bard, P.Y. and Dangla, P., 2006. Seismic site–city interaction: main governing phenomena through simplified numerical models. Bulletin of the Seismological Society of America, 96(5), pp.1934-1951.

38. Kramer, S.L., 1996. Geotechnical earthquake engineering. Pearson Education India.

39. Kumar, N. and Narayan, J.P., 2018. Quantification of site–city interaction effects on the response of structure under double resonance condition. Geophysical Journal International, 212(1), pp.422-441.

40. Kumar, N. and Narayan, J.P., 2019. Effects of site–city interaction and polarization of the incident S-wave on the transfer function and fundamental frequency of structures. Natural Hazards, 97(2), pp.747-774.

41. Leonard, M., 2010. Earthquake fault scaling: Self-consistent relating of rupture length, width, average displacement, and moment release. Bulletin of the Seismological Society of America, 100(5A), pp.1971-1988.

42. Liu, P., Archuleta, R.J. and Hartzell, S.H., 2006. Prediction of broadband ground-motion time histories: Hybrid low/high-frequency method with correlated random source parameters. Bulletin of the Seismological Society of America, 96(6), pp.2118-2130.

43. Lu, X., Tian, Y., Wang, G., & Huang, D. (2018). A numerical coupling scheme for nonlinear time history analysis of buildings on a regional scale considering site-city interaction effects. Earthquake Engineering & Structural Dynamics, 47(13), 2708-2725.

44. Mai, P.M. and Beroza, G.C., 2002. A spatial random field model to characterize complexity in earthquake slip. Journal of Geophysical Research: Solid Earth, 107(B11), pp.ESE-10.

45. Mai, P.M., Galis, M., Thingbaijam, K.K., Vyas, J.C. and Dunham, E.M., 2018. Accounting for fault roughness in pseudo-dynamic ground-motion simulations. In Best Practices in Physics-based Fault Rupture Models for Seismic Hazard Assessment of Nuclear Installations (pp. 95-126). Birkhäuser, Cham.

46. Mena, B., Dalguer, L.A. and Mai, P.M., 2012. Pseudodynamic source characterization for strike-slip faulting including stress heterogeneity and super-shear ruptures. Bulletin of the Seismological Society of America, 102(4), pp.1654-1680.
47. Merritt, R.G. and Housner, G.W., 1954. Effect of foundation compliance on earthquake stresses in multistory buildings. Bulletin of the Seismological Society of America, 44(4), pp.551-569.
48. Michel, C. and Gueguen, P., (2018), Interpretation of the velocity measured in buildings by seismic interferometry based on Timoshenko beam theory under weak and moderate motion. Soil Dynamics and Earthquake Engineering, 104, pp.131-142.
49. Narayan, J.P. and Kumar, V., 2013. A fourth-order accurate finite-difference program for the simulation of SH-wave propagation in heterogeneous viscoelastic medium. Geofizika, 30(2), pp.173-189.
50. Pulido, N. and Dalguer, L.A., 2009. Estimation of the High-Frequency Radiation of the 2000 Tottori (Japan) Earthquake Based on a Dynamic Model of Fault Rupture: Application to the Strong Ground Motion Simulation Estimation of the High-Frequency Radiation of the 2000 Tottori Earthquake. Bulletin of the Seismological Society of America, 99(4), pp.2305-2322.
51. Sahar, D., Narayan, J.P. and Kumar, N., 2015. Study of role of basin shape in the site–city interaction effects on the ground motion characteristics. Natural Hazards, 75(2), pp.1167-1186.
52. Schmedes, J., Archuleta, R.J. and Lavallée, D., 2010. Correlation of earthquake source parameters inferred from dynamic rupture simulations. Journal of Geophysical Research: Solid Earth, 115(B3).
53. Schmedes, J., Archuleta, R.J. and Lavallée, D., 2013. A kinematic rupture model generator incorporating spatial interdependency of earthquake source parameters. Geophysical Journal International, 192(3), pp.1116-1131.
54. Schwan, L., Boutin, C., Padrón, L.A., Dietz, M.S., Bard, P.Y. and Taylor, C., 2016. Site-city interaction: theoretical, numerical and experimental crossed-analysis. Geophysical Journal International, 205(2), pp.1006-1031.
55. Semblat, J.F., Kham, M. and Bard, P.Y., 2008. Seismic-wave propagation in alluvial basins and influence of site-city interaction. Bulletin of the Seismological Society of America, 98(6), pp.2665-2678.
56. Shi, Z., and S. M. Day (2013). Rupture dynamics and ground motion from 3- D rough-fault simulations, J. Geophys. Res. 118, no. 3, 1122–1141, doi: 10.1002/jgrb.50094.

57. Snieder, R. and Safak, E., (2006), Extracting the building response using seismic interferometry: Theory and application to the Millikan Library in Pasadena, California. Bulletin of the Seismological Society of America, 96(2), pp.586-598.
58. Somerville, P., Irikura, K., Graves, R., Sawada, S., Wald, D., Abrahamson, N., Iwasaki, Y., Kagawa, T., Smith, N. and Kowada, A., 1999. Characterizing crustal earthquake slip models for the prediction of strong ground motion. Seismological Research Letters, 70(1), pp.59-80.
59. Taborda, R. & Bielak, J. (2011a). Full 3D integration of site-city effects in regional scale earthquake simulations, in Proceedings of 8th International Conference on Structural Dynamics, Eurodyn, pp. 511–518, eds De Roeck, G., Degrande, G., Lombaert, G. & M¨uller, G., Leuven, Belgium.
60. Taborda, R., & Bielak, J. (2011b). Large-scale earthquake simulation: computational seismology and complex engineering systems. Computing in Science & Engineering, 13(4), 14-27.
61. Varone, C., Lenti, L., Martino, S., & Semblat, J. F. (2020). Spatial variability of the urban ground motion in a highly heterogeneous site-city configuration. Bulletin of Earthquake Engineering, 1-19, October.
62. Vidale, J., 1988. Finite-difference calculation of travel times. Bulletin of the Seismological Society of America, 78(6), pp.2062-2076.
63. Wells, D.L. and Coppersmith, K.J., 1994. New empirical relationships among magnitude, rupture length, rupture width, rupture area, and surface displacement. Bulletin of the seismological Society of America, 84(4), pp.974-1002.
64. Wirgin A, Bard PY., 1996. Effects of building on the duration and amplitude of ground motion in Mexico City. Bull Seism Soc Am 86: 914–920.
65. Wong HL, Trifunac MD., 1975. Two dimensional antiplane building-soil-building interaction for two or more buildings and for incident plane SH waves. Bull Seism Soc Am 65:1863–1885.
66. Zeng, Y., Anderson, J.G. and Yu, G., 1994. A composite source model for computing realistic synthetic strong ground motions. Geophysical Research Letters, 21(8), pp.725-728.

Figures

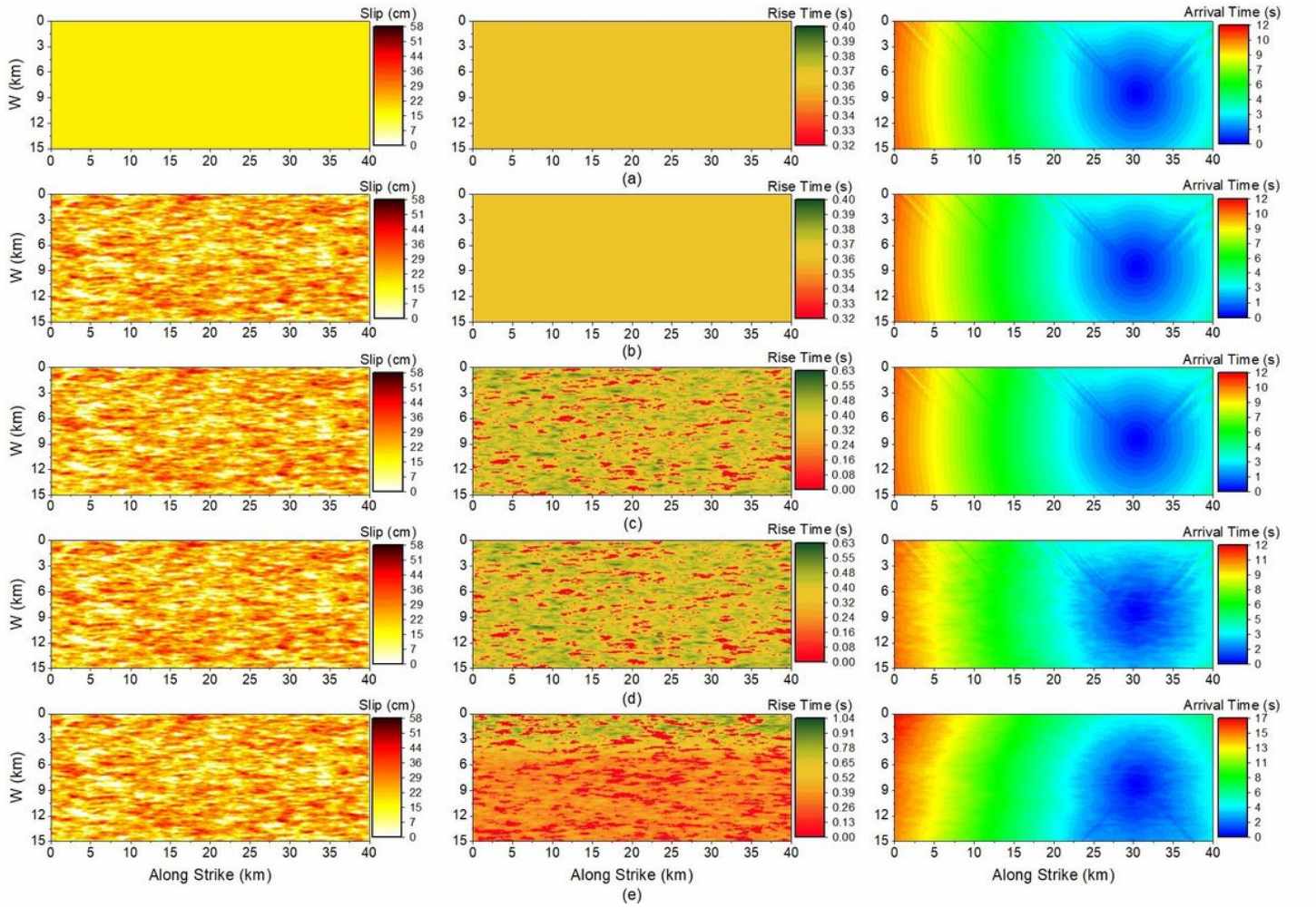

Figure 1

a-e Spatial variation of slip (left panel), rise-time (middle panel) and rupture arrival time (right panel) on the rupture plane of the considered PRM1-PRM5 pseudo-dynamic rupture models, respectively.

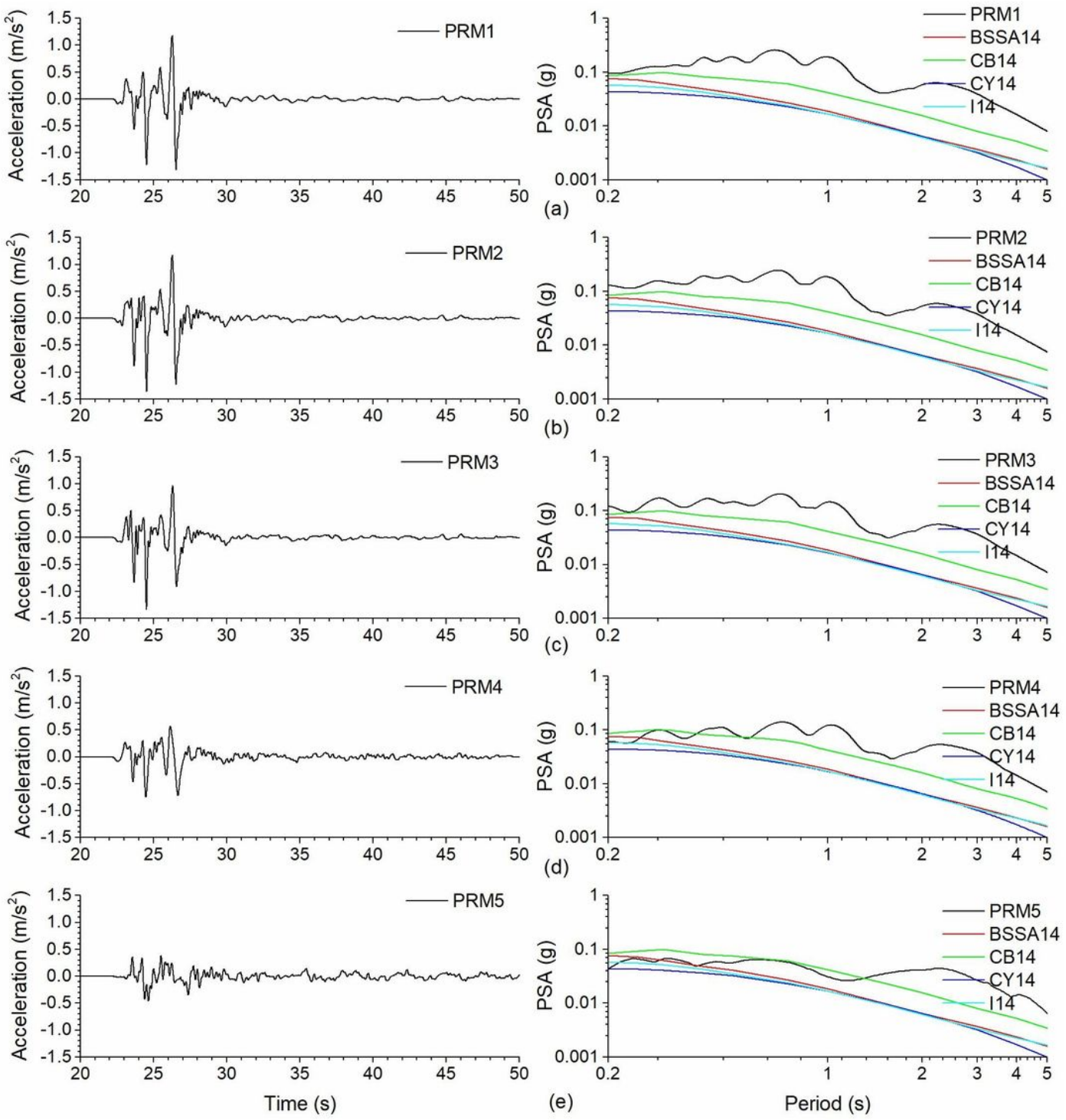

Figure 2

a-e Simulated ground motion acceleration at the free surface (left panels) and a comparison of computed PSA using simulated ground motion with the same calculated using NGA-West2 empirical relations in the case of PRM1-PRM5 pseudo-dynamic rupture models, respectively (right panels).

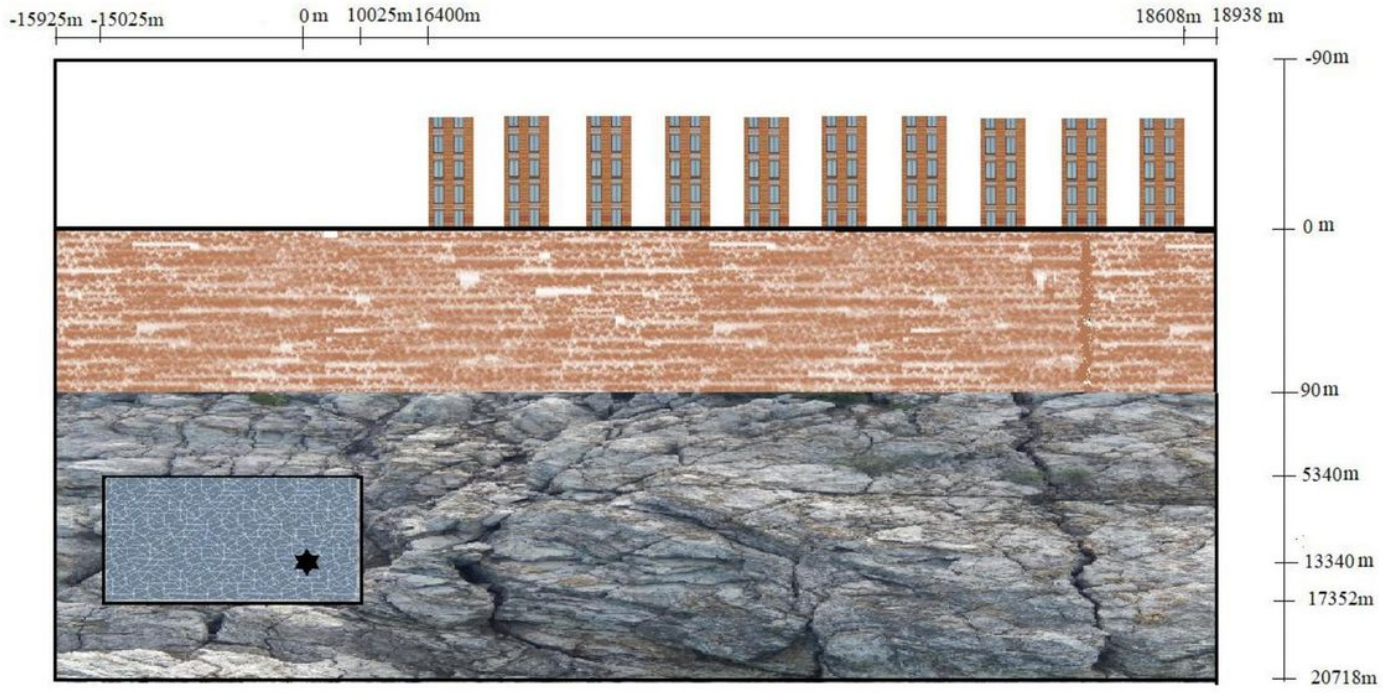

Figure 3

A vertically staggered site-city model along with the earthquake rupture and epicenter of a postulated earthquake of moment magnitude 5.4 (Note: all the horizontal distances are measured with respect to the epicenter and all the vertical distances are measured with respect to the free surface)

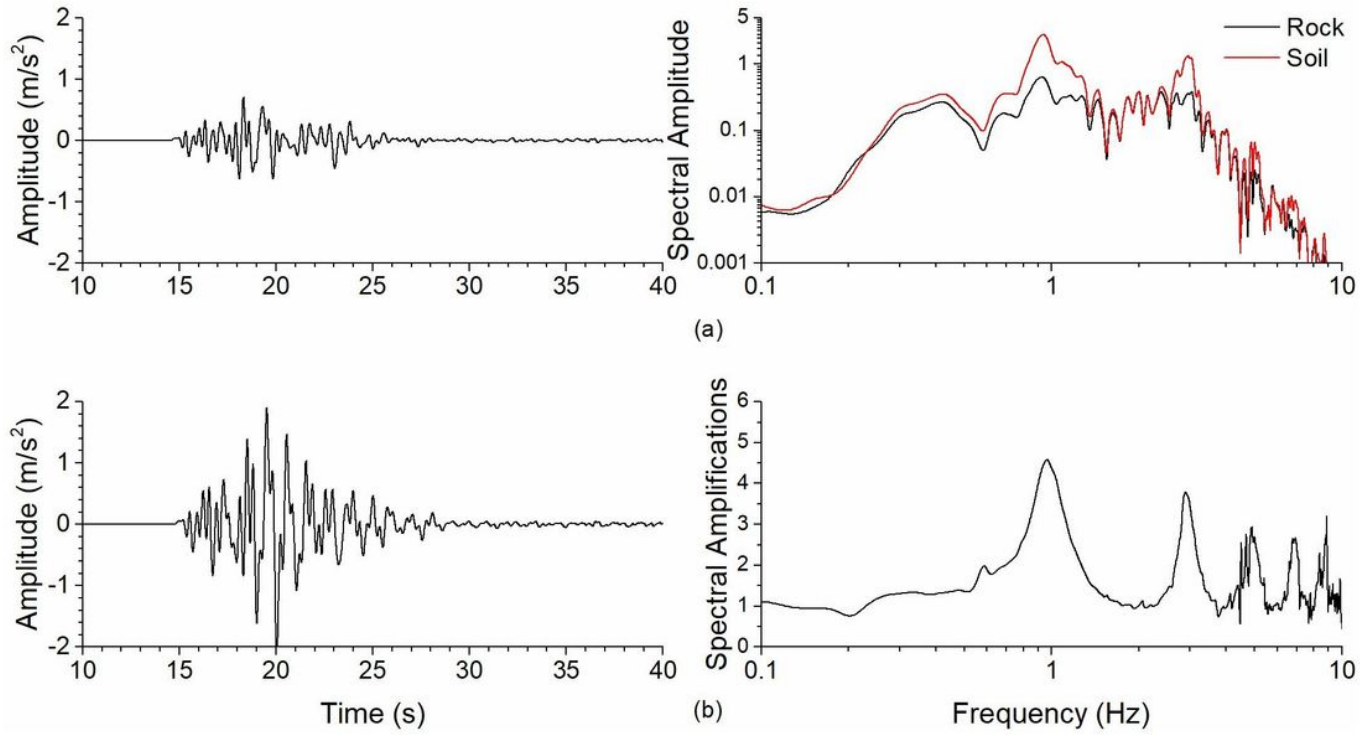

Figure 4

Free surface ground acceleration recorded on the out-cropping rock and sediment at an epicentral distance of 17.50 km (left panels of Fig. 4a&b); a comparison of spectra of responses of out-cropping rock and sediment (right panel of Fig. 4a) and spectral amplifications (transfer function) caaused by the sediment layer (right panel of Fig. 4b).

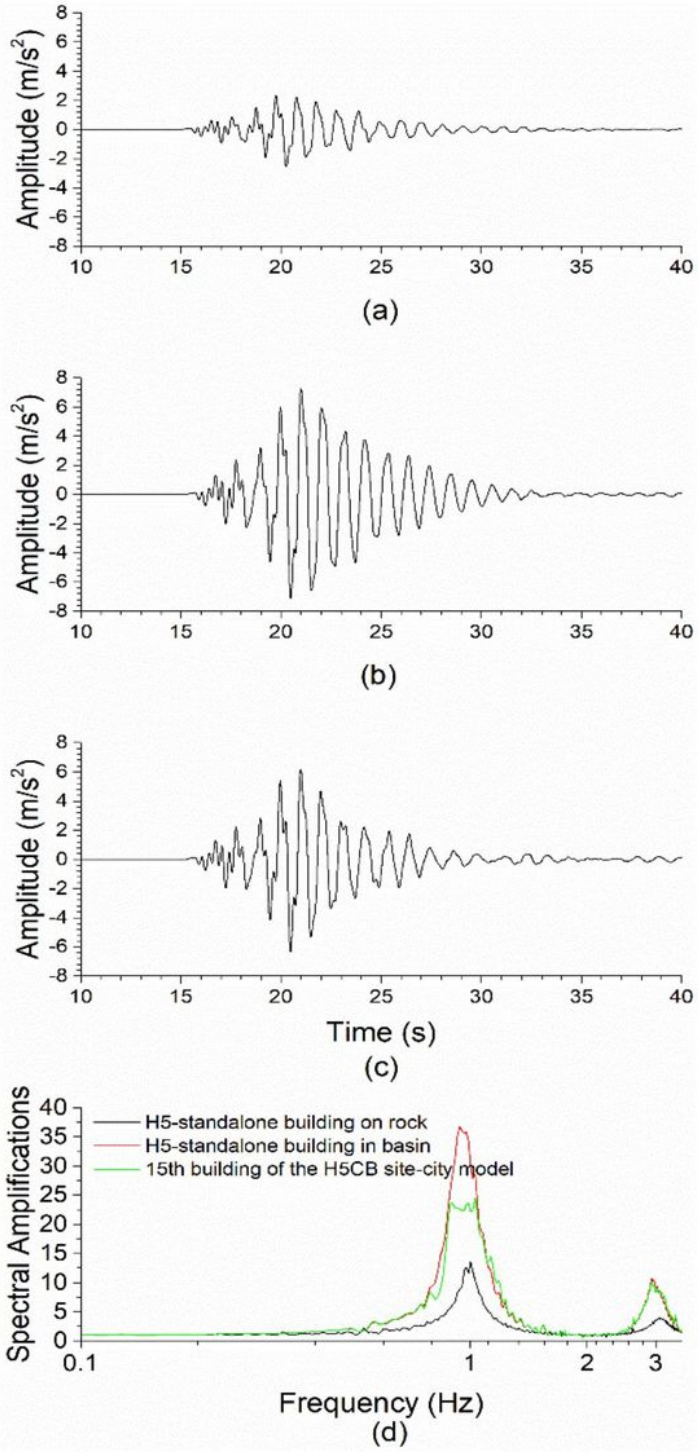

Figure 5

a-c The responses H5-standalone building on rock, H5-standalone building on horizontal sediment layer (H5SB model) and 15th building of the H5CB site-city model, respectively (thickness of sediment is 84 m in both the H5SB and H5CB models); (5d) Comparison of TFs of H5-standalone building on rock, H5-standalone building on horizontal sediment layer (H5SB model) and 15th building of the H5CB site-city model.

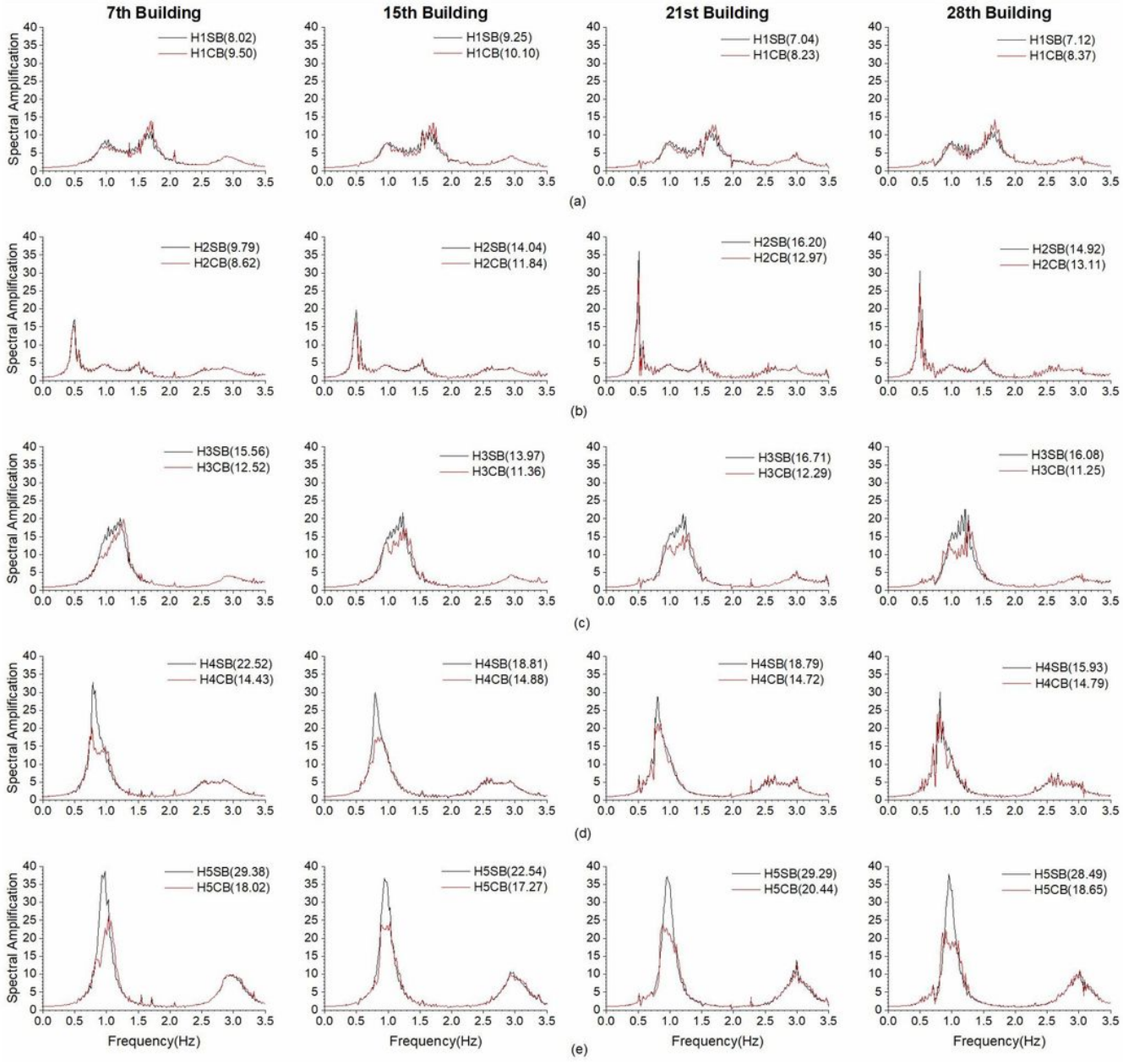

Figure 6

a-e A comparison of transfer functions of standalone buildings of H1SB-H5SB models with that of the corresponding building of cities H1CB-H5CB at different locations (Note: ATF in the BP of buildings of city and standalone buildings are given in brackets).

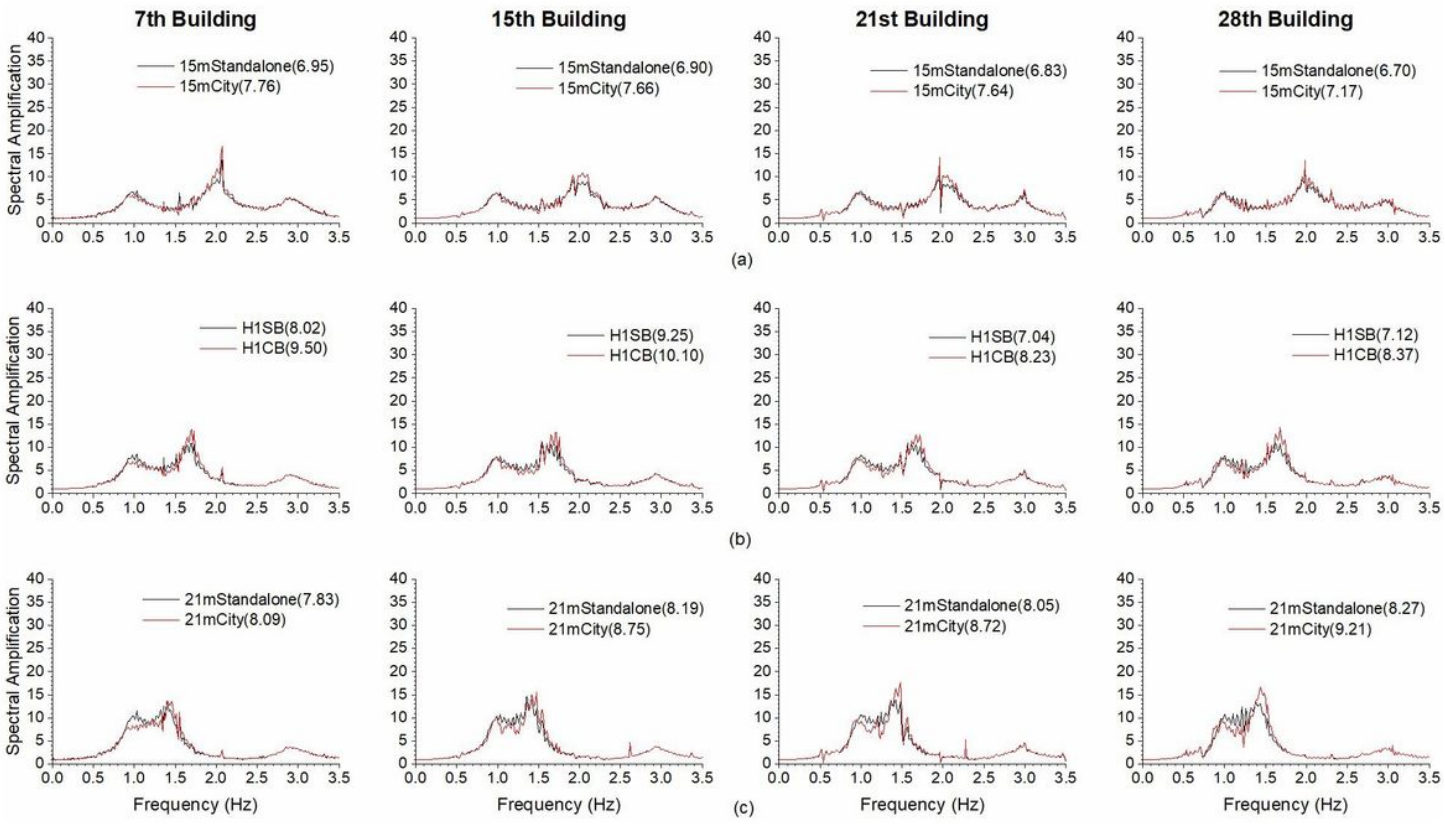

Figure 7

a-c A comparison of transfer functions of buildings of 15m,18m and 21m homogeneous city models, respectively with the standalone building at the corresponding location (Note: ATF in the BP of buildings of city and standalone buildings are given in brackets).

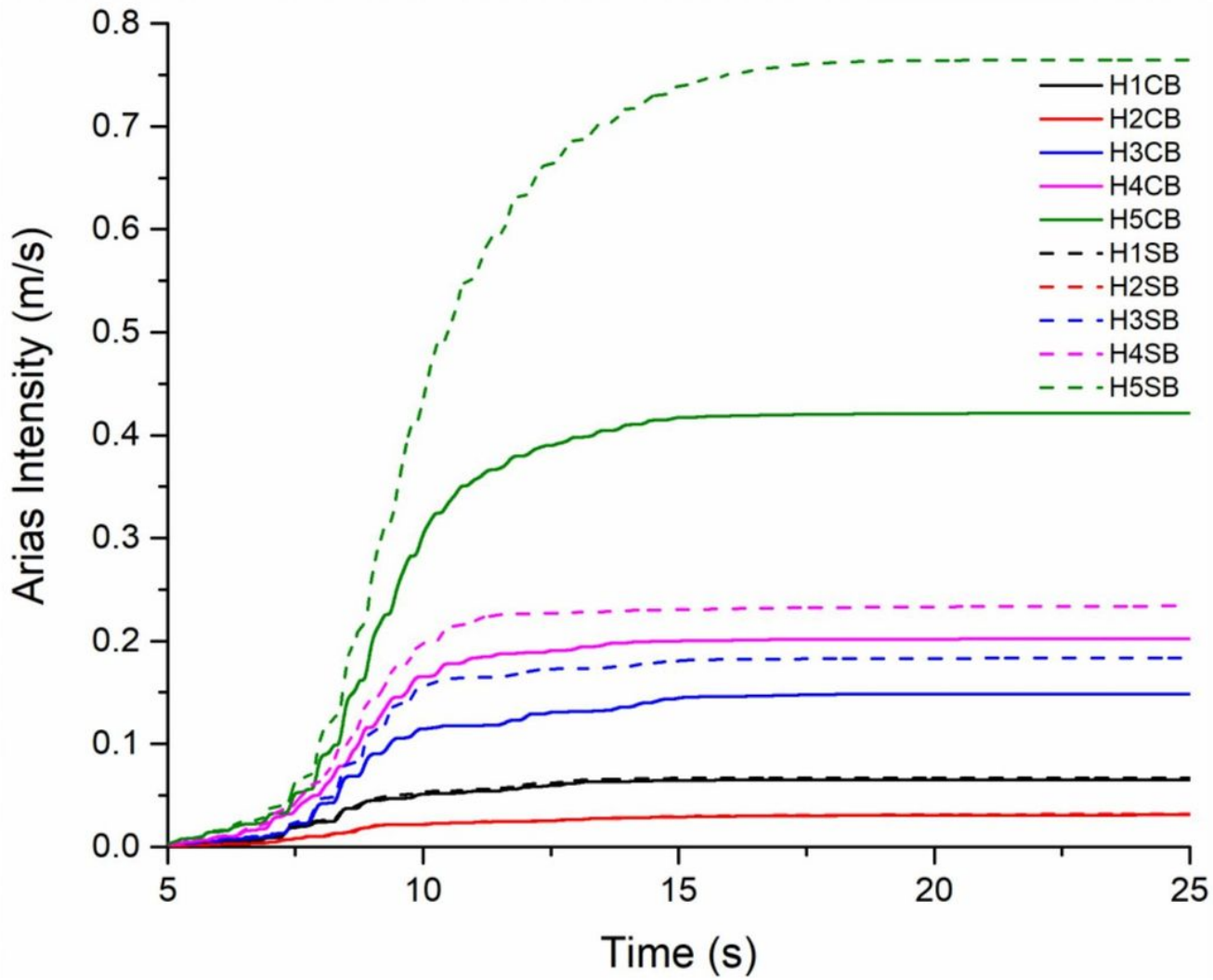

Figure 8

A comparison of Arias intensity of 15th building of the H1CB-H5CB city models with the respective standalone building.

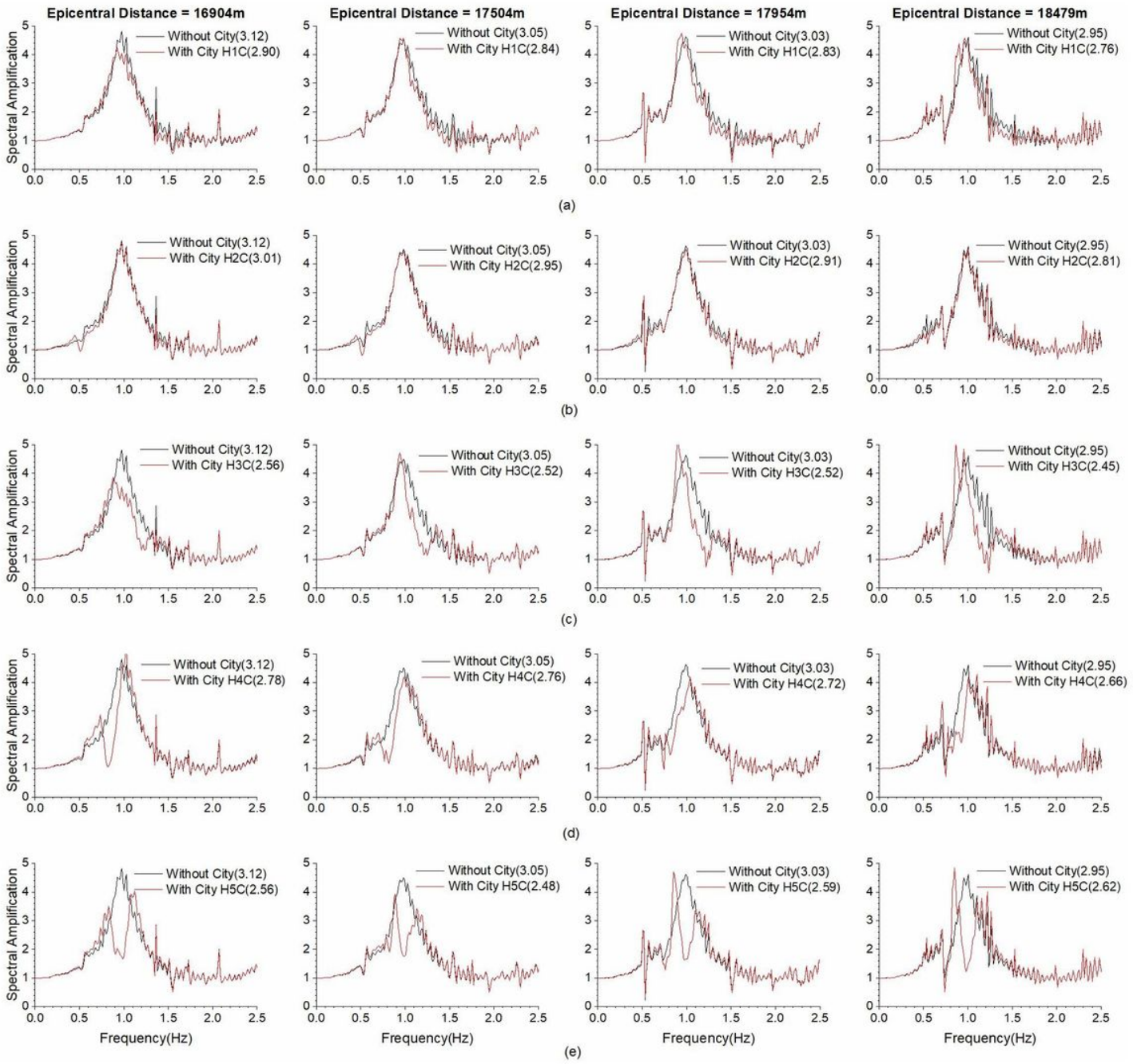

Figure 9

A comparison of transfer functions of sediment layer at various locations in the absence and presence of homogeneous H1CB-H5CB city models (Note: ATF of sediment layer in absence of city and ATF of the same in a frequency bandwidth (0.75-1.25Hz) in the presence of city are given in brackets).

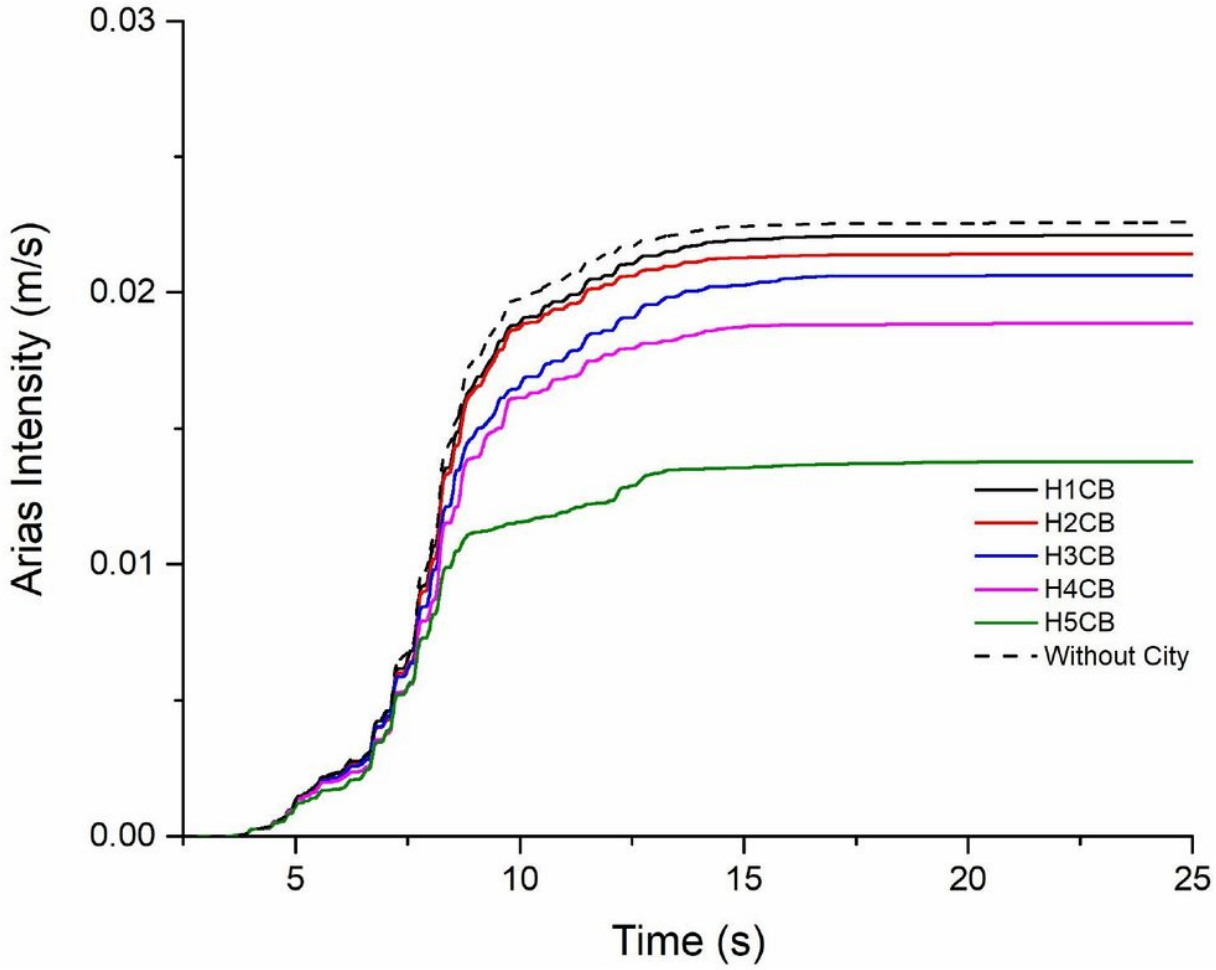

Figure 10

A comparison of free field Arias intensity at an epicentral distance of 17504m in the presence and absence of H1CB-H5CB city.

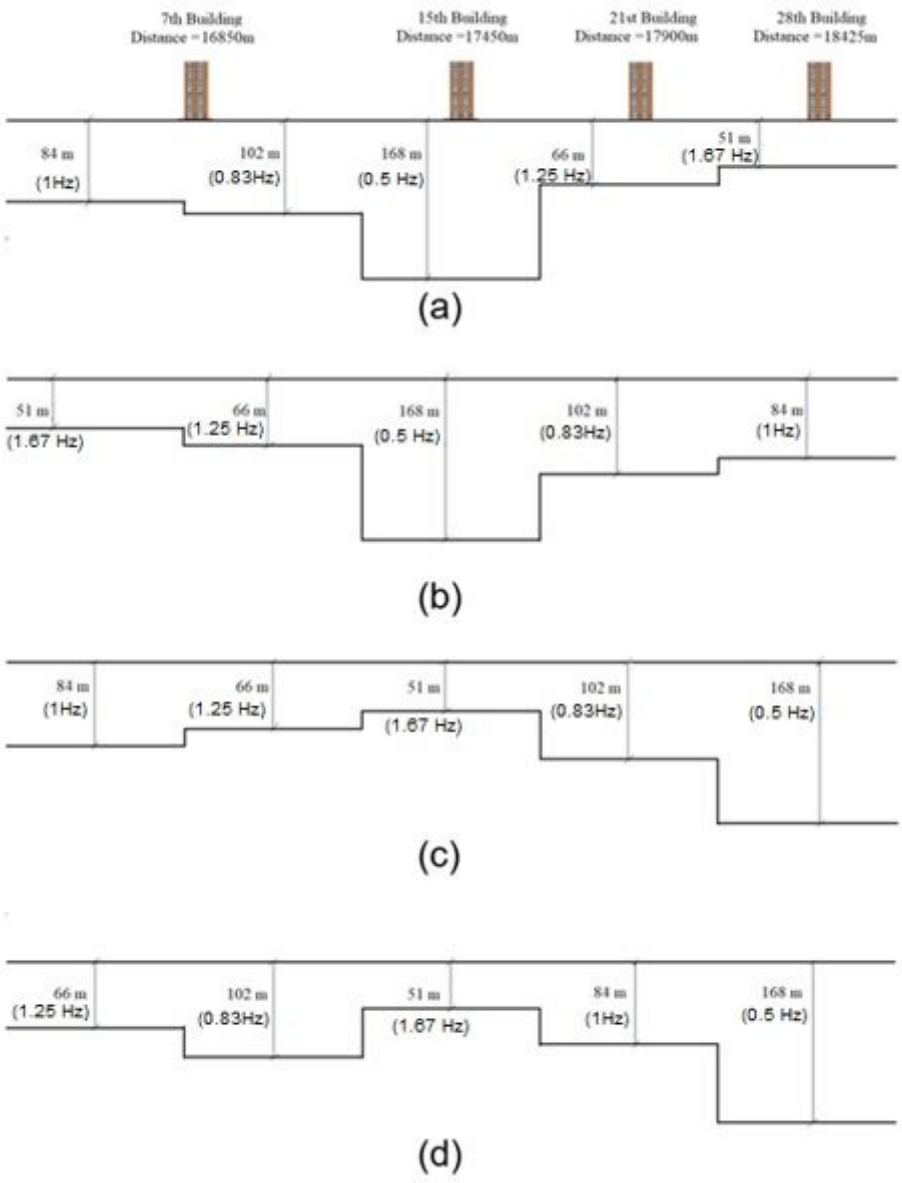

Figure 11

a-d Sketches for B1-B4 basin models, respectively and the sediment thicknesses along with the fundamental frequency in the different segments.

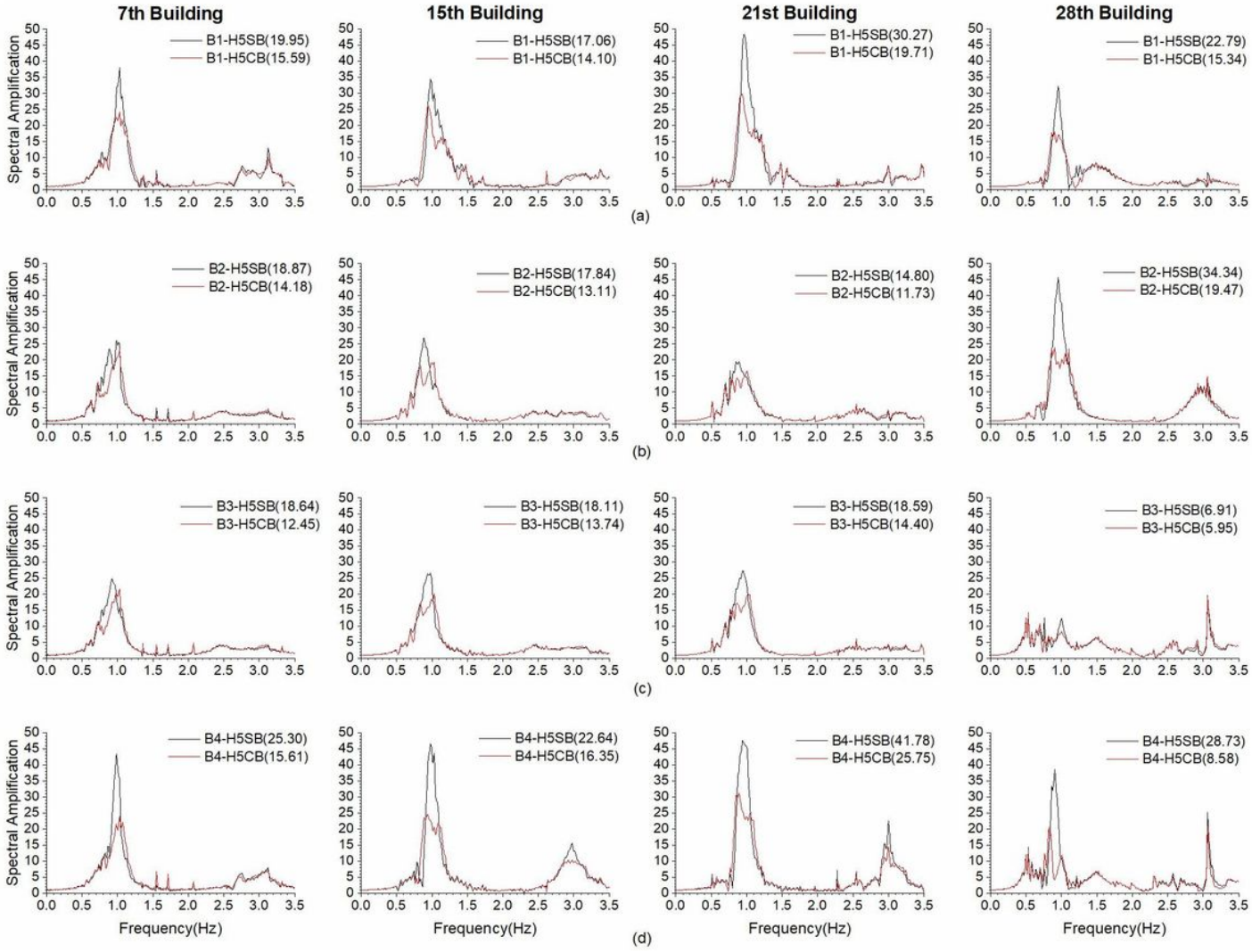

Figure 12

a-d A comparison of transfer functions of standalone buildings of B1-H5SB to B4-H5SB models with that of corresponding building of cities B1-H5CB to B4-H5CB at different locations (Note: ATF in the BP of buildings of city and standalone buildings are given in brackets).

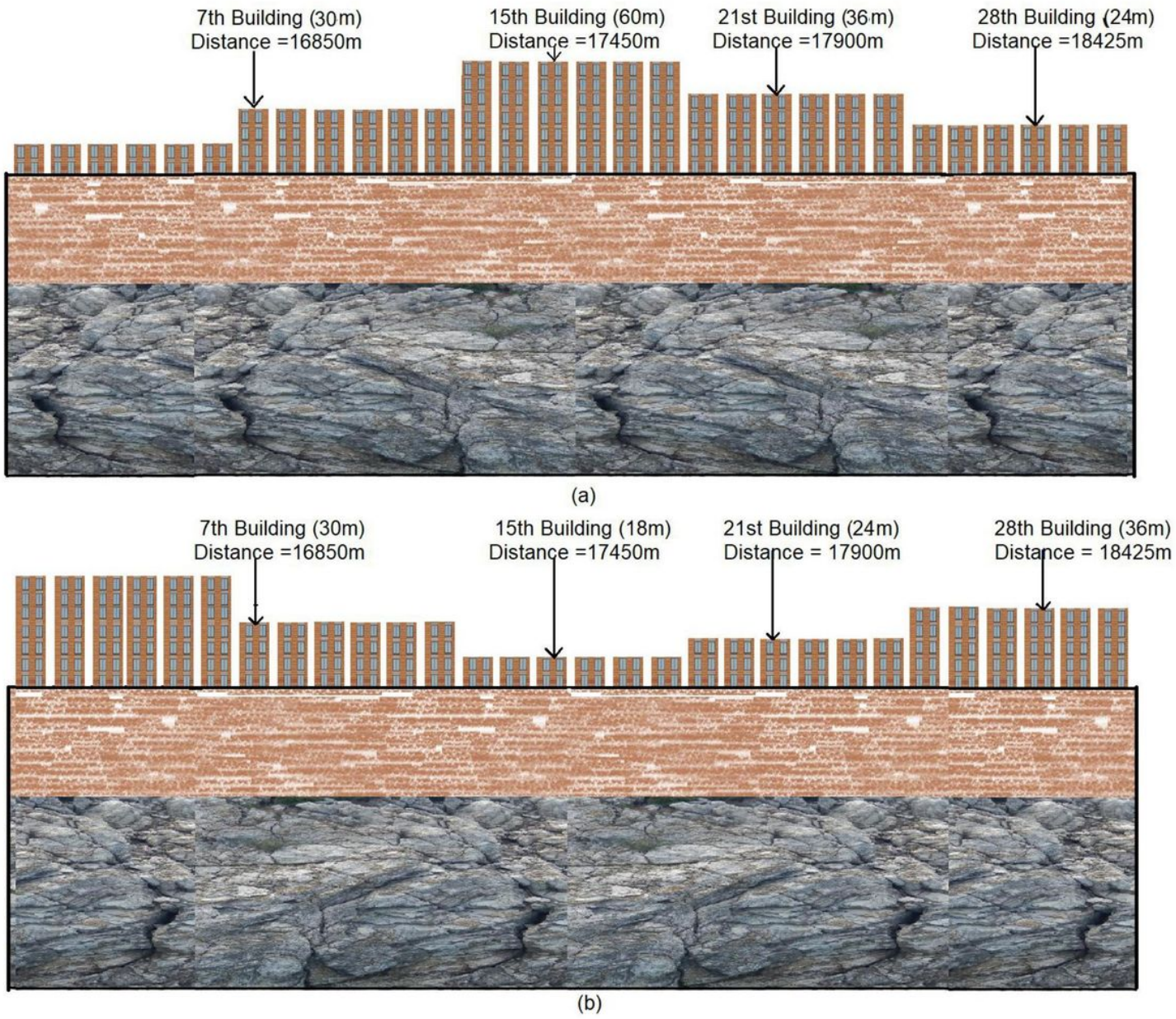

Figure 13

a&b Sketches for the HT1CB and HT2CB heterogeneous site-city models, respectively

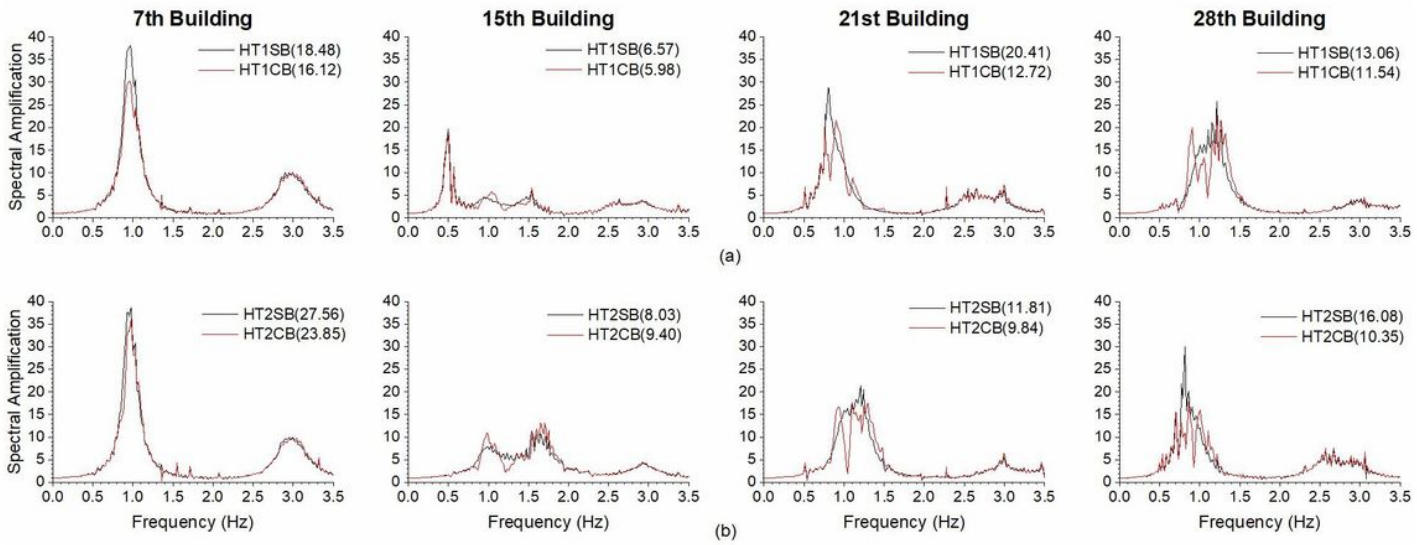

Figure 14

a&b A comparison of transfer functions of standalone building at different location with that of corresponding building of heterogeneous cities HT1CB and HT2CB (Note: ATF in the BP of buildings of city and standalone buildings are given in brackets).

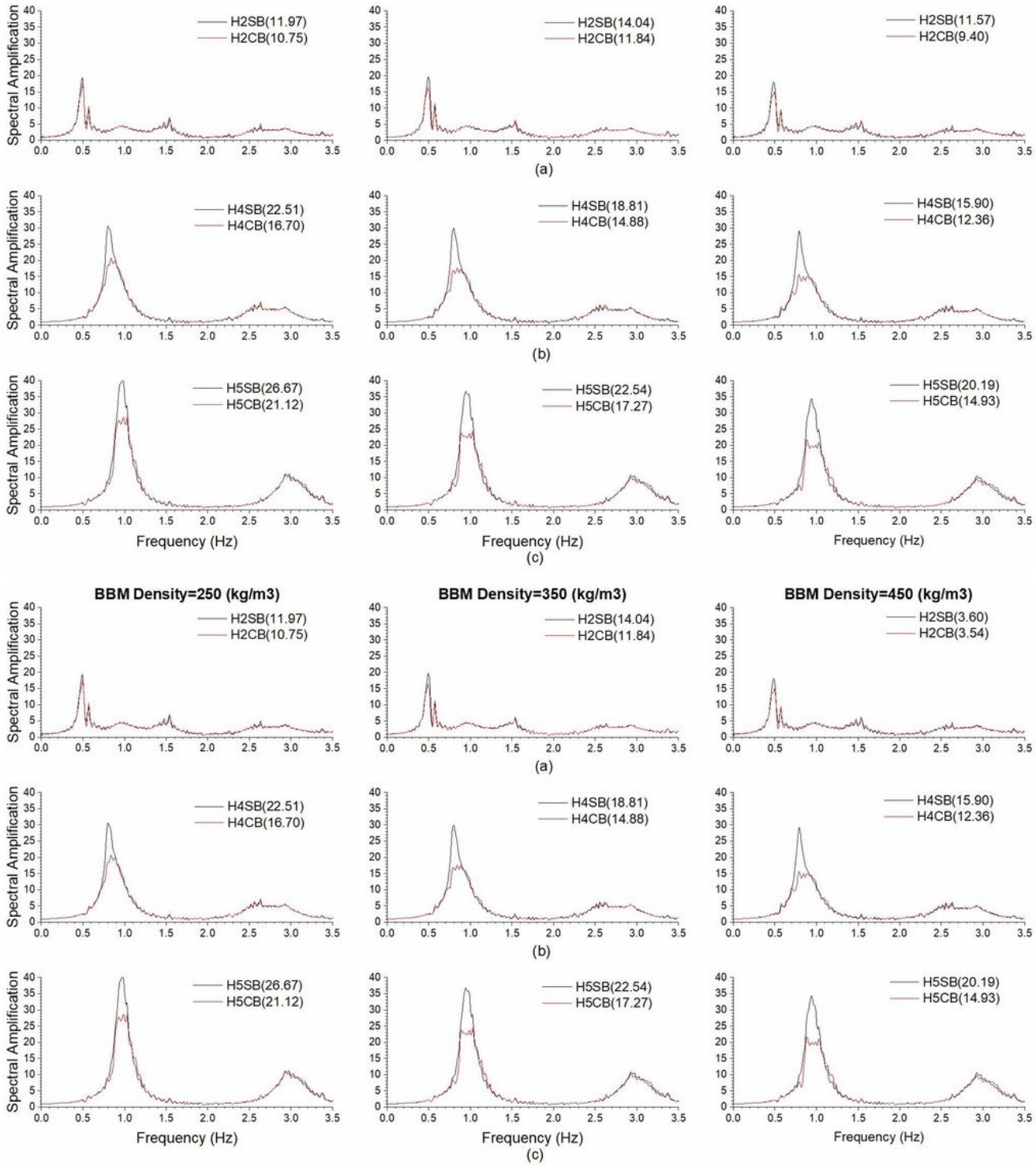

Figure 15

a-c A comparison of transfer functions of standalone buildings of H2SB, H4SB and H5SB models with that of corresponding 15th building of cities H2CB, H4CB and H5CB, respectively for different density of the BBM (Note: ATF in the BP of buildings of city and standalone buildings are given in brackets).

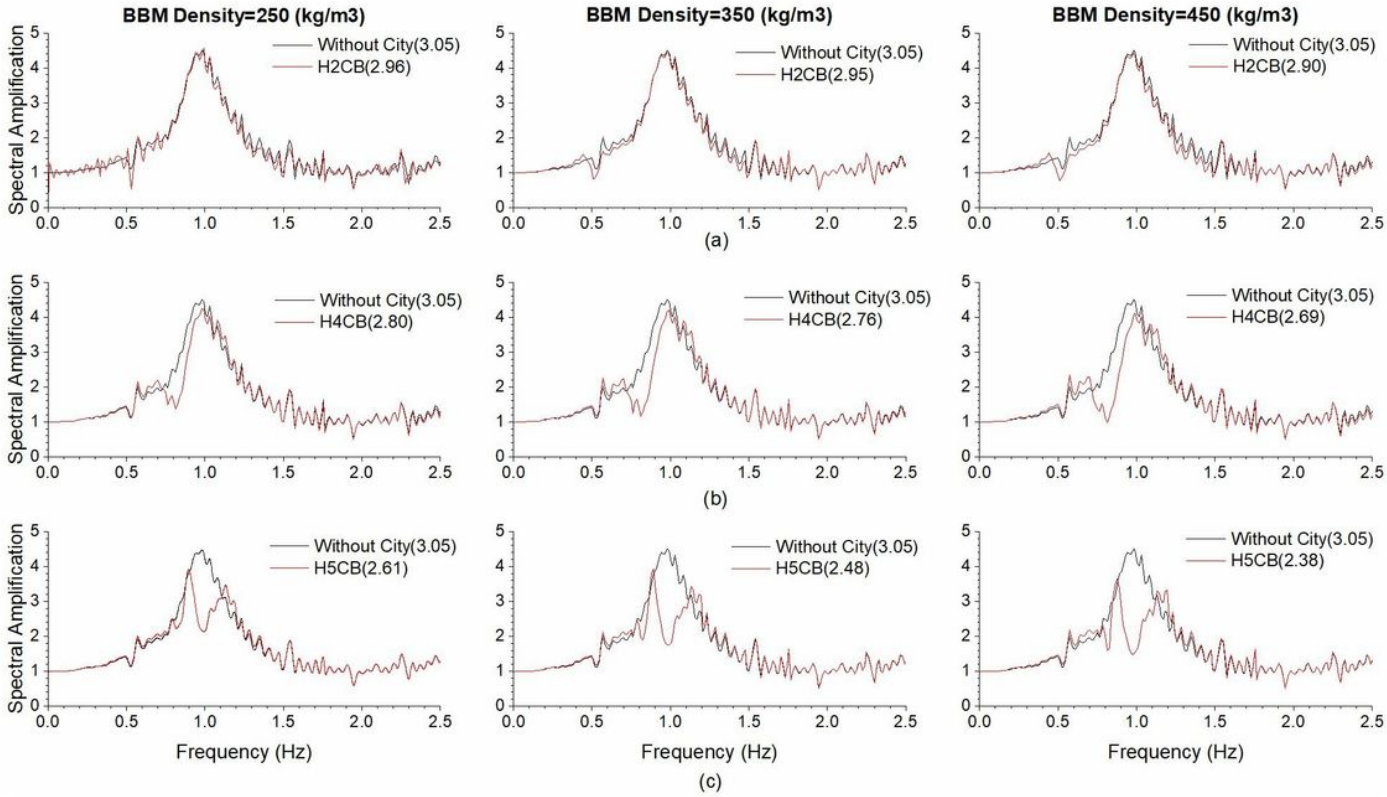

Figure 16

a-c A comparison of transfer function of sediment layer in the presence and absence of H2CB, H4CB and H5CB cities, respectively at an epicentral distance of 17.50 km for different density of BBM (Note: ATF of sediment layer in absence of city and ATF of the same in a frequency bandwidth (0.75-1.25Hz) in the presence of city are given in brackets).

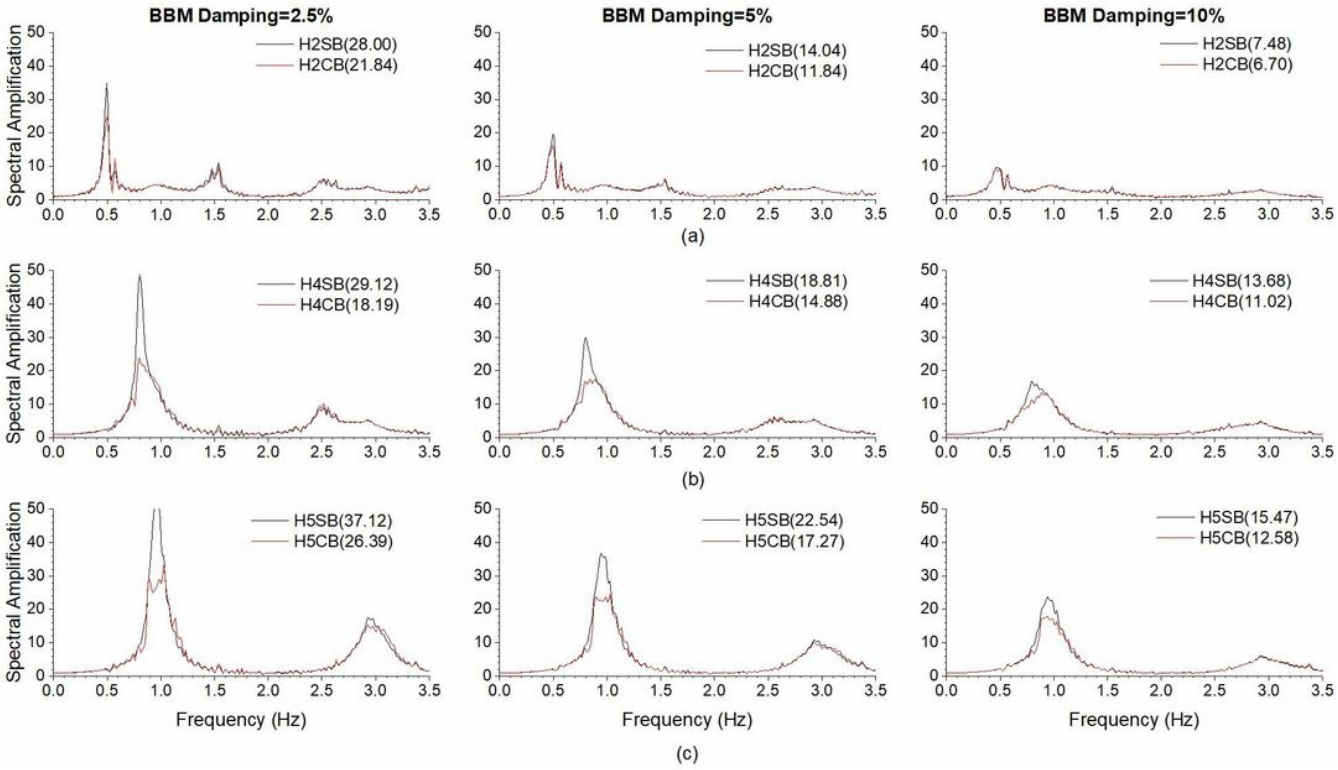

Figure 17

a-c A comparison of transfer functions of standalone buildings of H2SB, H4SB and H5SB models with that of corresponding 15th building of cities H2CB, H4CB and H5CB, respectively for different damping of BBM (Note: ATF in the BP of buildings of city and standalone buildings are given in brackets).

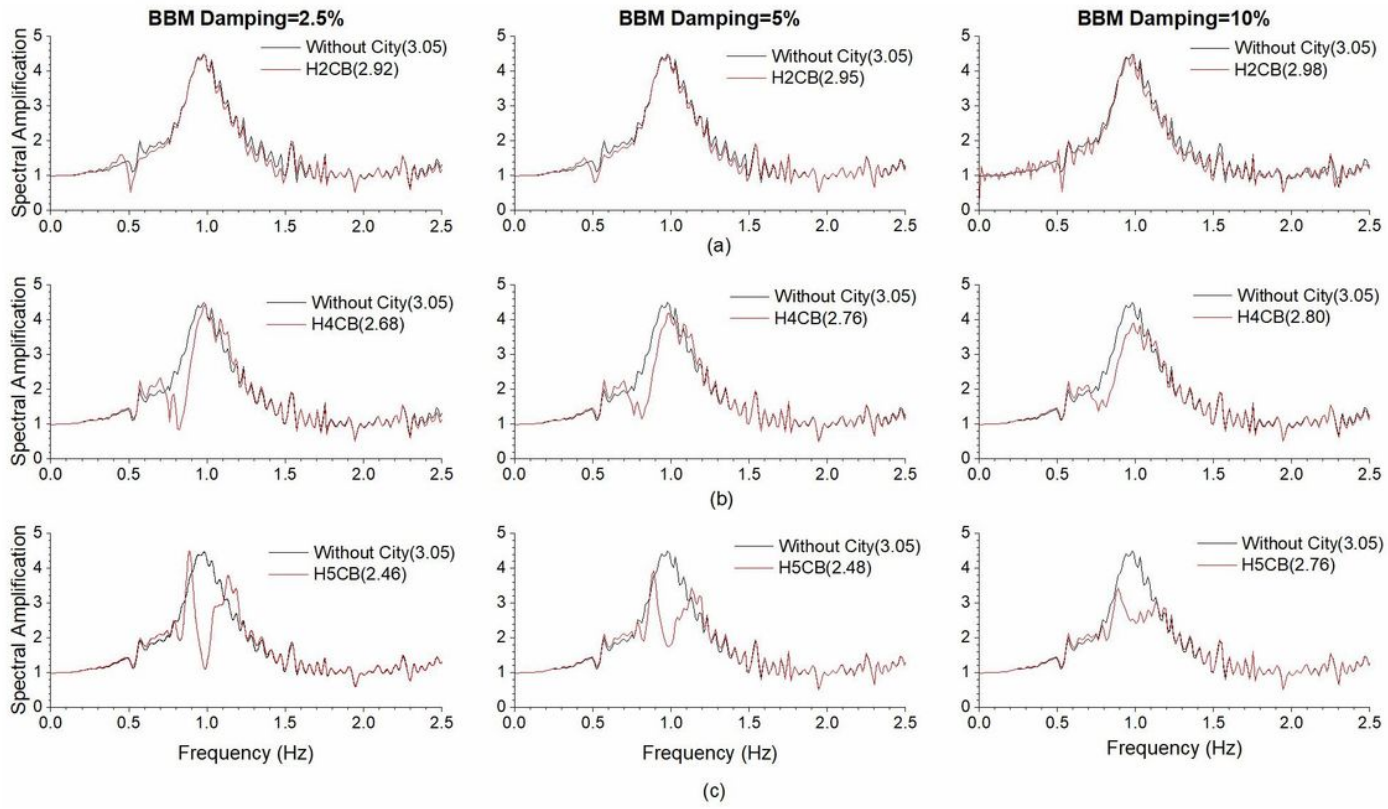

Figure 18

a-c A comparison of transfer function of sediment layer in the presence and absence of H2CB, H4CB and H5CB cities, respectively at an epicentral distance of 17.50 km for different damping of BBM (Note: ATF of sediment layer in absence of city and ATF of the same in a frequency bandwidth (0.75-1.25Hz) in the presence of city are given in brackets).